MICRO- AND NANO-PRECISION TESTING ON LOW TEMPERATURE SOLDERS

by

Colin Greene

A Thesis

Submitted to the Faculty of Purdue University

In Partial Fulfillment of the Requirements for the degree of

Master of Science in Mechanical Engineering

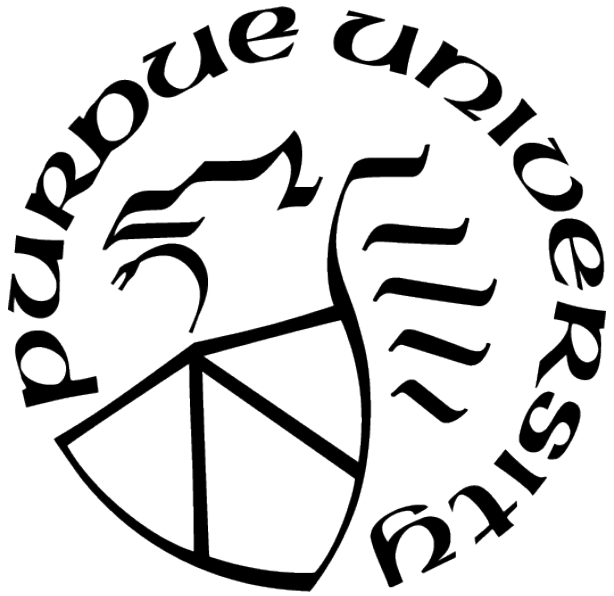

School of Mechanical Engineering

West Lafayette, Indiana

May 2021

THE PURDUE UNIVERSITY GRADUATE SCHOOL
STATEMENT OF COMMITTEE APPROVAL

Professor Ganesh Subbarayan, Chair

School of Mechanical Engineering

Professor John Blendell

School of Materials Engineering

Professor Keije Zhao

School of Mechanical Engineering

Approved by:

Nicole L. Key

ACKNOWLEDGMENTS

First, I would like to thank my advisor, Professor Subbarayan, for his patience, guidance, and support during my studies. I also would like to thank Professors Blendell and Zhao for serving in my committee.

I would also like to thank my labmates, who all helped me in their own ways. Yuvraj Singh took me under his wing during my undergraduate research, and introduced me to the world of metalworking. Travis Dale was a mentor and a friend during my graduate studies, even after he himself graduated. Sukshitha Achar was always available to brainstorm and helped me organize my thoughts. I would also like to thank Chetan, Pavan, Sai Sanjit, Sudarshan, and Yaxoing for conversations and banter across a great range of topics.

Finally, I would like to acknowledge my parents and grandmother, who had no small role in my scientific interests.

TABLE OF CONTENTS

LIST OF TABLES

LIST OF FIGURES

NOMENCLATURE

CAD	computer aided design, commonly referring to a 3D modelling software
CTE	linear coefficient of thermal expansion, commonly denoted α_L
ENIG	electroless nickel immersion gold, a common surface finish used in electronic packages
FR4	a standardized glass-reinforced epoxy laminate material, commonly used in printed circuit boards
L27	a proprietary lead-free solder composition
L29	a proprietary lead-free solder composition
load train	all components within a tester that are load bearing
OSP	organic solderability preservative, a common surface finish used in electronic packages
PID control	a control scheme involving proportional, integral, and derivative corrections
SAC305	a solder alloy composed of 3 wt% Ag, 0.5 wt% Cu, balance Sn
SEM	scanning electron microscope
Sn58Bi	a solder alloy composed of 58 wt% Bi, balance Sn
Sn57Bi1Ag	a solder alloy composed of 57 wt% Bi, 1 wt% Ag, balance Sn
RoHS	the Restriction of Hazardous Substances Directive (European Union directive 2002/95/EC)

ABSTRACT

Presently, a critical requirement in electronic assemblies is the reliability of solder joints. Accurate characterization of the mechanical behavior of solder alloys is challenging due to their micro-scale size, microstructural complexity, and complex rate-dependent mechanical behavior. This research presents two mechanical testers designed to acquire accurate mechanical response of the solder alloys. The testers allow using micro-scale test samples that replicate real solder joints in size and soldering pad metallurgy.

The first mechanical tester presented in this research is the micro-precision tester. It is capable of monotonic, creep and fatigue test profiles at testing temperatures between 25 and 75°C. Using a closed-loop control scheme and an external capacitance sensor to minimize measurement of the load train compliance, the tester is capable of precision on the order of 0.1 µm. For load controlled tests, the tester is capable of precision on the order of 0.5 N. The design and construction processes are presented, including rationale for major design choices. Additionally, the development of custom squat-joint samples for use in this tester is presented. These samples allow for increased data reliability while maintaining realistic dimensions. Both validation and test data are presented to demonstrate the capabilities of the micro-precision tester.

A second mechanical tester, the nano-precision tester, was developed to address the need for increased accuracy as solder geometries shrink. Again, the design choices and limitations are presented, with emphasis on improvements over the micro-precision tester. The load and displacement control are approximately and order of magnitude better than that of the micro-precision tester. Example tests are presented to demonstrate the accuracy and capabilities of the nano-precision tester.

Finally, the thesis concludes with recommendations on methods to further improve the two testers. Specifically, for the micro-precision tester, thermal expansion during high-temperature testing is a significant concern. For the nano-precision tester, both validation of the tester the capability of multi-temperature testing are future work.

1. INTRODUCTION

Solder is widely used to connect components within electronic packaging, both mechanically and electrically. One common mode of failure for electronics is mechanical fracture at the solder joints, leading to electrical failure of the component. For the majority of electronics, the primary loading condition is thermomechanical fatigue caused by thermal expansion as the device generates heat while in use. For many electronics, such as handheld devices, impact loading is a significant concern. In other applications, such as automotive electronics, extreme temperatures must be considered in addition to impact loads.

Broadly speaking, experimental methods to characterize solder fall into two categories. The first category is fatigue testing, where a load profile representative of the application is imposed on the sample. Generally, fatigue testing is accelerated, and use acceleration factor to determine field life. However, there is no universally accepted method to extrapolate between load conditions, which limits the direct applicability of fatigue test results without an accompanying damage accumulation model. A more directly usable test outcome is a constitutive model, where the stress-strain response to arbitrary load conditions is predicted. For solder, the experimental methods used to generate a constitutive model are typically monotonic and creep tests.

Many research groups have developed experimental solutions designed for mechanical testing of solder. One of the first published results on the mechanical behavior of solder was by Darveaux [1], which serves as a basis for most subsequent research. A non-exhaustive list of custom mechanical testers includes those by Wiese [2], Ma [3], Chan [4], [5], and Dale [6]. This demonstrates both the need for solder data, as well as the drive to create custom testers.

Solder alloys demonstrate some interesting behavior that result in difficulties obtaining accurate mechanical data. Bhate noted that mechanical data derived from bulk solder was not representative of interconnect-sized solder joints due to microstructural differences. Additionally, Bhate demonstrated the need for both accurate strain-rate measurements and closed-loop control due to the strain-rate sensitivity of solder alloys [7]. Chan described

the difficulties of dynamic testing of solder on commercial test equipment due to the use of universal joints [5].

Recent trends in the electronics and packaging industries have placed emphasis on achieving higher density, better temperature performance, and improved reliability of electronic packages. Further compounding this issue is the RoHS ban on lead-based solders due to the documented health effects of lead exposure. Lead-free alternative solders need significant mechanical validation since experience with these newer alloys is limited. This places a greater need for mechanical characterization of lead-free solders in general and, in particular, newer solder alloys with lower melting temperatures currently being considered in the industry.

This research presents two mechanical testers designed to meet the need for accurate and reliable characterization of solder joints. Chapter 2 presents the micro-precision mechanical tester, the latest in a long line of custom testers developed by the research group. Chapter 4 presents the nano-precision tester, a similar machine designed for higher precision at the cost of range. Technical drawings, components, and operating procedures for these testers are presented in the appendices.

2. THE MICRO-PRECISION MECHANICAL TESTER

Mechanical testing for bulk material has long been an established field, and commercial testing machines are available for a wide variety of applications. In the past, this research group used an Instron Microtester 5848, a tester specifically advertised towards evaluating microelectronics. However, several issues were present in the Instron machine, and in commercial testing equipment in general.

The first issue is that of displacement measurement. The Instron determines position with the use of an encoder mounted at the actuator, and claims sub-micron accuracy with this setup. This setup is typical of commercial testing machines. However, measurement of the actuator position is not an adequate measure of the strain at the sample due to load train compliance. This has been demonstrated in several publications, initially by Bhate et al. [7]. The behavior of solder is strongly strain-rate dependent, and requires closed-loop control with measurements of displacement as close to the sample as possible, so as to minimize load train compliance.

The second issue is that of cyclic testing, which for solder requires the load train to support compressive loads. The load train of the Instron uses ball joints to absorb off-axis loading produced by misalignment, rather than transfer the off-axis loads to the sample. This allows for looser manufacturing tolerances and less stringent alignment procedures. However, these joints cannot transfer compressive loads without significant deflection. This means that it is challenging to use Instron and similar commercial testing equipment for cyclic testing of solder.

The micro-precision tester is a custom machine designed to overcome the issues typical to commercial mechanical testing machines. This chapter presents the design, assembly, and validation of the micro-precision tester, as well as improvements made over the previous revision of the tester. It should be noted that this tester is only the latest revision. Many research group members have spent considerable time testing solder alloys. The tester design presented in this research is draws heavily on their work. Dale et al. presented the direct predecessor of this tester in the 2019 InterPACK conference [6].

2.1 Design

The micro-precision tester is a universal mechanical tester designed on the same principles as Instron and MTS testing machines. The tester is designed primarily to test solder samples in shear, or combined shear and compression. The overall design can be seen in the CAD model as well as a photograph of the tester in Figure 2.1 and 2.2. The following sections will elaborate on the major components of the tester, including the rationale behind significant design choices.

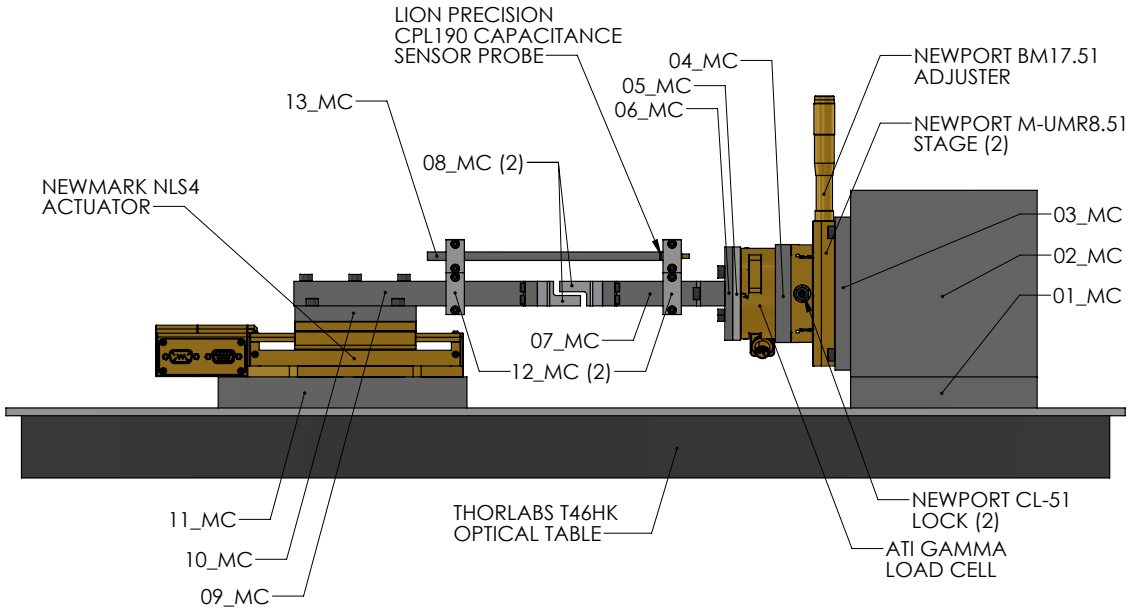

Figure 2.1. CAD model of the micro-precision mechanical tester. Purchased components are marked by manufacturer and name. Custom manufactured components are numbered 01_MC through 13_MC.

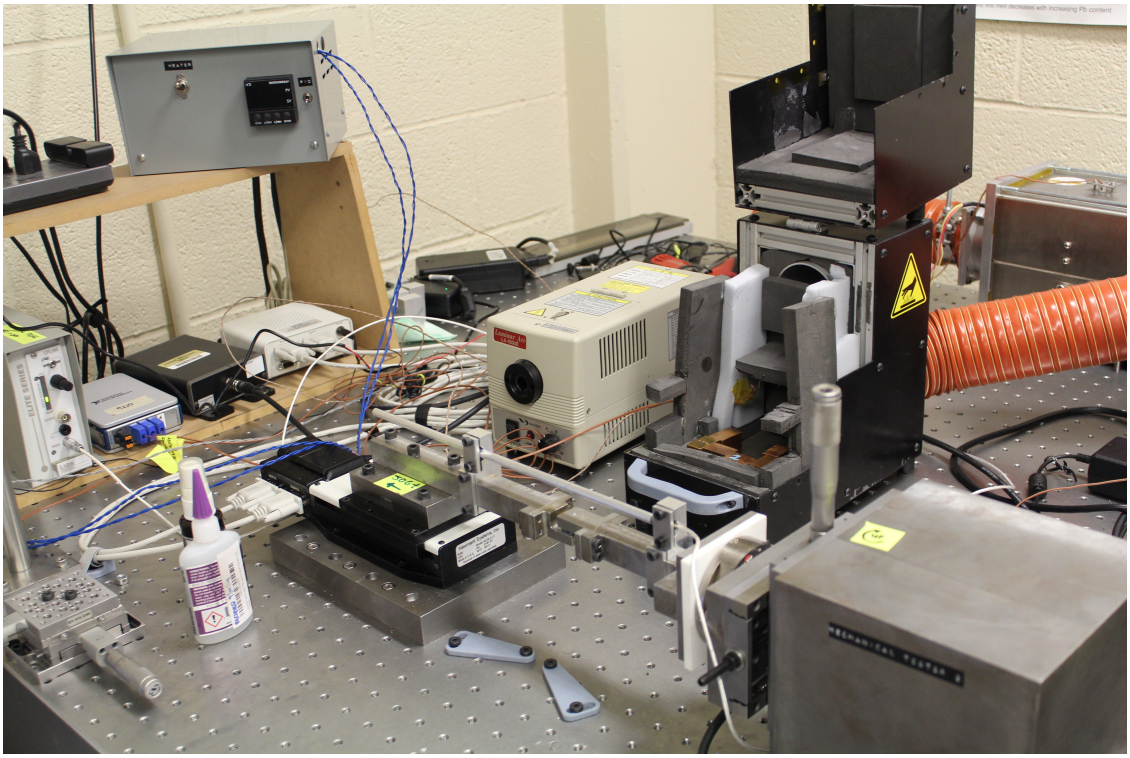

Figure 2.2. Photograph of the micro-precision mechanical tester. Drivers for the capacitance sensor, load cell, and actuator can be seen on the left. The environmental chamber is located behind the tester on the right, and its controller is located above the drivers on the left.

2.1.1 Sample and Workholding

The solder test specimen are deliberately constructed to be squat-joint samples, with a diameter of 730 µm and a standoff height of 150 µm. Eight joints are sandwiched between two FR4 substrates, see Figure 2.3. These samples are primarily intended for single lap shear, or combined shear and compression.

The dimensions of the solder sample are not particularly representative of typical solder joints, which tend to have a higher ratio of height to diameter. The choice to test low aspect ratio joints is to produce a more uniform state of stress at the solder-pad interface, thereby relating a given applied load to a unique state of stress at the interface. A numerical study by Bhate et al. determined that lower aspect ratio joints generate a more homogeneous shear stress at the pad interface [7], [8].

The choice to test joint-sized samples, as opposed to bulk solder, is to fully capture the behavior of field-use solder joints. It has been shown that the mechanical behavior of solder is markedly different in bulk than in joints, likely due to microstructural differences caused by pad finish [1], [2], [9]. Similarly, the choice to test the samples in shear is to emulate field use solder joints, which typically see shear loading due to a difference in the thermal expansion coefficient of the components in electronic packages. Fundamentally, isotropic plastic behavior of solder alloys assures that test observations are translatable between shear, tensile, or compressive loading modes. However, the choice to test in shear more accurately captures the failure modes of solder joints, commonly by Mode II shear fracture.

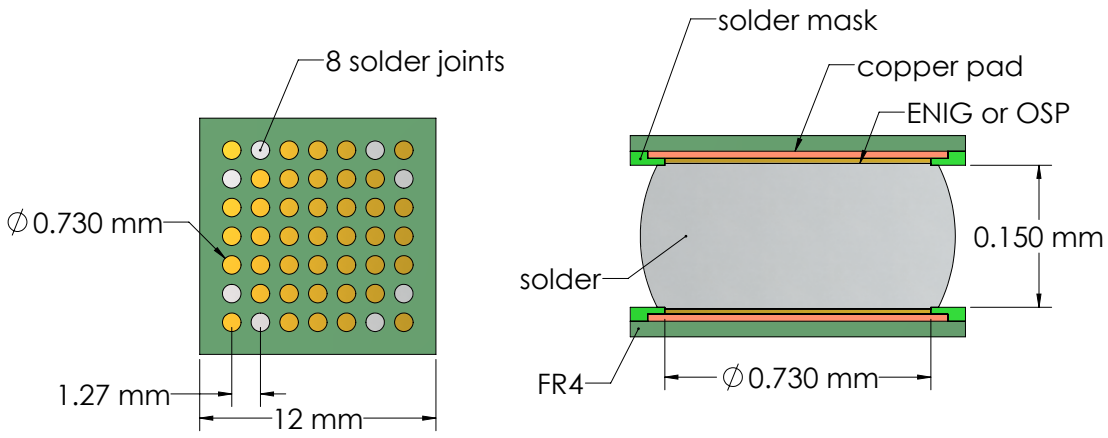

Figure 2.3. Typical squat-joint samples used in the micro-precision mechanical tester. Figure is not to scale.

In order to test the samples, they are attached to removable fixtures with cyanoacrylate adhesive. Adhesive is recommended for clamping samples with large surface area but insufficient height for a traditional clamp [10]. In this case, adhesive is required as positive clamping would bend the FR4 substrate. Additionally, the removable glue fixtures allow for preservation of the sample after testing for microstructure and failure analysis.

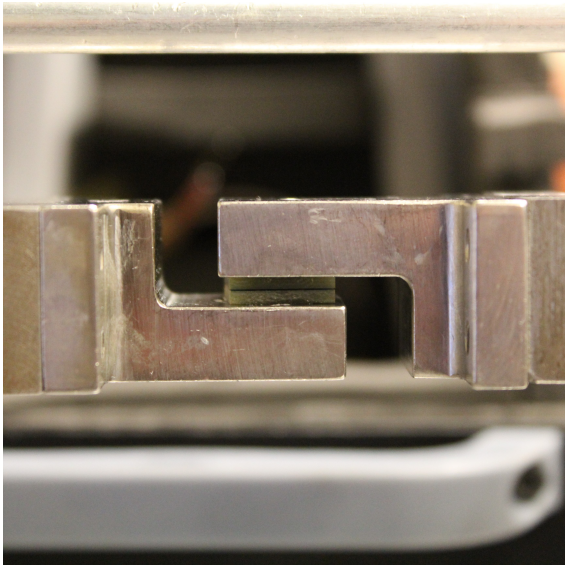

Figure 2.4. A sample fixed to the micro-precision tester with adhesive.

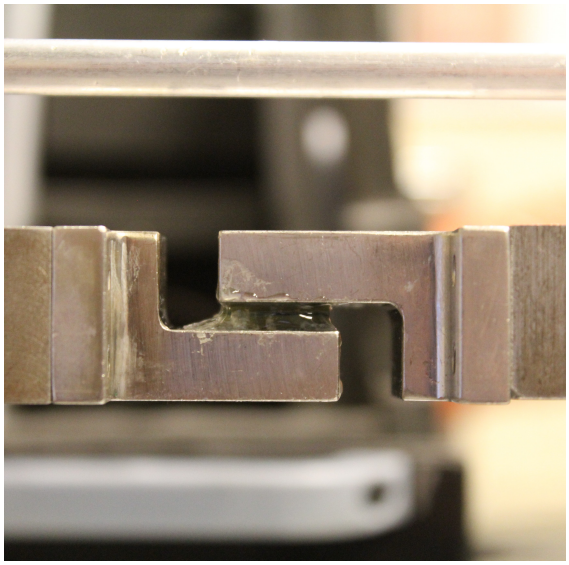

Figure 2.5. Fixtures glued together for removal after a test.

Based on these dimensions, the samples are expected to withstand loads of 60-150 N and displacements of 20-100 µm before failure, depending on temperature and test parameters. This controls the requirements of the actuator, as well as the load and displacement measurements. It should be noted that the load requirements can be lowered by populating fewer joints on the FR4 substrate.

2.1.2 Actuator

A Newmark NLS4-2-11 linear stage provides the testing machine's actuation. The stage is driven by a stepper motor coupled to a 1/16" (1.5875 mm) pitch ball screw. The step size is 32 nm when at 250 microsteps/step.

Manufacturer advertisements of 'backlash free' screw-based actuators are misleading. Many methods exist for reducing backlash in a screw-based actuator, and none are completely successful. A more accurate description would be 'reduced backlash' and a determination must be made if the amount of backlash is acceptable for the application. This determination is made more difficult by the lack of a manufacturer specified backlash.

As an example, Newmark Systems claims their NLS4 series has "zero backlash for the life of the stage" by the use of a trapezoidal leadscrew with a plastic nut. The backlash of the NLS4 of the micro-precision tester was measured by commanding the actuator to move while also measuring the position with the capacitance sensor. The observed backlash is between 6 and 8 µm, as shown in Figure 2.6.

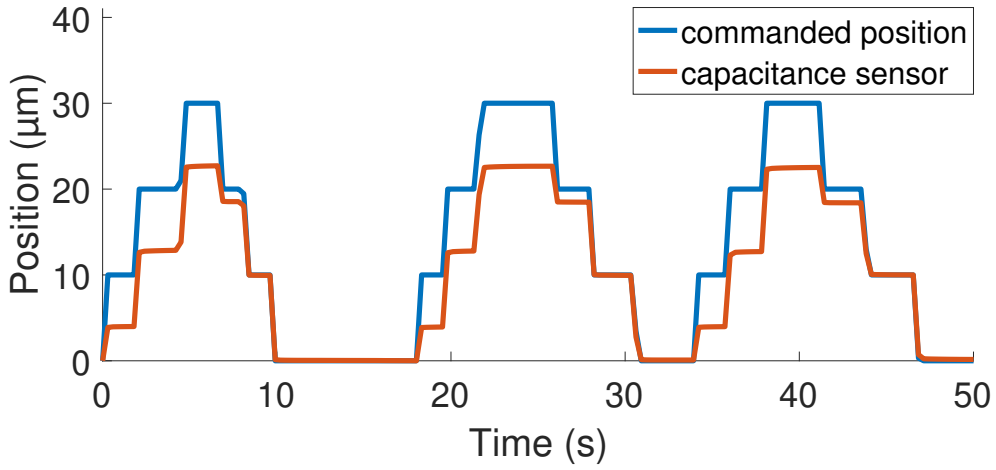

Figure 2.6. The commanded and the measured positions of the NLS4 actuator while unloaded.

2.1.3 Load and Displacement Measurement

Load is measured by an ATI Gamma 6-axis load cell. The shear load on the sample is measured by the z-axis, which has a range and resolution ±200 N and 0.025 N, respectively. For both x- and y-axes, the range and resolution are ±65 N and 0.0125 N, respectively.

A Lion Precision CPL190 capacitance sensor system measures displacement applied to the sample. It has a range of 250 µm and a resolution of 7.5 nm. Capacitance sensors are non-contact measurement systems, and therefore do not introduce any error in the load cell measurement.

The capacitance sensor is mounted as close to the sample as possible in order to minimize measurement of load train compliance. This is especially relevant for solder, as these materials display strongly strain rate dependent mechanical properties. The measurement

from the capacitance sensor is used for closed-loop control, so as to avoid the issue of load train compliance affecting the strain rate at the sample [6], [8].

For context, the nominal compliance of the load cell in the z-direction is 56 nm/N. If a 100 N load results in a 4 µm displacement at the sample, the load cell would deform an additional 5.6 µm. The displacement measured at the stage would be, at minimum, 9.6 µm, a greater than 100% error. Note that this error would not include any other sources of load train compliance, such as elongation of the actuator lead screw.

2.1.4 Temperature Measurement and Control

A custom environmental chamber provides the means to control the temperature at the sample. The chamber operates by forcing heated air over the sample with a high temperature fan. An insulated enclosure isolates the sample from the rest of the tester. Temperature at the sample is measured and controlled using a thermocouple placed next to the sample. The maximum temperature of the environmental chamber is limited by the fan, which is 85°C. To verify that the chamber can maintain a constant temperature, two tests were run, one at 30°C and one at 75°C. Based on these tests, the environmental chamber can maintain a constant temperature to within ±0.5°C.

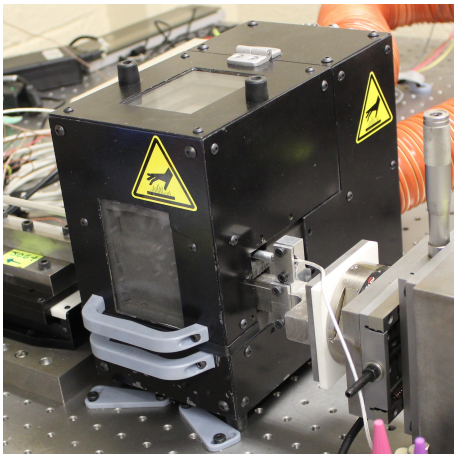

(a) Image of the insulated enclosure.

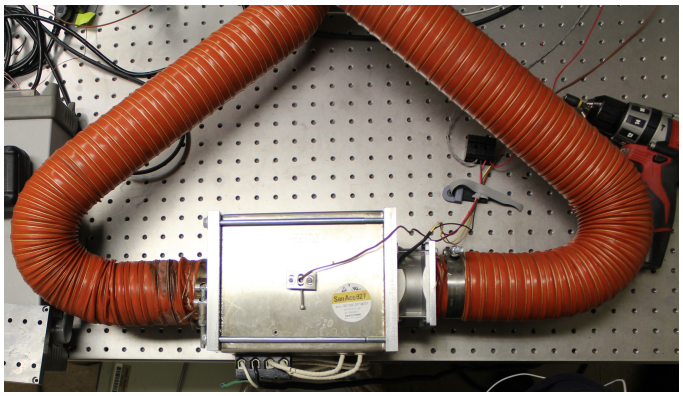

(b) Image of the resistive heater, fan, and ducting.

Figure 2.7. Images of the environmental chamber used to heat the sample.

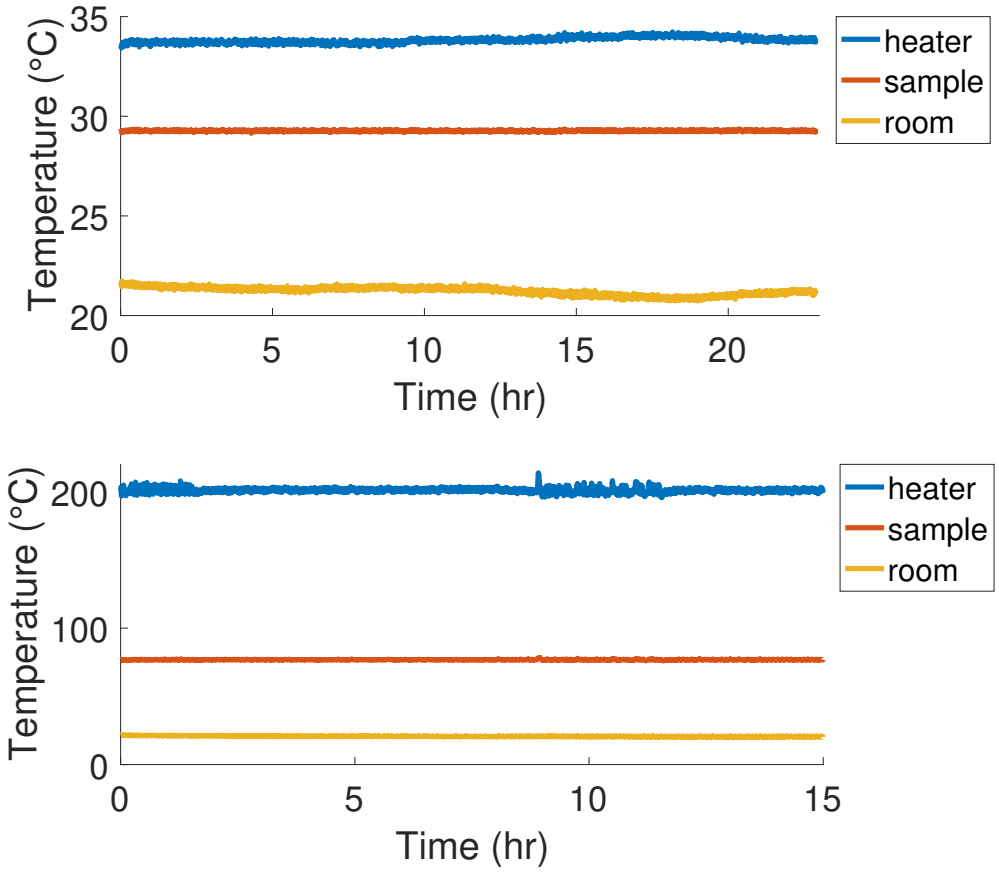

Figure 2.8. Verification tests of the environmental chamber. Temperatures are measured by thermocouples near the heater, sample, and in the room.

2.1.5 Data Acquisition and Control

The data acquisition and control is handled by a desktop computer running a custom LabVIEW program. The use of a desktop computer is convenient but presents a few challenges, primarily due to the operating system. The operating system, Windows 10, is a general purpose operating system designed with user interaction in mind, not a real time operating system designed to run a closed-loop control system. Due to the intended use-case, general purpose operating systems cannot guarantee precision timing, such as a discrete PID algorithm commanding an actuator at a rate of 1000 Hz.

Due to the use of desktop computer running a general purpose operating system, efforts must be taken to improve timing consistency. To accomplish this, the producer/consumer design pattern is used to decouple time-critical and time-insensitive processes by placing them into separate, parallel loops [11]. The producer loop only handles time-critical processes, namely sampling measurement data, implementing the PID algorithm, and commanding the actuator. From the producer loop, data is pushed to a queue and buffered for reading by the consumer loop. The consumer loop handles all time-insensitive tasks, including writing data to storage and updating operator-facing plots.

The program processes and records the measurement data, and implements a PID algorithm used for closed-loop control. For monotonic tests, the control variable is the backward difference velocity, computed from the capacitance sensor readings.

$$v_{\mathrm{i}} = \frac{z_{\mathrm{i}} - z_{\mathrm{i}-1}}{t_{\mathrm{i}} - t_{\mathrm{i}-1}}$$

where

v_{i}	the backwards difference velocity
z_{i}	the current capacitance sensor reading
$z_{\mathrm{i}-1}$	the previous capacitance sensor reading
t_{i}	the current time
$t_{\mathrm{i}-1}$	the previous time

For fatigue tests, the position from the capacitance sensor is the control variable. For creep tests, the F_z reading is used as the control variable. The PID output to the actuator is a velocity command.

A flowchart of the LabVIEW data acquisition and control loop is shown in Figure 2.9.

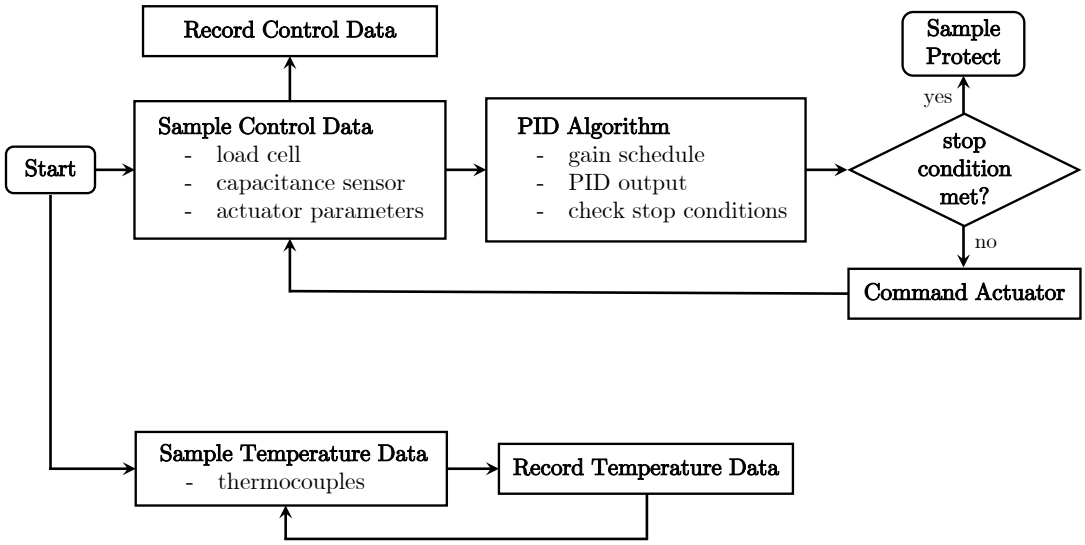

Figure 2.9. Data flow within the LabVIEW program, separated into two parallel processes.

Load and displacement measurements are sampled by a National Instruments PCIe-6323 DAQ. Using manufacturer provided calibrations, the measurements are converted from voltage into workable units [12], [13]. The DAQ samples 500 data points per channel at a rate of 25 kHz. The mean value is computed from these sampled data points, which then serve as the referenced load and displacement measurement.

Temperature is measured using thermocouples installed near the sample, in the room, and inside the heater. The thermocouple readings are sampled at 2 Hz using a NI-9210, a DAQ designed for thermocouple measurements.

All data is recorded to a binary file as they are received. The use of a binary file instead of a text file is for speed. After a test is completed, the data is converted into a tab-delimited text file, a more convenient format for post-processing.

Built into the control software are a set of stopping conditions, which determine whether or not to continue the test. For monotonic and creep, the most common stopping condition met is a time limit. For fatigue tests, it is possible to stop when a displacement cycle does not produce significant load, implying the sample has fully fractured. Alternatively, it is possible to study crack growth by stopping the test when the current cycle load has decreased a certain amount from the first cycle.

After the test has stopped, the tester begins a sample protect test with the goal of preventing additional damage to the sample. The sample protect test is simply a creep test with a setpoint of 0 N. The sample is then removed and the failure modes can be studied under optical or electron microscope.

2.1.6 Other Considerations

Two design criteria are challenging to address, namely load train stiffness and external vibration. The design of the micro-precision tester includes efforts to maximize stiffness, with the ultimate goal of minimizing off-axis loading from deflection. To do this, the length of all lever arms were minimized. All components were aligned to the common centerline of the actuator and load cell.

The entire tester is mounted on an optical table in order to minimize the effect of vibrations on the experiment. While usually used for optics and laser experiments, optical tables are also well suited for mechanical experiments. The table is designed to be highly rigid by the use of honeycomb reinforcing, and versatile by the use of a grid of mounting holes. The table rests on pneumatic cylinders, which mechanically decouple the work surface from the environment. This vibration reduction is particularly useful in buildings that are not isolated from the surrounding and do not include any special purpose stiffened flooring construction.

2.2 Changes from the Previous Tester

While the micro-precision tester presented is a revision on the previous tester, several incremental changes were made with the goal of improving the overall design. These changes, and the motivation behind them, are presented here.

2.2.1 Orientation

In the previous tester, the faces of the glue fixture that contact the sample were vertical. For this orientation, the operator must simultaneously hold the sample in midair while adjusting the glue fixtures until they secure the sample. In the current tester, the sample is

simply placed on lower glue fixture. This reduces the chance of operator error when installing the sample. In the case of combined loading, this orientation removes the need for a pulley system to apply a compressive load, although not for tensile loads.

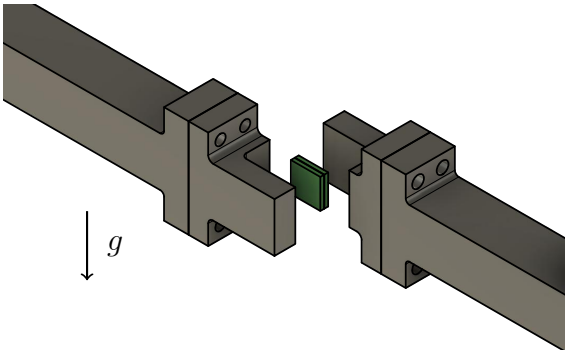

Figure 2.10. Orientation of the glue fixtures on the previous tester.

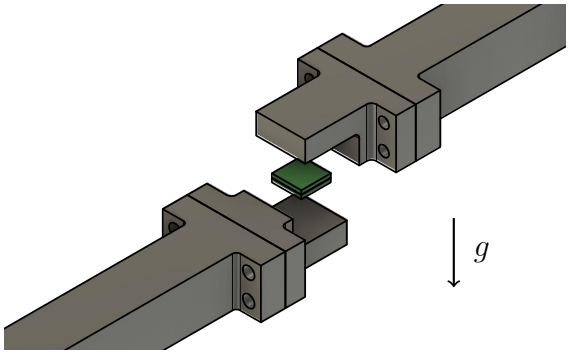

Figure 2.11. Orientation of the glue fixtures on the current tester.

2.2.2 Capacitance Sensor Fixtures

Two fixtures (12_MC) hold the the capacitance sensor and target onto the load cell and actuator arms. The previous tester used a 'split bore' style clamp. Note for this style of clamp, the clamping load distorts the bore so that it is no longer cylindrical. Due to this deformation, contact with the sensor is only made in two places, leaving a rotational degree of freedom. This is unacceptable for making micron and sub-micron measurements. This same issue is shared by 'set screw' style clamps. A more robust clamping method is the 'v-block' style, which guarantees contact in three places and fully constrains the capacitance sensor probe [14].

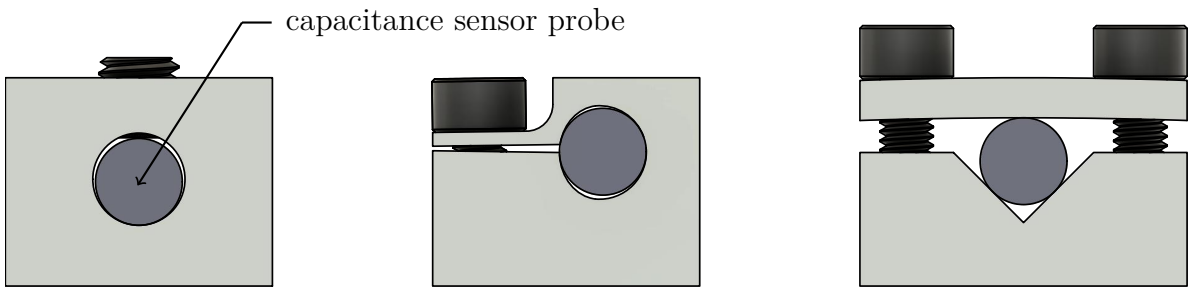

(a) set screw (b) split bore (c) v-block

Figure 2.12. Three common styles of clamp. Deformation due to clamping forces is exaggerated.

2.2.3 Data Acquisition Rate

Significant software changes accompanied the hardware changes to the new revision of the micro-precision tester. The most significant software change was the improvement to the data acquisition rate. The data acquisition software for the current tester is discussed more fully in Section 2.1.5.

The data acquisition and control algorithm of the previous tester performed the same functions as the current version, although in a slightly different manner. Figure 2.13 shows the data flow of the previous software, which is similar but not the same as the newly developed version.

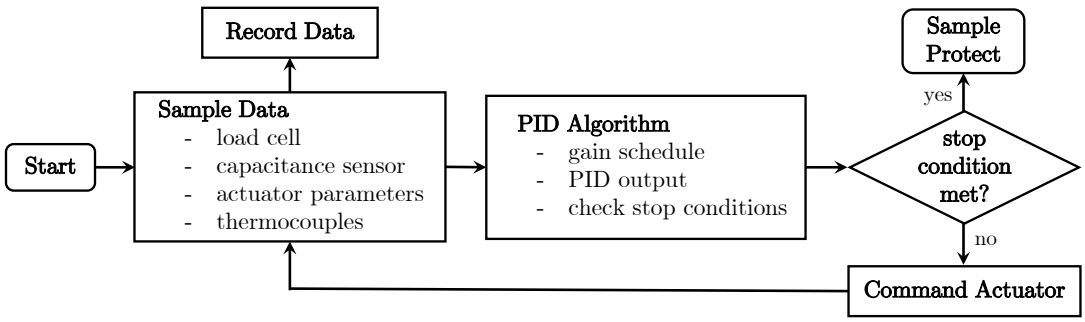

Figure 2.13. Data flow within the original LabVIEW program.

The measured data is processed via a discrete PID algorithm to generate a control signal for the motor. Receiving, processing, and transmitting data takes a finite amount of time. It

is desirable to reduce that time as much as possible, both to gather more data points, and to improve control. In order to improve the sampling speed, first it was necessary to determine where improvement was possible. To do this, the control software was run for one minute while recording the duration of each operation. Table 2.1 shows the timing data measured from this procedure.

Table 2.1. Timing data for the original micro-precision mechanical tester.

Operation	**Typical Duration (ms)**	**Maximum Duration (ms)**
sample data		
temperature	370	425
load and displacement	205	216
actuator parameters	110	198
generate actuator command		
gain schedule	<0.001	<0.001
PID algorithm	0.006	0.01
check stop conditions	<0.001	<0.001
send actuator command	4	10

This table is organized in the same manner as the data flow within the control software. Operations that are performed in series have a row in the table. Each sub-operation within that row is performed in parallel. For example, the software is capable sampling temperature and load data simultaneously, but is not able to generate an actuator command until all sampling has completed. Therefore, each operation is only as fast as its slowest sub-operation. From this data it can be seen that discrete PID loop can only run slightly above 2 Hz, largely due to the time taken to acquire the temperature data.

Using the information from this exercise, the following changes were made:

- Data acquisition was separated into two parallel processes. One process handles all data required for closed-loop control. The other process handles the remaining data.
- Communication with external devices was minimized.
- Data transfer, both internal and external, is made in bulk.
- No effort was made to improve the PID algorithm performance, as efforts led to little improvement.

Using the same timing procedure as before, the timing data was re-sampled with the improvements implemented in the control software. The results of this procedure are reported in Table 2.2.

Table 2.2. Timing data after efforts to improve overall sampling rate.

Operation	**Typical Duration (ms)**	**Maximum Duration (ms)**
sample control data		
load and displacement	23	25
actuator parameters	25	31
sample temperature data	370	425
generate actuator command		
gain schedule	<0.001	<0.001
PID algorithm	0.006	0.01
check stop conditions	<0.001	<0.001
send actuator command	4	10

After improvements, the maximum duration of the control loop recorded was ~30 ms. In order to maintain a consistent duration, the duration was set to a nominal 50 ms. The improvements and consistency of the timing were validated by running a 20 hr test. The

results are a 54ms average over 20hr duration test, which is approximately an order of magnitude improvement over the previous tester (∼2Hz to 20Hz).

2.3 Manufacturing

The custom components required for micro-precision tester were manufactured in-house at Purdue's Bechtel Innovation and Design Center. All parts required milling to size, and clearance and tapped holes for bolts. Some parts required reamed holes for alignment pins. A Haas 3-axis CNC mill was used to manufacture all custom parts. Care was taken to ensure datum features, such as perpendicular surfaces, were manufactured as accurately as possible. Figure 2.14 shows a representative part, both in the design phase as a technical drawing, and in the manufacturing phase.

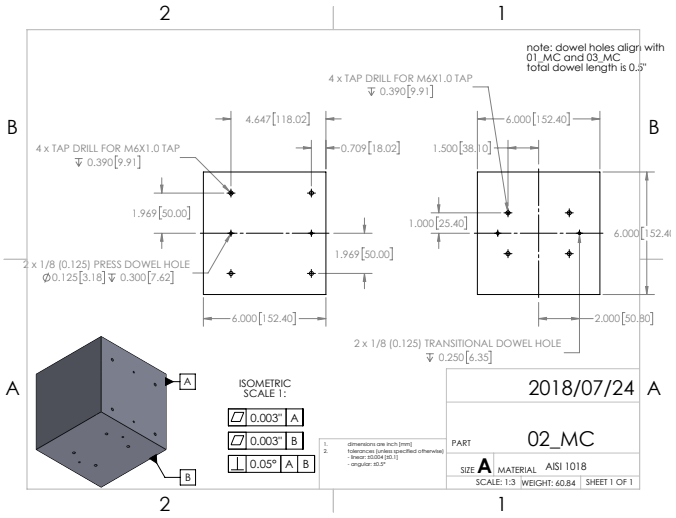

(a) technical drawing

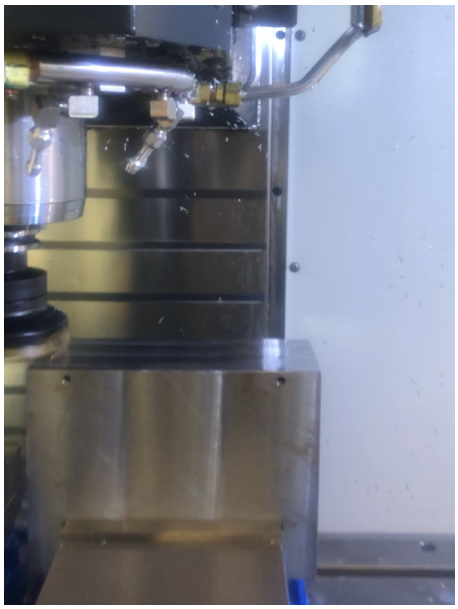

(b) face milling to size

Figure 2.14. Technical drawing and manufacturing of the angle plate supporting the load cell side (02_MC).

2.4 Assembly and Alignment

Efforts were made to manufacture all features as square and parallel as possible, and dowel pins were used to align many components. However, there is a limit on manufacturing

accuracy, and many purchased components had no alignment features. Because of this, care was needed to assemble the tester as designed.

Figure 2.15 illustrates one possible type of manufacturing error. Here, the actuator arm is not aligned with the actuator motion because the two faces of the fixture plate are not parallel. If uncorrected, this would produce combined loading on a sample that would need to be in pure shear.

Figure 2.16 illustrates a misalignment possible due to the play within a bolted connection. This can be corrected by manufacturing an alignment feature, such as a key or dowel holes, but there are no such features on this particular actuator. However, this is a relatively benign error, and would only introduce moderate bending in the arm.

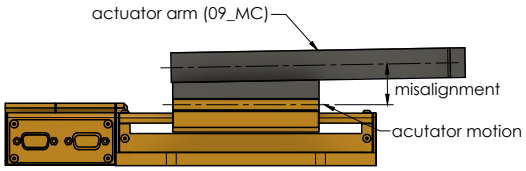

Figure 2.15. Potential misalignment due to manufacturing error.

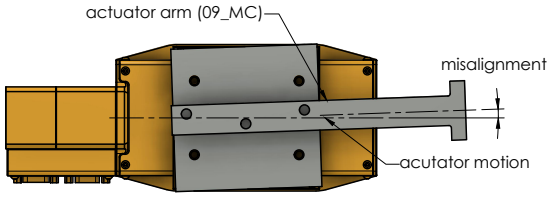

Figure 2.16. Potential misalignment due to a lack of alignment features.

In order to measure and correct any misalignment between the axis of the actuator with the arm, a datum and measurement device were used. The motion of the actuator itself provides the datum, and the tester's own capacitance sensor serves as the measurement device. In this case, the maximum angular deviation measured was 0.05°, which was an error too small to correct with a shim.

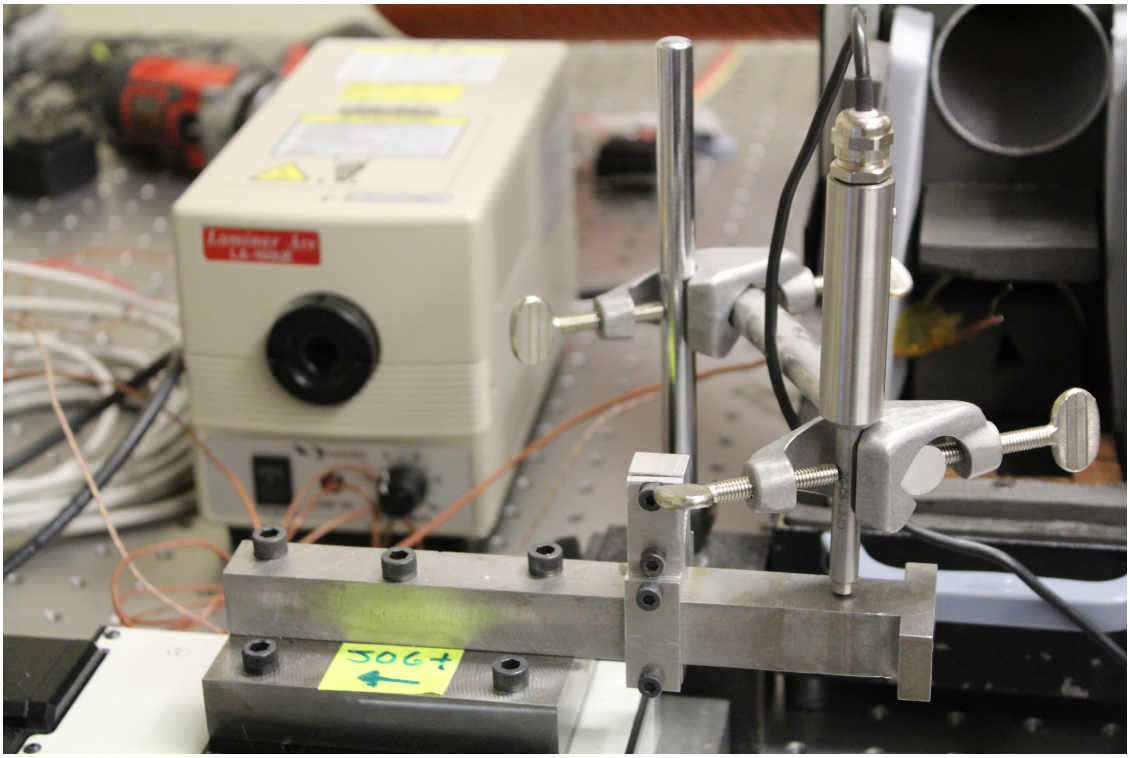

Figure 2.17. Quantifying the misalignment between the actuator motion and arm.

After the actuator arm was adequately aligned, the z-axis of the load cell was aligned with the actuator motion. This ensures the shear load imposed by the actuator is fully resolved by the z-axis of the load cell. Additionally, this alignment serves to minimize bending of the load cell arm (07_MC). Figure 2.18 and 2.19 show these two potential misalignments. The misalignment shown in the upper illustration would need to be corrected using shim stock. The lower misalignment can be corrected by rotating the fixtures bolting the load cell side to the optical table. See 01_MC through 03_MC in Figure 2.1.

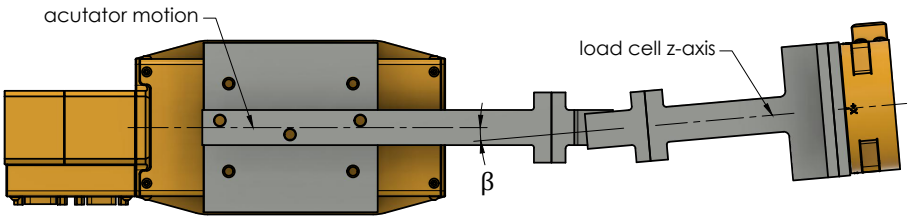

Figure 2.18. Actuator and load cell misalignment in the yz-plane.

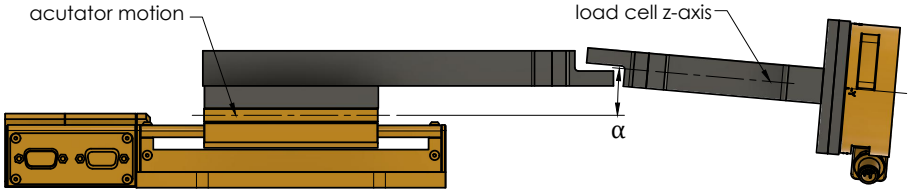

Figure 2.19. Actuator and load cell misalignment in the xz-plane.

To quantify and correct the load cell misalignment, a different procedure was developed, inspired by the principles governing coordinate measurement machines. Two fixtures were manufactured, one fixture to hold a domed-head dowel pin and another fixture to provide a flat surface for the pin to contact. The procedure is as follows (see Figure 2.20 to 2.22):

1. The actuator was advanced until contact was detected by the load cell.
2. At this point the displacement was recorded using the capacitance sensor.
3. Steps 1 and 2 were repeated with the dowel pin in the other 3 positions.
4. The angular misalignments were calculated.
5. The misalignment in the load cell's xz-plane was corrected using shim stock.
6. The misalignment in the load cell's yz-plane was corrected by rotation of the entire right side of the tester.
7. Steps 1 through 4 were repeated to confirm the alignment was corrected.

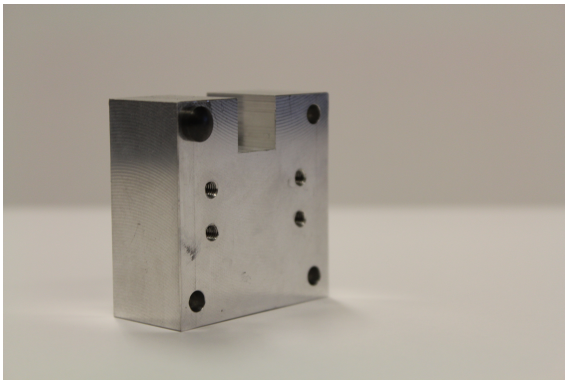

Figure 2.20. The fixture for holding the domed-head dowel pin.

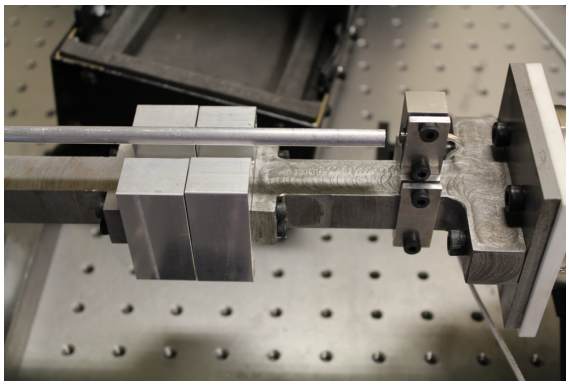

Figure 2.21. The procedure for alignment of the actuator and load cell.

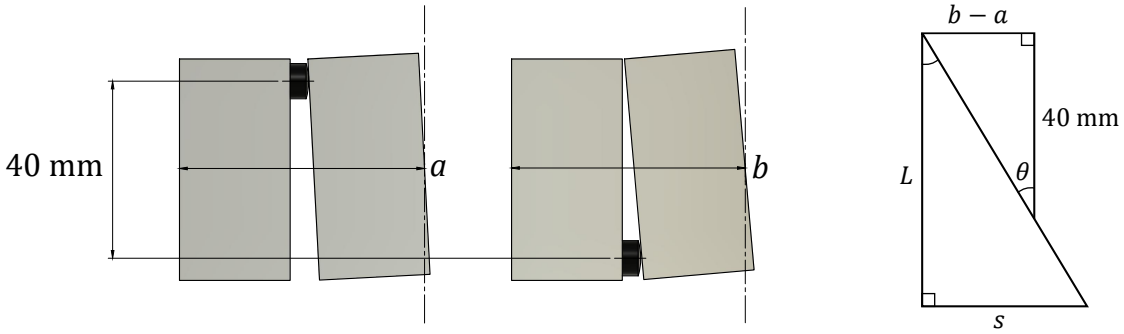

Figure 2.22. The geometric relationship between the displacement measurements taken (a and b), the angular misalignment (θ), the shim thickness (s), and the shim's lever arm (L).

The final α misalignment was 2 µm over 40 mm (0.03°), and the β misalignment was 12 µm over 40 mm (0.17°). Misalignment due to β error does not produce combined loading, therefore deemed acceptable. (much more tedious to correct).

2.5 Validation

The design of the micro-precision mechanical tester was validated in two parts. First, the efforts made to align the load cell were checked. This was done by comparing the F_z reading of the tester load cell to a higher resolution (0.0041 N) load cell, as shown in Figure 2.23.

The higher precision load cell was placed where a sample would be, and compression loads were applied from 0.5 to 4 N, in 0.5 N increments. An equal number of samples were selected from each increment, and the mean errors computed. Figure 2.24 shows a plot of the mean error versus the nominal load. The maximum error recorded was 0.029 N, and there does not appear to be a correlation between the the error and the nominal load. If the load cell z-axis was significantly misaligned from the load arm, then the error and the nominal load would be proportional. Instead, the error is at or near the sum of the two load cell resolutions.

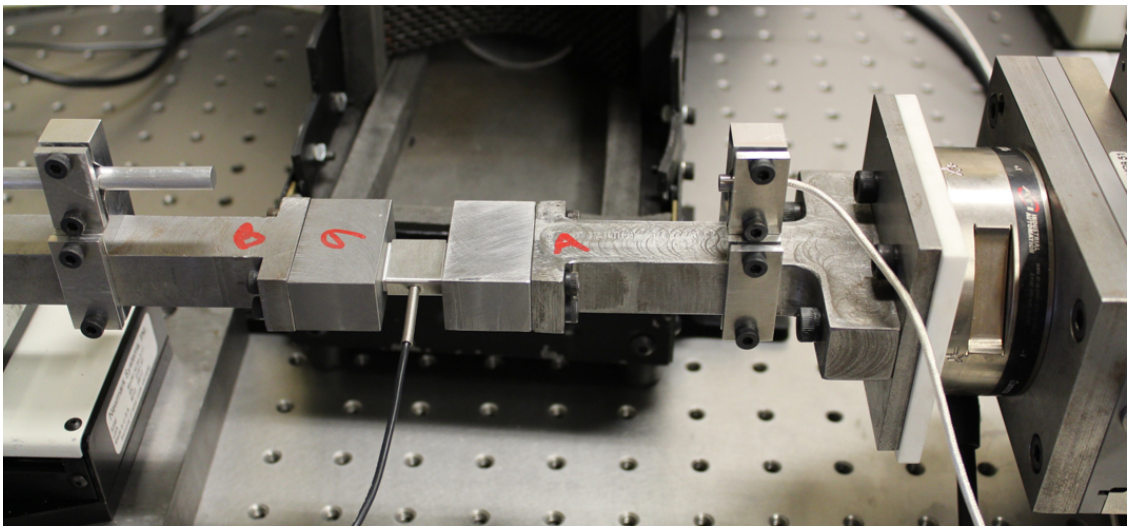

Figure 2.23. Procedure used to validate the load cell F_z reading against an auxiliary load cell.

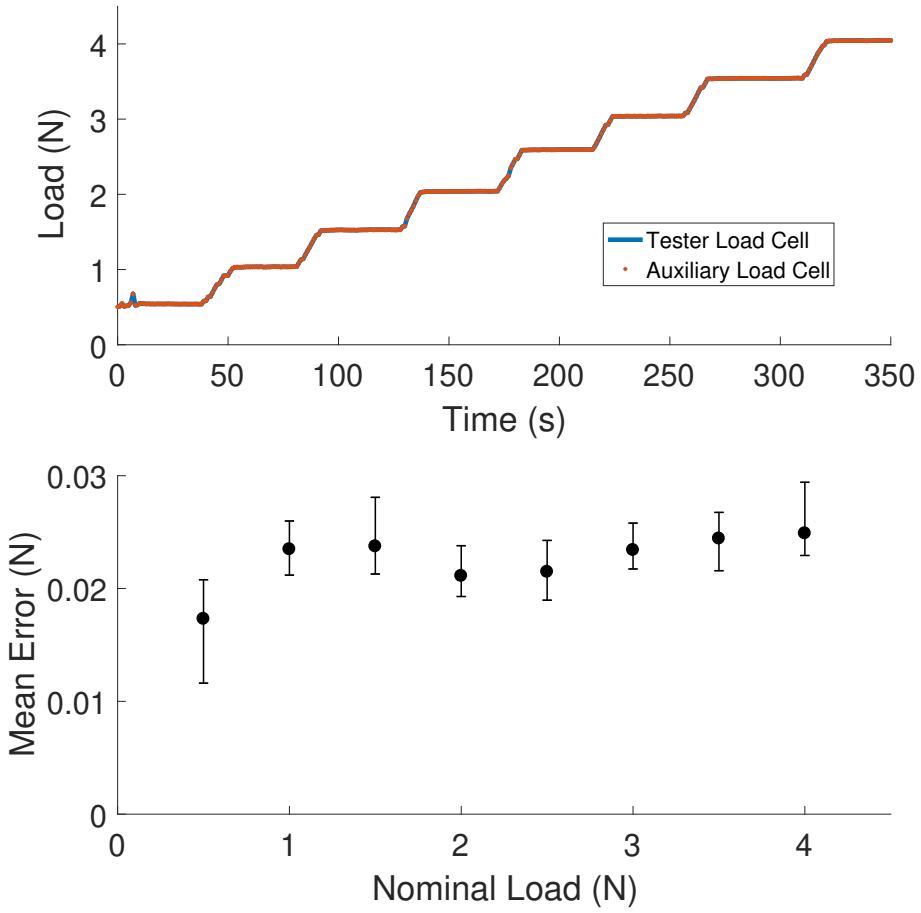

Figure 2.24. Raw data and the calculated absolute error of the sampled data.

The overall design of the micro-precision tester was verified by determining the elastic modulus from tensile testing and comparing to the accepted value. In this case, the materials were AISI 1010 steel, with a commonly accepted elastic modulus of 200 GPa, and UNS 6061 aluminum, with a modulus of 69 GPa. Rectangular samples were cut to a nominal 5 × 50 mm using a squaring shear, then measured individually using a micrometer with a 1 µm resolution. Both the thickness and width were measured, and parallelism of the sheared edges was checked. The dimensions were chosen so that the samples would have similar stiffness to the typical solder samples tested in the machine.

The procedure used during the tensile tests was as follows:

1. Align the faces of the clamping fixtures. See Figure 2.25.

2. Set the gauge length of the sample by jogging the stage until contact is made with a reference block. See Figure 2.26.

3. Fix the sample to the clamping fixtures. See Figure 2.27.

4. Load and unload the sample. Here, a trapezoidal profile was used, ramping between 20 and 180 N at 2 N/s, with a dwell of 20 s at 180 N. See Figure 2.28.

5. Perform a second load/unload cycle, as some slipping in the clamping fixtures was noticed during the first cycle.

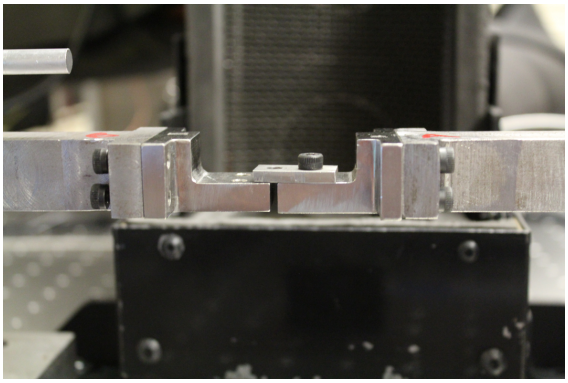

Figure 2.25. Procedure for alignment of the clamping fixture faces.

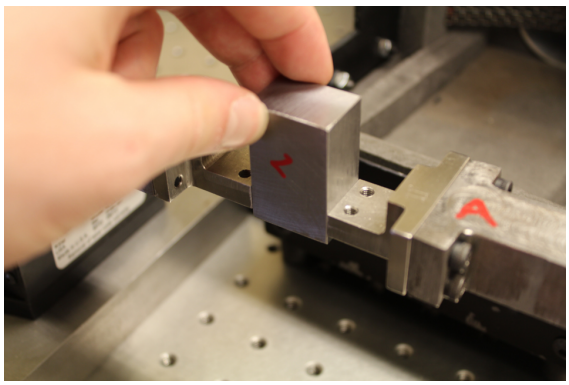

Figure 2.26. Procedure for setting the gauge length of the validation sample.

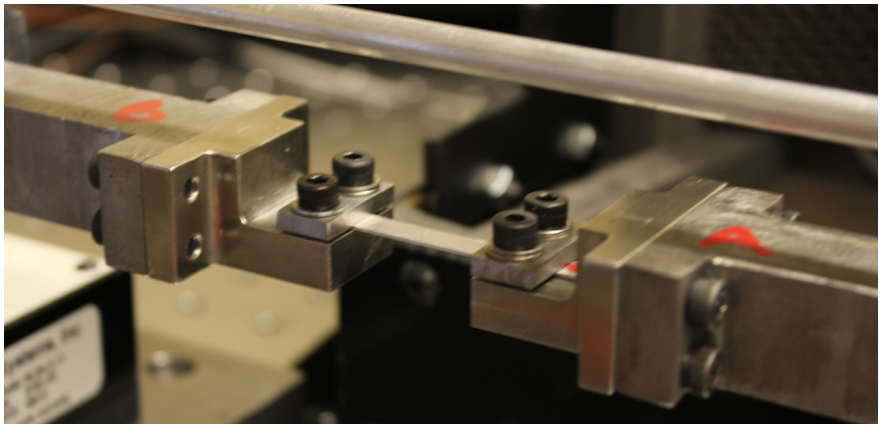

Figure 2.27. An aluminum validation sample clamped in place for tensile testing.

The elastic modulus was calculated as

$$E = \frac{\sigma}{\varepsilon} = \frac{F/A}{\Delta L/L_0} \tag{2.1}$$

where

E	elastic modulus
σ	stress
ε	strain
F	measured load along the z-axis
A	measured cross-section area
ΔL	measured displacement
L_0	gauge length

Here, ΔL was not computed as a difference of two measurements, but from the least-squares fit of all data between 50 and 150 N. In this manner, an average of many data points was taken, as opposed to only two data points, therefore increasing the statistical reliability of the measurement.

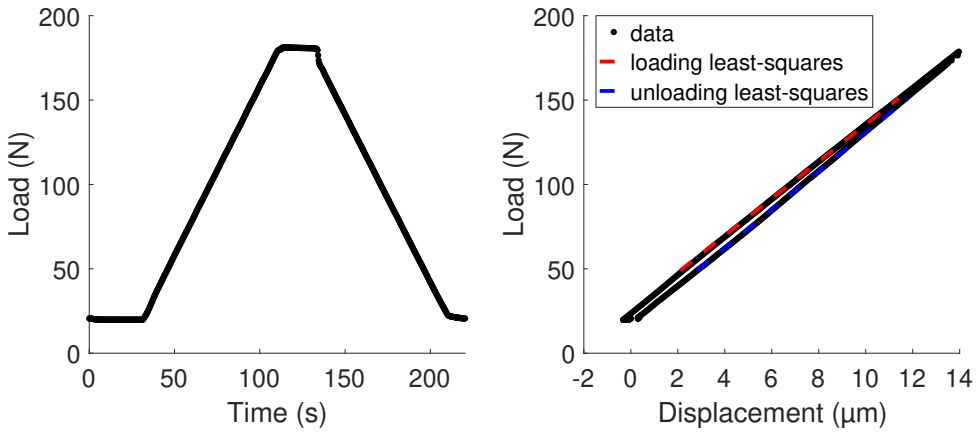

Figure 2.28. Applied load profile, measured load and displacement data, and least-square fits of the loading and unloading curves.

With this procedure, the elastic modulus was calculated for 5 steel samples and 5 aluminum samples. The error in comparison to the accepted value is shown for the steel samples

in Figure 2.29, and for the aluminum samples in Figure 2.30. The maximum error for steel was 7.5%, which occurred during the first loading cycle. The maximum error for aluminum was 15%, which also occurred during the first loading cycle. The error for the second loading cycle was consistently lower, which is likely due to the samples slipping in the clamping fixtures. Only looking at the second cycle, the mean absolute errors were 3.3% and 2.6% for steel and aluminum, respectively.

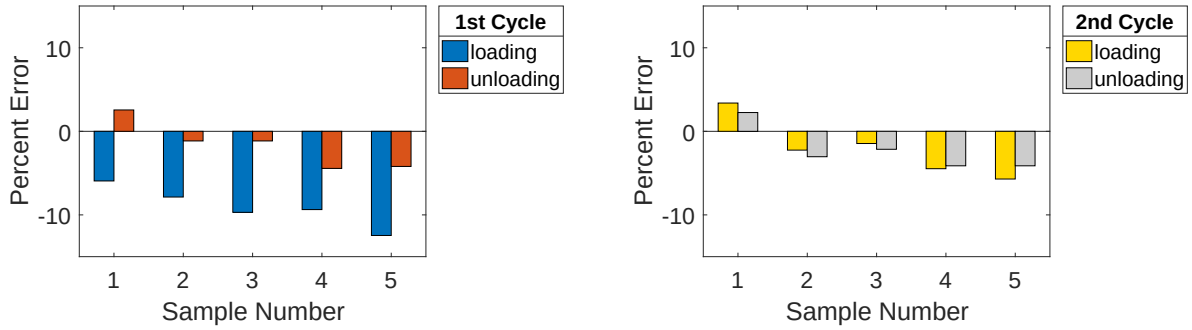

Figure 2.29. Error in the calculated elastic modulus of 5 steel samples, separated by loading cycle.

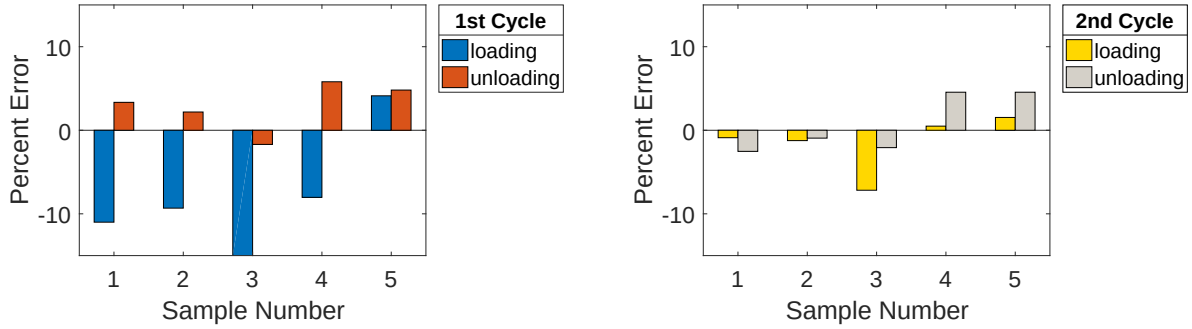

Figure 2.30. Error in the calculated elastic modulus of 5 aluminum samples, separated by loading cycle.

3. MECHANICAL BEHAVIOR OF LOW THEMPERATURE SOLDERS

The purpose of this chapter is to demonstrate the capabilities of the tester to mechanically evaluate solder compositions. The results of monotonic, creep, and fatigue tests are presented. In particular, improvements in control over the previous version of the tester are demonstrated.

3.1 Sample Preparation

The test samples consist of eight discrete solder joints sandwiched by two custom built substrates. The assembly process is as follows. First, the printed circuit boards are created. They are custom fabricated by a commercial vendor (Bay Area Circuits). The manufacturing process begins with large sheets of FR4 substrate, which is a glass fibre reinforced composite. A copper sheet is laminated to the FR4 substrate, then chemically etched to generate a grid of circular pads. The exposed copper pads are then plated with electroless nickel immersion gold (ENIG) or coated with organic solder preservative (OSP) to prevent the copper pads from oxidation and to ensure subsequent solderability. To confine the solder to the pad area, an organic solder mask is coated over board covering all the area but the solder pads. Finally, the fabricated boards are diced into coupons, resulting in the final printed circuit boards.

Next, two boards are soldered together to create a test sample. The assembly process begins by silk-screening a layer of solder flux onto a coupons. Then eight solder balls are placed onto their copper pads, and held in place by the tacky flux. The boards and solder are placed in an oven, which reflows the solder balls into semi-spherical solder bumps. Finally, the silk-screen, flux and reflow process is repeated with a second coupon to finish the assembly of the test sample.

After the samples are manufactured, they are stored at -10°C . This is to prevent microstructural changes within the solder.

3.2 Design of Experiments

Table 3.1 contains the list of experiments that were run in this study using the microscale tester that was described earlier in Chapter 2.

Table 3.1. Design of Experiments

Surface Finish	Aging Condition	Test Temperature	Solder Composition
ENIG	none	30°C	L27
			L29
			Sn58Bi
	10 days at 125°C		Sn57Bi1Ag
	none	75°C	L27
			L29
			Sn58Bi
	10 days at 125°C		Sn57Bi1Ag
OSP	none	30°C	L27
			L29
			Sn58Bi
	10 days at 125°C		Sn57Bi1Ag
	none	75°C	L27
			L29
			Sn58Bi
	10 days at 125°C		Sn57Bi1Ag

3.3 Extraction of Stress and Strain

Several assumptions were used to convert the load and displacement measurements captured during testing into usable data. The assumptions are as follows.

1. The measured displacement is wholly due to solder deformation, i.e. the tester arms and FR4 substrates are infinitely stiff in shear [6].
2. A uniform state of pure shear exists within the solder joints [7].
3. The stress and strain can be computed from the pad area and standoff height [9].
4. The von Mises distortion energy theory is applicable [9].

Note there is no assumption regarding the shear load F_z because the load cell reading has been validated. Therefore, the equivalent uniaxial tensile stress and strain within the solder joints is approximated as

$$\sigma = \sqrt{3}\frac{F_z}{A} \qquad \varepsilon = \frac{1}{\sqrt{3}}\frac{\Delta z}{h} \tag{3.1}$$

where

σ	equivalent engineering stress
F_z	measured shear load
A	total pad area
ε	equivalent engineering strain
Δz	measured shear displacement
h	standoff height

3.4 Results of Monotonic Testing

A total of 32 monotonic tests were performed, not including unsuccessful tests. All tests were performed with a displacement rate of 0.2 µm/s, equivalent to a strain rate of 7.7×10^{-4} s^{-1}. The variable parameters were composition, aging condition, pad surface finish, and test temperature.

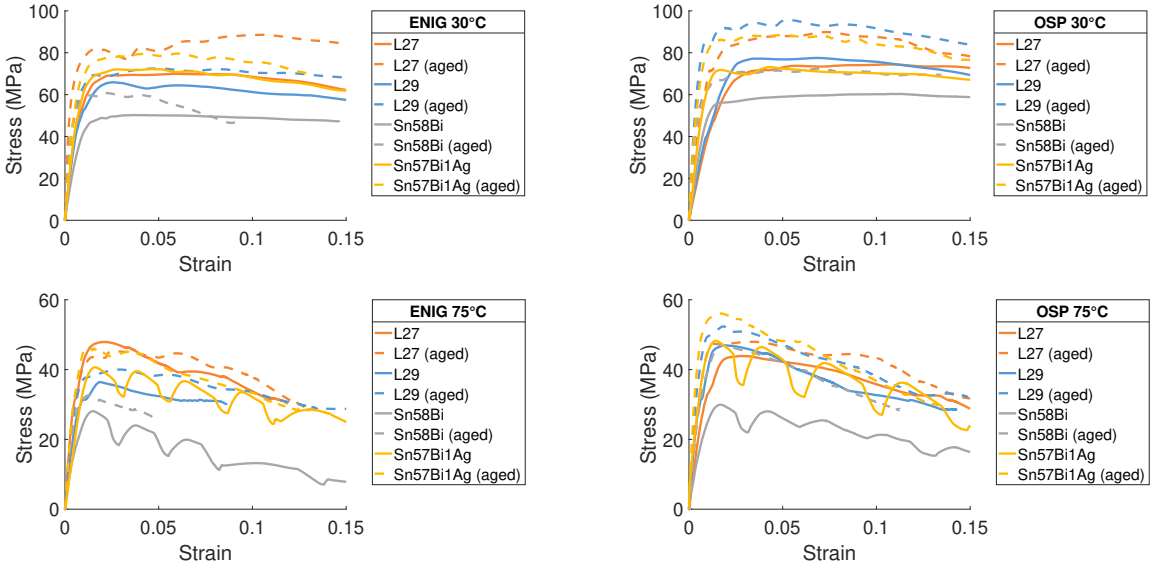

Figure 3.1. Stress-strain data extracted from monotonic testing at a strain rate of 7.7×10^{-4} s^{-1}.

Note that the SnBi samples display unexpected behavior at high temperature. Rather than a smooth curve, the SnBi and SnBiAg stress-strain responses show multiple sharp reversals. This is possibly due to the sample failing joint by joint. In order to test this hypothesis, three SnBi samples from the same batch were re-tested, and all displayed the same stress-strain response (see Figure 3.2). While this is not conclusive, it suggests that the issue may lie within the sample, not the testing methodology.

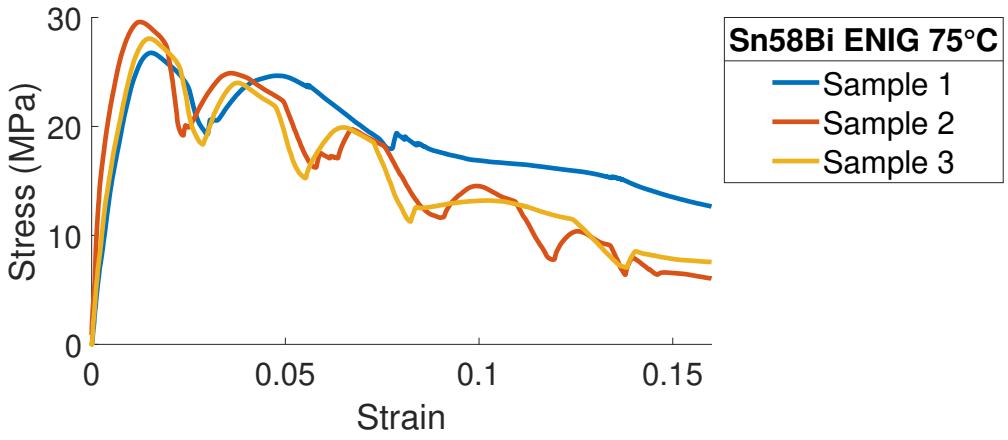

Figure 3.2. Three retests of Sn58Bi samples demonstrating consistency of test results.

The data in this section benefits from the improved sampling rate discussed in Section 2.2.3. The faster sampling rate allows for improved control of the test velocity. This is demonstrated in Figure 3.3, where a retest of one monotonic test performed on the previous tester is compared to a test on the current tester. All test and sample parameters were identical. The previous tester took over 150 seconds to reach a steady state velocity, while the current tester takes around 20 seconds. This is clearly visible in the stress-strain curves in the lower initial slope.

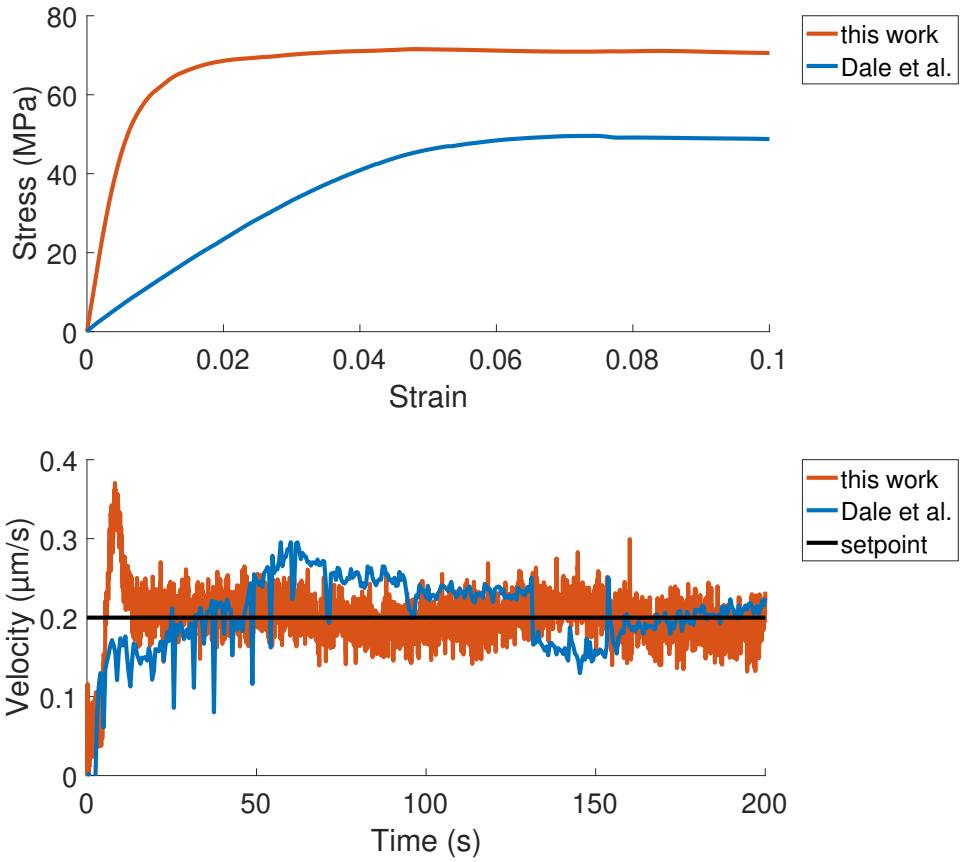

Figure 3.3. Demonstration of improvement in velocity control.

3.5 Results of Creep Testing

A total of 32 creep tests were performed, not including unsuccessful tests. All tests were performed at a load of 50 N, equivalent to a stress of 25.9 MPa. Just as with the monotonic tests, the variable parameters were composition, aging condition, pad surface finish, and test temperature.

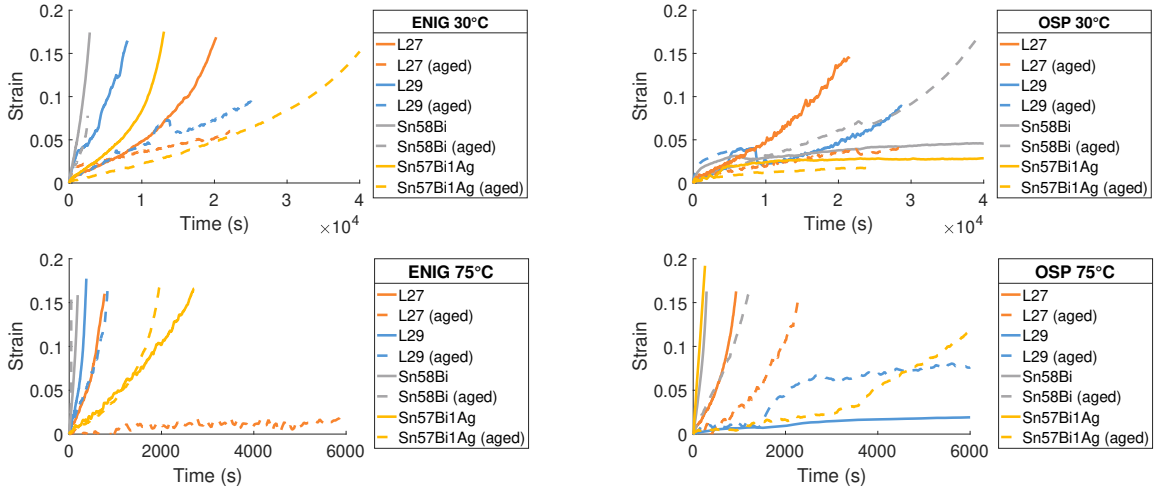

Figure 3.4. Strain data extracted from creep testing at with 25.9 MPa load.

Just as with the monotonic data, the creep data also benefits from an improvement in control. Figure 3.5 shows a representative portion of a creep test, and the ability of the previous and current testers to maintain a constant load. The previous tester could maintain a constant load to within ±0.5 N, while the current tester is within ±0.1 N. This improvement is strictly due to the increase in sampling rate, as no other parameters were changed.

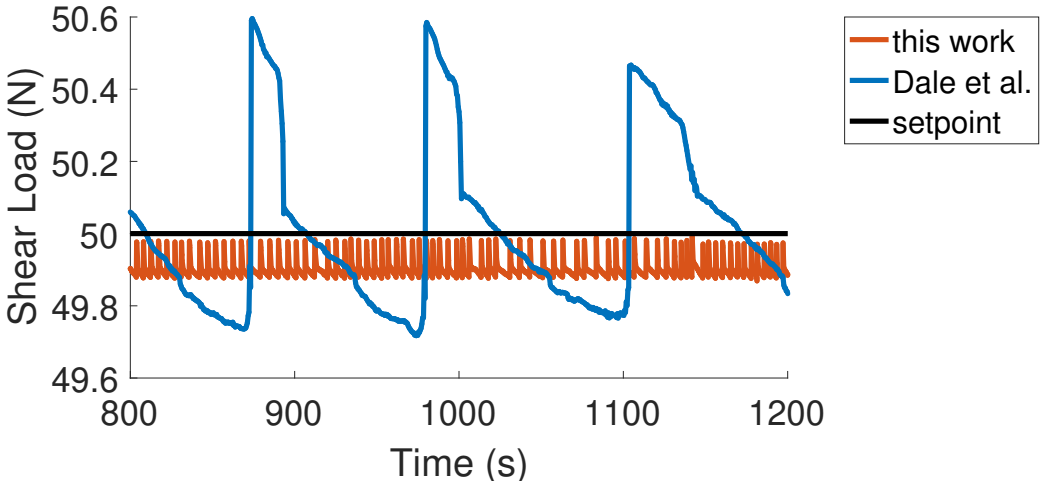

Figure 3.5. Improvement in load control.

3.6 Results of Fatigue Testing

A total of 32 fatigue tests were also performed, not including unsuccessful tests. A trapezoidal displacement profile was used, with a rate of 0.2 µm/s (7.7×10^{-4} s^{-1}), a total displacement of 39 µm (15% strain), and a dwell of 200 s (see Figure 3.6). This profile emulates the strain profile placed on field solder joints by thermal cycling. This profile was repeated until failure, which can take anywhere from an hour to several days. As before, the variable parameters were composition, aging condition, pad surface finish, and test temperature.

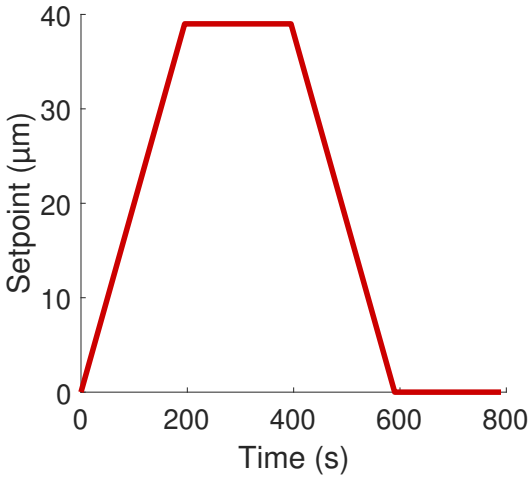

Figure 3.6. Trapezoidal fatigue profile. One full cycle shown.

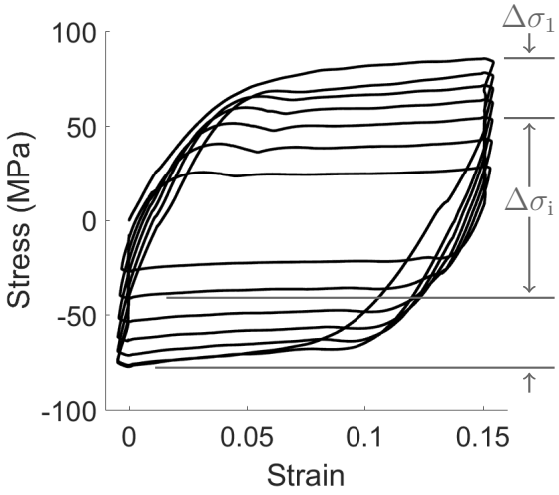

Figure 3.7. Determining damage from fatigue data.

The post processing of the fatigue tests is different from that of monotonic or creep tests. For fatigue tests, first the stress-strain curves are determined, which exhibit a hysteresis loop as seen in Figure 3.7. Cumulative damage is then calculated from the stress amplitude drop, a method presented by Lemaitre [15].

$$D_i = 1 - \frac{\Delta\sigma_i}{\Delta\sigma_1} \tag{3.2}$$

where

D_i cumulative damage of the ith cycle

$\Delta\sigma_i$ the range of stress in the ith cycle

$\Delta\sigma_1$ the range of stress in the 1st cycle

The data presented in Figure 3.8 is the number of cycles for the damage to reach 50%, denoted as N_{50}.

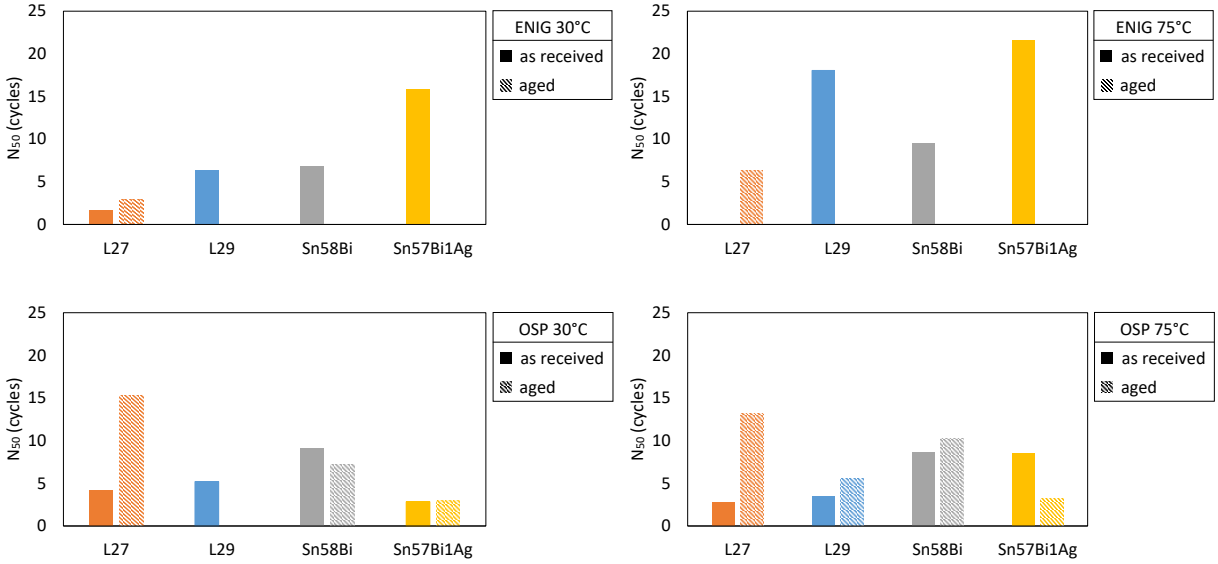

Figure 3.8. N_{50} data extracted from fatigue testing.

Additionally, a small number of tests were performed with a reduced displacement of 13µm (5% strain). The dwell duration did not change. Only 2 compositions and 2 test temperatures were tested, in order for a quick comparison with the primary/other data.

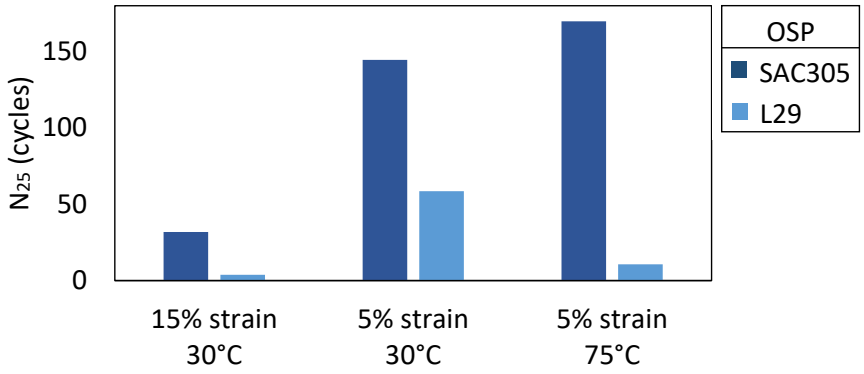

Figure 3.9. Comparison of fatigue life for 5% and 15% strain cycles.

4. THE NANO-PRECISION MECHANICAL TESTER

The primary motivation to design a new mechanical tester was to improve control performance, especially on smaller sample geometries. As solder joint geometry shrinks, the need for accuracy increases.

For example, take the micro-precision mechanical tester's NLS4 actuator. It is powered by a 1.8° stepper motor coupled to a 1/16" pitch leadscrew. The minimum step size is 1 microstep. At 250 microsteps per step, this is equivalent to

$$(1 \text{ microstep}) \left(\frac{1 \text{ step}}{250 \text{ microsteps}} \right) \left(\frac{1.8^\circ}{1 \text{ step}} \right) \left(\frac{1 \text{ rev}}{360^\circ} \right) \left(\frac{1/16"}{1 \text{ rev}} \right) f \left(\frac{25400 \text{ µm}}{1"} \right) = 0.032 \text{ µm}$$

Ideally, this is the lower limit of control. However, this is not an ideal scenario and losses are present in the tester. As noted in section 2.1.2, the actuator displays between 6 and 8 µm of backlash, which is difficult to fully compensate. The load train compliance causes additional deformation that is proportional to load, and not displacement. Specifically, the load train compliance is at least 56 nm/N, the nominal compliance of the load cell. With these non-ideal additions, the practical limit of control is an order of magnitude larger, approximately 0.1 µm.

To put this number in context, convert it to strain on the sample. A displacement of 0.1 µm is equivalent to 0.04% strain on a joint with a standoff height of 150 µm. For smaller geometries, such as a microbump sample with a standoff height of 10 µm, the same 0.1 µm is equivalent to 6% strain. This is an unacceptably large error.

4.1 Design

The design of the nano-precision tester is conceptually identical to that of the micro-precision tester. The primary use of the nano-precision tester is to test solder samples in shear, just like its larger cousin. The components that make up the tester perform the same functions, although the specifications differ. These components are discussed in the following sections, with emphasis on the improvements they bring.

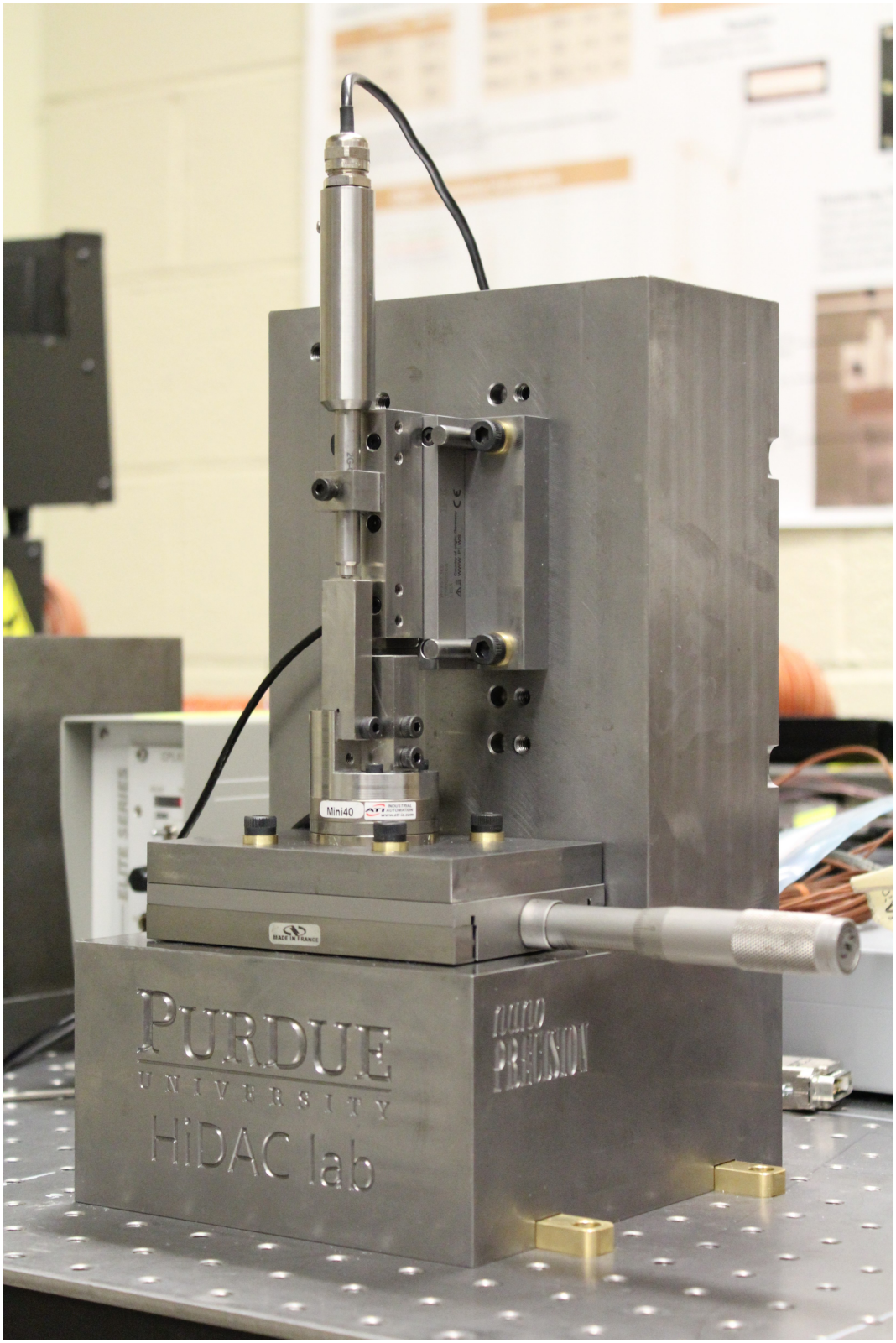

Figure 4.1. Image of the nano-precision mechanical tester. In the background, the drivers for the capacitance sensor and actuator are visible.

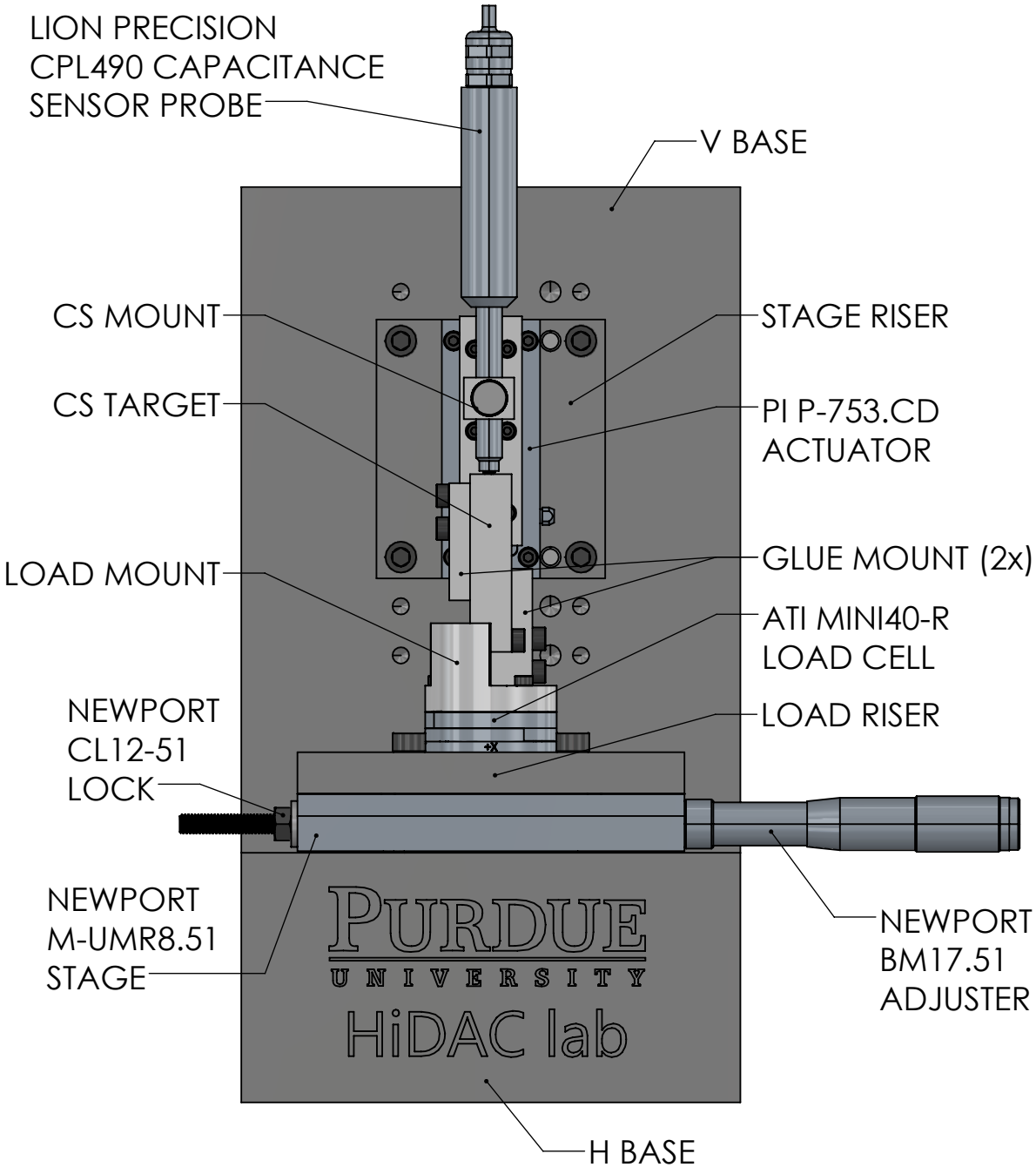

Figure 4.2. Technical drawing of the micro-precision mechanical tester. Purchased components are marked by manufacturer and name. The remaining components are custom machined.

4.1.1 Sample and Workholding

The nano-precision tester is primarily designed for test assemblies of up to 12×12×4 mm. This includes the custom built coupons used in the micro-precision tester (Figure 2.3). The samples are secured to removable glue fixtures with adhesive, similar to the setup used in the micro-precision tester. However, one key difference is the addition of grooves to allow for adhesive overflow. This reduces the chance for glue to flow inside the solder joint while still maintaining surface area for sufficient adhesion. This is particularly helpful for samples with less height, which are more likely to be glued shut. Additionally, the new fixtures have all critical features on one side, improving manufacturability.

It is possible to both test other geometries and other loading conditions, but a new method of workholding would need to be designed and manufactured.

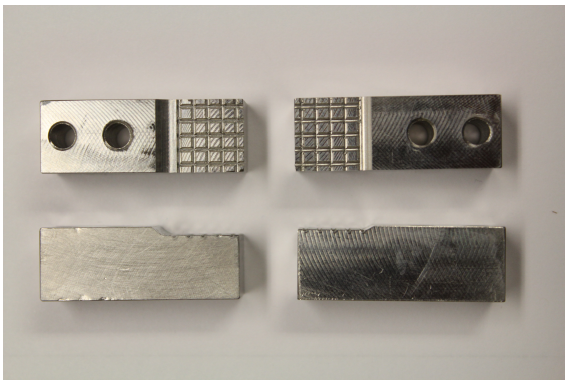

Figure 4.3. Two sizes of glue fixtures for use in the nano-precision tester.

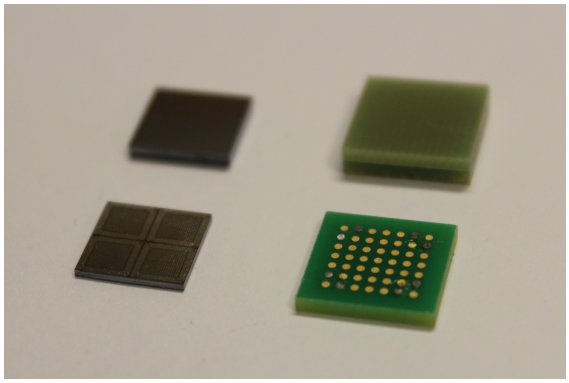

Figure 4.4. Two examples of solder assemblies used for testing with the nano-precision tester.

4.1.2 Actuator

Actuation for the nano-precision tester is provided by a P-753.3CD linear stage from Physik Instrumente. The stage is a piezo-actuator with an integrated capacitance sensor for closed loop control. Commands are sent to the controller, which then regulates the voltage at the piezo-stack until the internal capacitance sensor confirms the command has been completed. The actuator has a displacement range of 40 µm, a push capacity of 100 N, and

a pull capacity of -20 N. Because the load cell and external capacitance sensor have greater ranges than the actuator, these specifications are also the capacity of the tester.

Due to the asymmetrical load capacity, the orientation of the actuator is relevant. The orientation of the actuator was chosen so that the push direction results in tension within the load train. Uni-directional tests are performed in the push direction, fully utilizing the load capacity of the actuator. This minimizes the possibility of compressive loads producing lateral displacements and therefore off-axis loads.

The piezo-actuator does not use the same motion or bearing system as the NLS4 used in the micro-precision tester. The NLS4 converts rotation into rectilinear motion through the use of a leadscrew and linear bearings. In contrast, the piezo-actuator does not need a screw because the piezo-stack directly produces linear motion. Flexure elements constrain this motion to a straight line and also serve to absorb off-axis loads. These two changes eliminate both backlash and friction, which produces a higher precision actuation system. The effective limit on the resolution of a piezo-actuator is the precision of the voltage source used to drive the piezo-stack.

4.1.3 Load and Displacement Measurement

Load is measured by an ATI Mini40 6-axis load cell, a smaller cousin of the ATI Gamma used on the micro-precision tester. The shear load on the sample is measured by the z-axis with a resolution of 0.02 N. The x- and y-axes measure off-axis loads with a resolution of 0.01 N.

A Lion Precision CPL490 capacitance sensor system is used to measure the displacement at the sample. The sensor is similar to the CPL190 system used in the micro-precision tester, with additional electronics designed to improve the measurement resolution. The CPL490 has a resolution of 0.15 nm.

As with the micro-precision tester, the capacitance sensor is mounted as close to the sample as possible to minimize measurement of load train compliance. Most significantly, the compliance from the load cell is accounted for. The Mini40 load cell has a nominal

compliance of 50 nm/N in the z-axis. At the actuator's maximum rated load of 100 N, the load cell displacement will be 5 µm, equal to 12% of the actuator range.

4.1.4 Data Acquisition and Control

The control software for the nano-precision tester is functionally identical to the micro-precision tester software. A LabVIEW program based on the producer-consumer architecture samples data, runs a closed-loop control algorithm, and records data to file. See Section 2.1.5. The most significant difference is the subroutines used to communicate with the actuator.

The data acquisition rate is set to a nominal 25 Hz. The actual rate was recorded over a 5 minute duration, with a mean observed rate of 110 Hz and a minimum of 52 Hz. If not artificially limited, the data acquisition rate would fluctuate between 50 and 100 Hz. In order to ensure a consistent rate, the rate was artificially limited to 25 Hz.

For high speed tests, the artificial rate limiting is removed in order to sample as much data as possible. As an example, note that a 20 µm/s monotonic test would reach the stage travel limit in only 2 seconds. The conservative 25 Hz data acquisition rate would acquire 50 data points for this test. Removing the rate limitation would record approximately 200 data points.

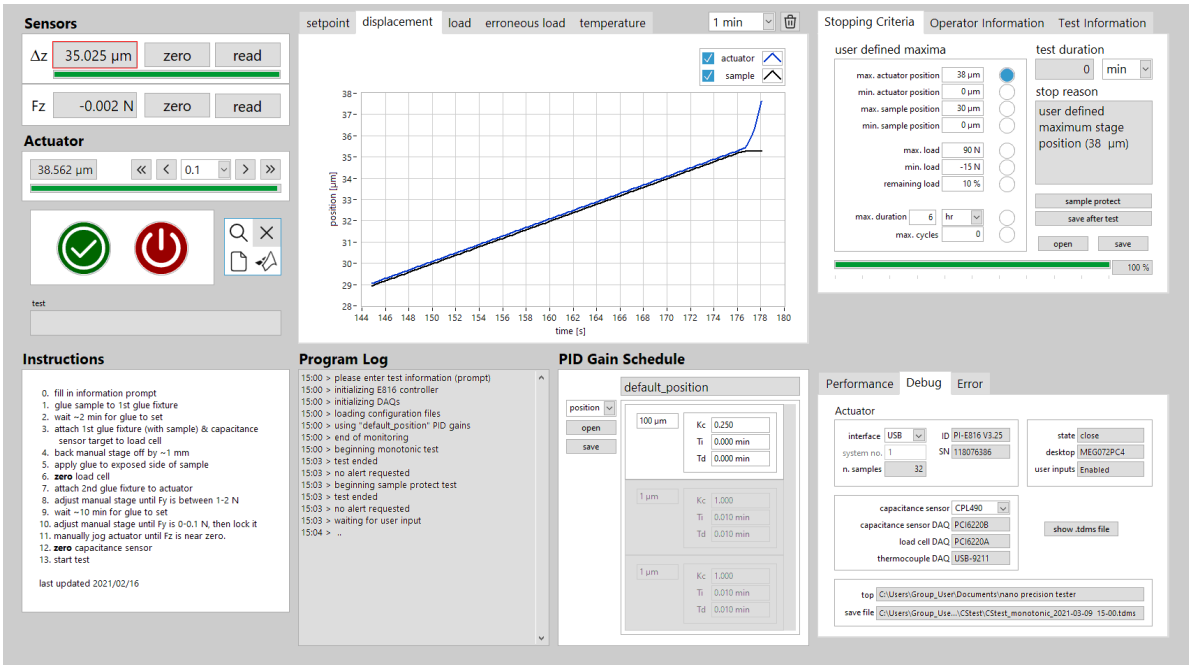

Figure 4.5. The nano-precision tester LabVIEW control program.

4.1.5 Other Considerations

Just as in the micro-precision tester, efforts were made to maximize the tester stiffness. This includes the use of a substantially large load frame, as well as significantly shortening the overall distance between the actuator and load cell. To minimize off-axis loading, the glue fixtures are offset so that the sample is located on the common centerline of the load cell and actuator. The tester is installed on the same vibration isolating table as the micro-precision tester.

4.2 Manufacturing

The nano-precision tester was manufactured in-house, at Purdue's Bechtel Innovation and Design Center. At minimum, each manufactured part required milling to size as well as clearance or tapped holes for bolts. Additionally, many parts required reamed holes for alignment pins and lapping to meet surface roughness and flatness requirements. The load mount is shown in Figure 4.6 as a representative part. On the left, the technical drawing of the part. On the right, the part clamped in a vise during manufacturing. At this point

in the manufacturing process, the upper surfaces are milled to size, but clearance holes for bolts are still required, and the bottom surface has yet to be milled to size and lapped for flatness.

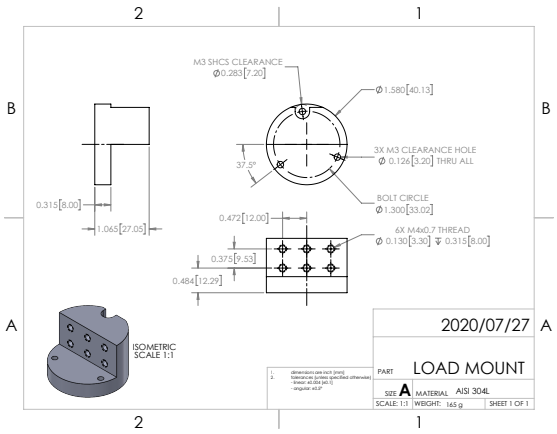

(a) technical drawing

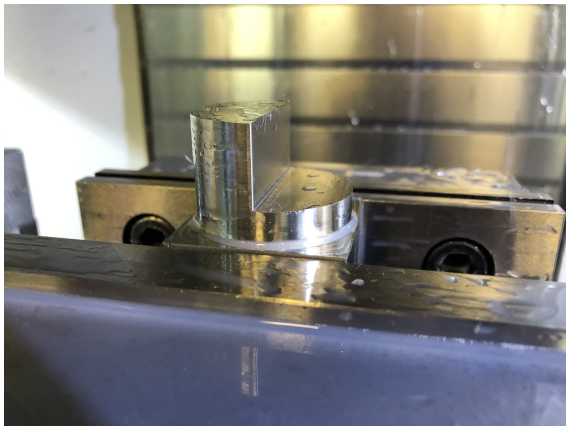

(b) manufacturing process

Figure 4.6. Technical drawing and manufacturing process of the load mount.

4.3 Assembly and Alignment

This section presents the procedure used to assemble and align the components of the tester. Just as with the micro-precision tester, the motivation of this procedure is to account for manufacturing tolerances. Note this is not the definitive method, only the method most convenient with the tools at hand.

First, all parts are thoroughly cleaned. This is perhaps the single most important step of assembly. Stray chips from machining will prevent proper alignment and oil and abrasive grit from manufacturing may degrade the tester. Next, all portions of the tester made of carbon steel are coated in rust-preventative. Throughout the assembly process, care is taken to torque all bolts equally, using a torque wrench.

The majority of alignment is ensured by manufacturing techniques or dowel pins. However, some off-the-shelf items do not have alignment features, namely the manual and piezo stages.

The alignment of the piezo-stage to the upper glue fixture was accomplished using a measurement device and a datum reference. A dial-test indicator with 1 µm resolution

serves as the measurement device and a spare linear stage as the reference datum. The accuracy of the linear stage was verified, as shown in Figure 4.7. Both the indicator and stage were fixed to the table, and the stage was moved while observing the indicator. There was a maximum of 6 µm deviation measured over 50 mm, which equates to 0.0069°. This meets manufacturer specifications.

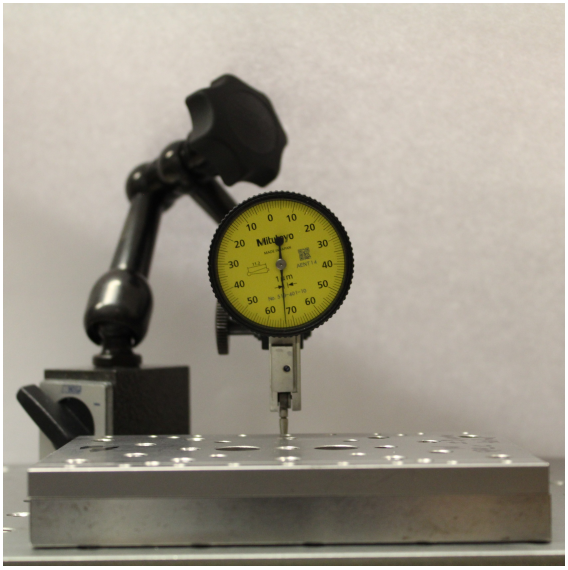

Figure 4.7. Determining the linearity of the manual linear stage.

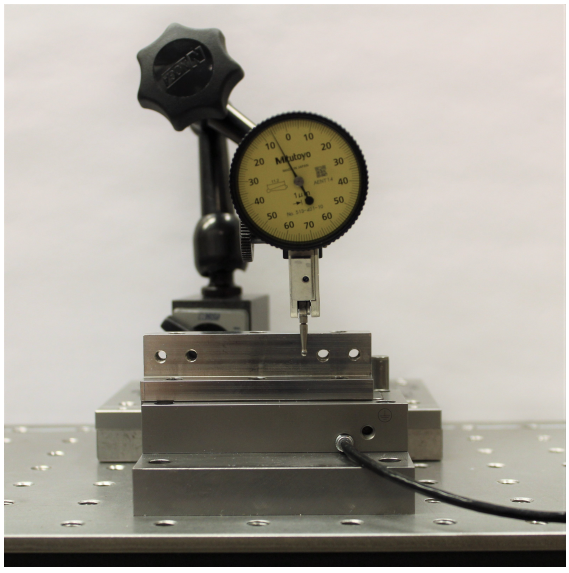

Figure 4.8. Alignment of the fixture with the axis of the piezo-actuator.

Next, the piezo-actuator was aligned with the datum. This was done by attaching the indicator to the manual stage and sweeping the edge of piezo-actuator, which is assumed to be parallel with the axis of motion. The piezo-actuator was gently tapped until sufficiently aligned. There was a maximum of 5 µm deviation measured over 30 mm, which equates to 0.0095°.

Using the same methods, the stage mount was aligned with the datum, and therefore the piezo-actuator. There was a maximum of 5 µm deviation over 30 mm, which equates to 0.0095°of angular deviation. Therefore, the total misalignment measured over a range of 30 mm of travel is less than 0.019°. For context, the piezo-actuator has a range of 40 µm, therefore, the maximum observable deviation over the entire travel would be 15 nm. At this point, the piezo-actuator sub-assembly is installed on the tester base.

Next, the load cell z-axis was aligned to the motion of the actuator so that the shear load is correctly resolved. To do this, first the indicator was mounted on the load cell riser plate and used to sweep the top face of the actuator (Figure 4.9). A misalignment of 12 µm over 16 mm was measured. An attempt was made to correct this error by shimming between the manual stage and the load riser. However, the smallest available shim was still too thick, and over-corrected the misalignment (almost exactly). Therefore, no shim was used, and the final misalignment remains the same as originally measured, 0.043°. Should this misalignment prove unacceptable, one possible solution is to manufacture a custom shim by sanding down an off-the-shelf shim.

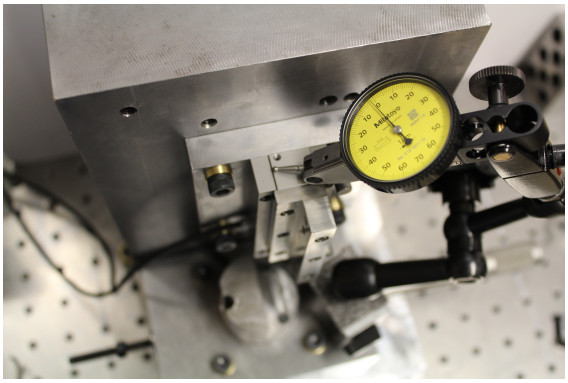

Figure 4.9. Measuring the misalignment between the load riser and the actuator.

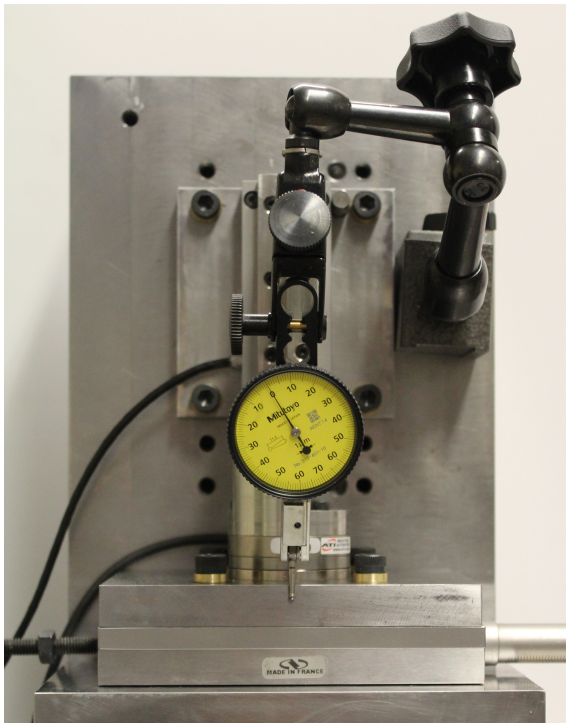

Figure 4.10. Measuring the misalignment between the load riser and the manual stage.

Using the same methods as described previously, the load riser was aligned to the motion of the manual stage. The final misalignment was less than 2 µm over 30 mm. Note that the load cell is aligned to the load riser by the use of locating dowel pins. The purpose of this

procedure is to align the y-axis of the load cell to the motion of the manual stage, so that the compressive/tensile load on the sample is correctly resolved.

Finally, the load mount was aligned to the piezo-actuator. This is accomplished by aligning the two components with a straight-edge, then torquing the bolts securing the load mount while maintaining the alignment with hand-pressure. This procedure ensures the sample is held between parallel surfaces.

5. CAPABILITIES OF THE NANO-PRECISION TESTER

The purpose of this chapter is to demonstrate the capabilities of the nano-precision mechanical tester, especially in comparison to the micro-precision tester. To quantify the tester's capabilities, tests were run on the custom squat-joint samples designed for the micro-precision tester. Monotonic, creep, and fatigue tests were performed with the same range of parameters usually used on the micro-precision tester. The stress and strain reported are calculated in the same manner as in section 3.3.

5.1 Monotonic Capabilities

Preliminary tests were performed on SAC305 samples in order to evaluate the strain rate capabilities of the nano-precision tester. Displacement rates of 0.02 µm/s to 20 µm/s were tested, equivalent to strain rates of 7.7×10^{-5} s^{-1} to 7.7×10^{-2} s^{-1}. The results of this exercise can be seen in Figure 5.1. The relative error between the measured and desired velocities is used to quantify the capabilities of the tester to control velocity.

$$v_i = \frac{z_i - z_{i-1}}{t_i - t_{i-1}} \qquad \mathrm{RE}_i = \frac{v_i - s}{s} \qquad \mathrm{RT}_i = \frac{t_i}{t_n} \qquad 1 \leq i \leq n \tag{5.1}$$

v_i	backward difference velocity of the i^{th} sample
s	setpoint velocity
RE_i	relative error of the velocity
RT_i	relative time

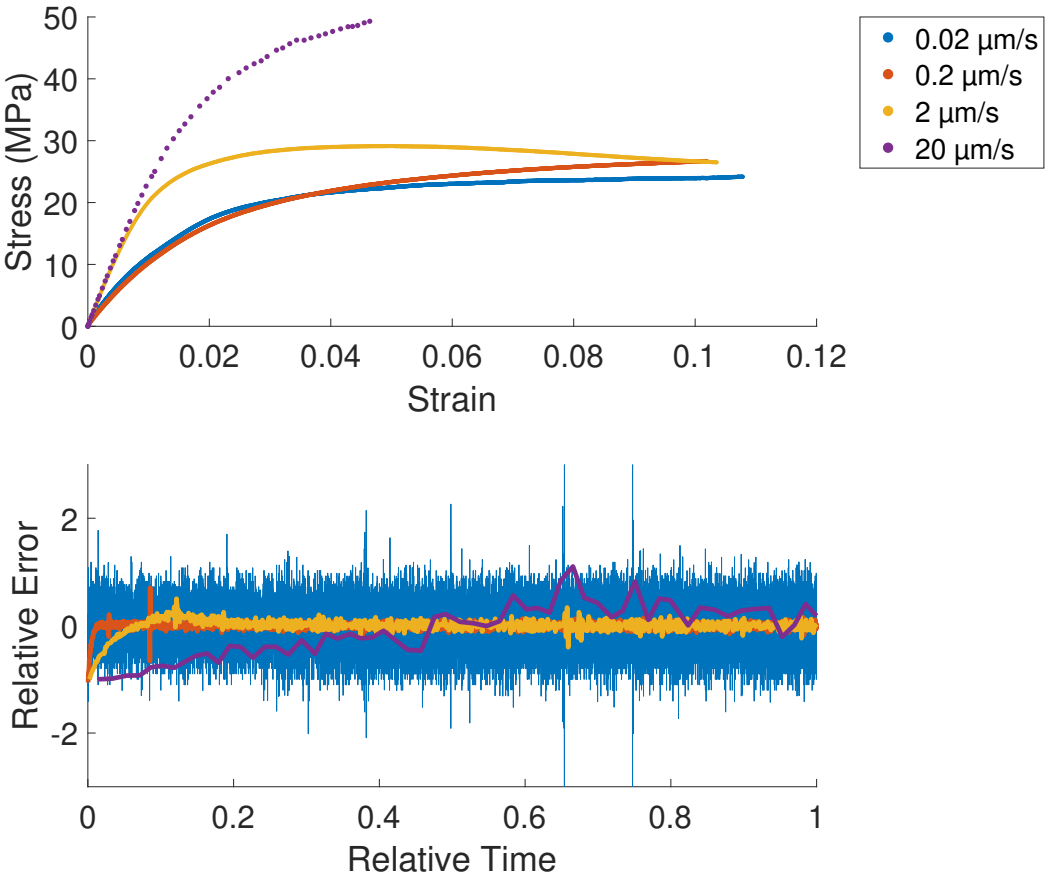

Figure 5.1. Results of monotonic tests

The upper plot shows the stress-strain curves extracted from the monotonic tests. The bottom plot shows the relative error in following the setpoint velocity, according to equation (5.1). The axes of this plot are normalized so that all tests fit in the same plot.

The relative error plot indicates that the 0.02-2 µm/s tests maintain the correct average velocity. However, the 20 µm/s test does not reach steady state before the test is over, but that can perhaps be improved with PID tuning.

The 0.02 µm/s test shows a large variability in displacement rate, as high as 250% relative error. This indicates that 0.02 µm/s is near the lower limit of the capability of the nano-precision tester. This is still an improvement over the micro-precision tester, which cannot reliably maintain a 0.02 µm/s velocity.

The most consistent tests were the 0.2 and 2 µm/s tests, which were usually within 15% relative error. These tests show significant improvement over the micro-precision tester, both in precision and range of strain rates. The nano-precision tester reaches a steady-state velocity faster, with less overshoot, and with less steady state variability than the micro-precision tester.

5.2 Creep Capabilities

Two tests were performed on SAC305 samples to evaluate the nano-precision tester capability for creep tests. Shear loads of 25 and 50 N were tested, equivalent to a uniaxial tensile load of 12.9 and 25.9 MPa. The error between the setpoint load and the load cell reading is used to quantify the load control capability of the tester.

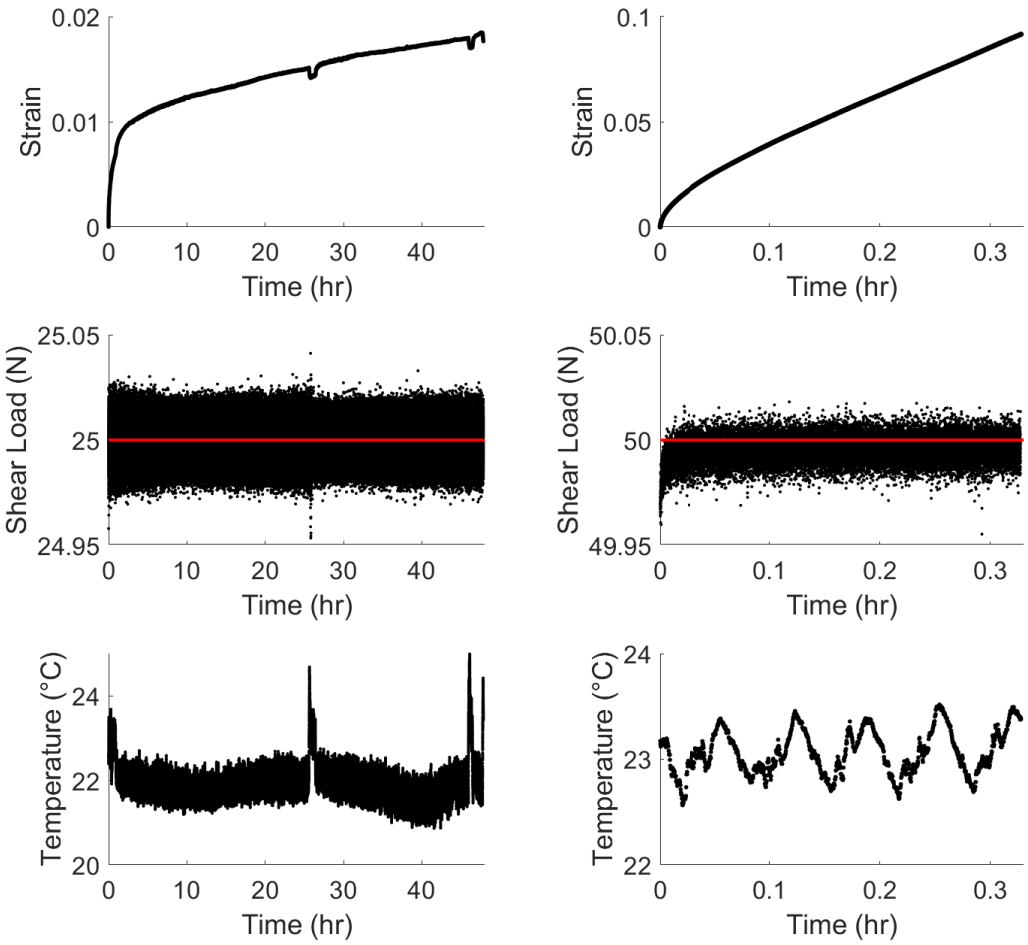

Figure 5.2. Creep test data. The 25 N test (left), and the 50 N test (right).

Table 5.1. Mean, standard deviation, and range of the error during the creep tests.

Setpoint (N)	Mean	SD	Range
25	25.0000	0.0054	0.1899
50	49.9966	0.0058	0.0628

Based on the standard deviation, the nano-precision tester is capable of maintaining a desired load with variation less than the resolution of the load cell. If this is true, the resolution of the load cell is the limiting factor, not the actuator.

5.3 Fatigue Capabilities

To evaluate the nano-precision tester's capability for fatigue tests, a trapezoidal displacement profile was run. The profile was similar to those typically run on the micro-precision tester, but scaled down to a total displacement of 10 µm. The results of this exercise are presented in Figure 5.3 below.

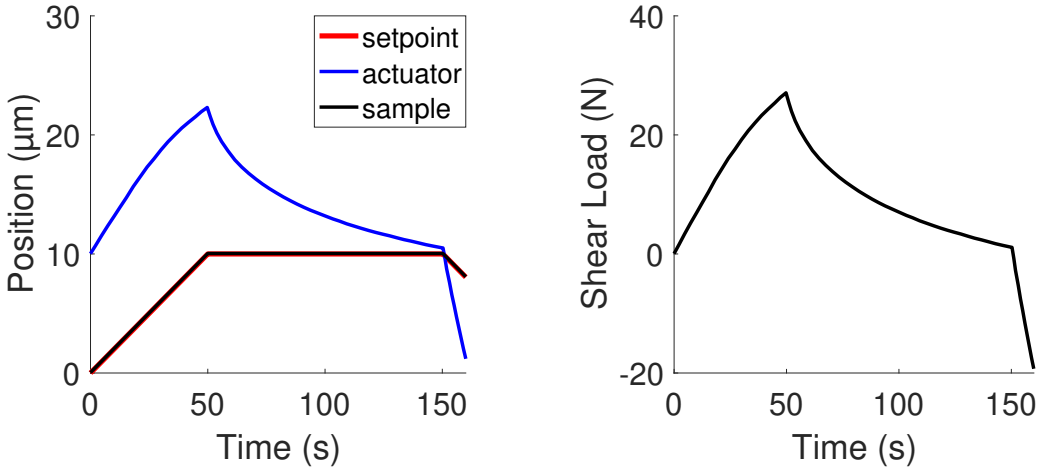

Figure 5.3. A displacement controlled fatigue test with a trapezoidal profile.

On the left, the setpoint, the actuator's internal capacitance sensor, and the sample position measured by the external capacitance sensor are plotted versus time. On the right, the resulting shear load measured by the load cell is plotted versus time. From the position plot it is clear the nano-precision tester has no issues following the trapezoidal profile. In fact, it is difficult to distinguish the capacitance sensor measurements from the setpoint. Additionally, the actuator was positioned at 10 µm at the start of the test and did not exceed its positional capabilities. However, from observing the load plot, the test ended due to exceeding the actuator pull capacity of -20 N.

Due to limitations of its actuator, the nano-precision tester is not as capable as the micro-precision tester at fatigue tests. The creep behavior of solder results in a large reverse shear required, which the piezo-actuator cannot apply. Since the piezo-actuator is limited to a pull force of only -20 N, the tester can only perform such displacement profiles on relatively compliant solder samples.

Because the actuator exceeds its load capacity while following a displacement profile, the logical solution is a load profile. A triangular load profile cycling between 0 and 20 N was used, with a cycle duration of 10 seconds. The test was run for just over 4 days, or 36000 cycles. The strain over time, as well as a representative cycle are plotted in Figure 5.4.

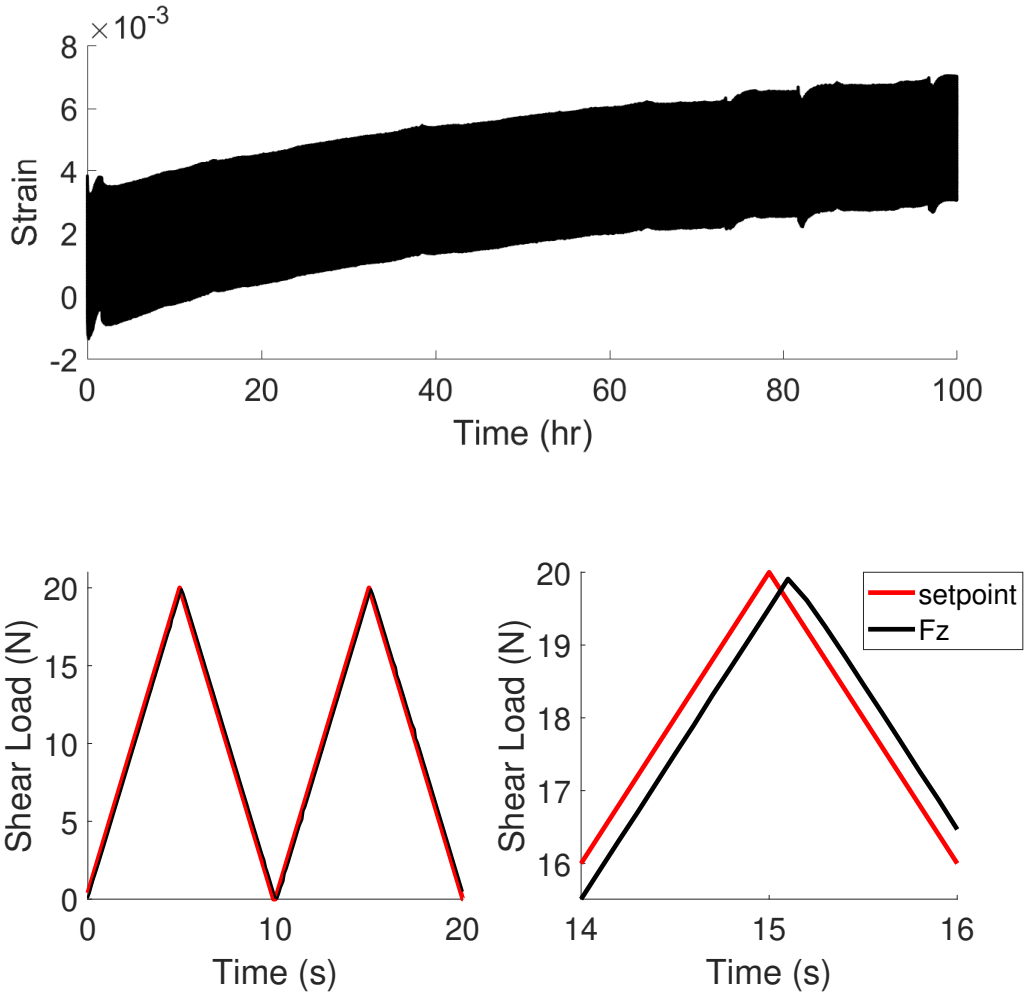

Figure 5.4. A load controlled fatigue test with a triangular profile.

Again, the error between the setpoint and the load cell reading is used to evaluate the tester's capability for this type of test. Because this is a cyclic test, the error has a bimodal distribution and the mean error is near zero. Therefore, the mean absolute error will be used to evaluate the testers capabilities instead of the mean error.

The mean absolute error during this test is 0.47 N, which is not insignificant. However, note that the value of F_z lags behind the setpoint. This is due to the use of strictly propor-

tional control. Shifting the setpoint data by 1 sampling period gives a mean absolute error of 0.073 N, and a standard deviation of 0.010 N. It should be noted that PID tuning efforts were minimal, representing room for improvement.

Up until this point, the profiles evaluated have been piecewise linear, and do not fully demonstrate the capabilities of the tester. It is common in fatigue analyses to approximate complex load profiles as sinusoidal curves [16]. Therefore, the capacity for the nano-precision tester to apply a sinusoidal profile was evaluated. Specifically, a sinusoidal profile with a period of 10 seconds, and a range of 0 to 20 N was used. The test was left to run for 1000 cycles.

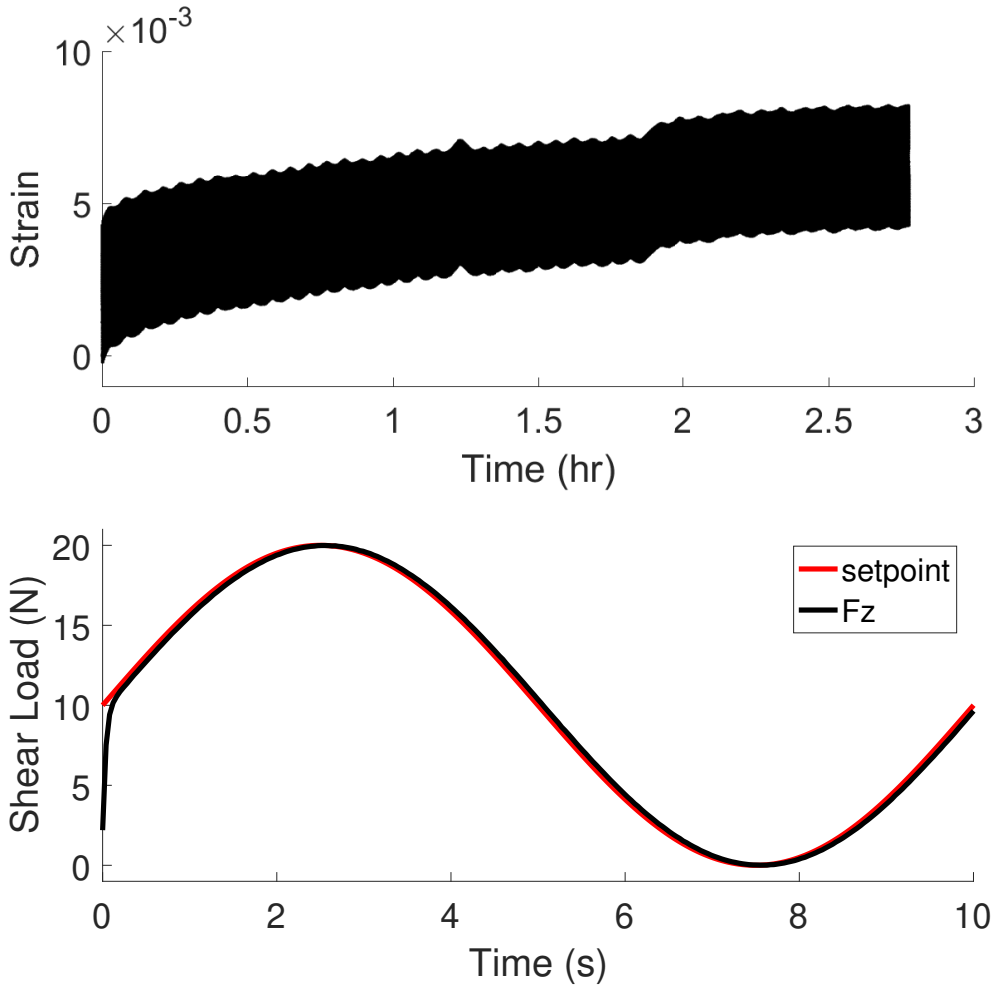

Figure 5.5. A load controlled fatigue test with a sinusoidal profile.

The strain data captured during this test as well as the first load cycle are plotted in Figure 5.5. The strain data displays fluctuations that do not seem to be fully explained by either the load profile, or the test temperature (which fluctuates slightly). Just as with the triangular profile test, the load cell reading lags behind the setpoint. Accounting for a delay of one sampling period, the mean and standard deviation of the absolute error are 0.068 N and 0.040 N, respectively.

6. CONCLUSIONS AND RECOMMENDATIONS

This research presents two mechanical testers designed to meet the need for reliable mechanical evaluation of solder. In particular, design criteria, validation, and control capability are presented, which are not commonly found in current literature.

The first tester presented, the micro-precision tester, is a revision on a previous mechanical tester. The tester is designed to evaluate the mechanical behavior of solder through multi-temperature testing in shear. Several improvements were made over the previous tester, including changes to the physical design and control software. The result is a tester with significant improvement in setpoint control during monotonic and creep tests. Therefore, the mechanical characterization derived from this data is more reliable.

The second tester presented is the nano-precision tester, a new design that sacrifices load and displacement capacity for superior control. The nano-precision tester is capable of significantly better velocity control, and load control of arbitrary profiles to nearly the resolution of the load cell (0.02 N). A drawback is the displacement range of the tester, which presents a significant challenge to displacement controlled tests.

6.1 Recommendations for the Micro-Precision Tester

The micro-precision tester is capable of fully evaluating the mechanical behavior of solders. However, there is always room for improvement. This section presents some proposed solutions to a few problems still present in the tester.

6.1.1 The Environmental Chamber

As discussed previously, the environmental chamber maintains the temperature at the sample to within 1°C ($\leq 0.003T_m$), which is sufficient for constitutive modelling. However, approximately 100 mm of the tester is also within the environmental chamber. An estimate of the expansion of the plain carbon steel that composes the tester arms is

$$\frac{\Delta L}{\Delta T} = \alpha_L L_0 = \left(12 \times 10^{-6} (^\circ\text{C})^{-1}\right) (100 \text{ mm}) = 1.2 \text{ µm}/^\circ\text{C}$$

More significantly, the aluminum capacitance sensor target expands with temperature change. The same calculation gives

$$\frac{\Delta L}{\Delta T} = \alpha_L L_0 = \left(22 \times 10^{-6} (^\circ\text{C})^{-1}\right) (100 \text{ mm}) = 2.2 \text{ µm}/^\circ\text{C}$$

Summing these two gives a total of 3.4 µm/°C, equivalent to 1.3% strain on the custom squat joints. This is significant because the temperature variation is erroneously measured as strain on the sample. As confirmation of this approximation, data from a creep test is plotted in Figure 6.1. Temperature fluctuations less than 0.4°C are visible in the displacement curve.

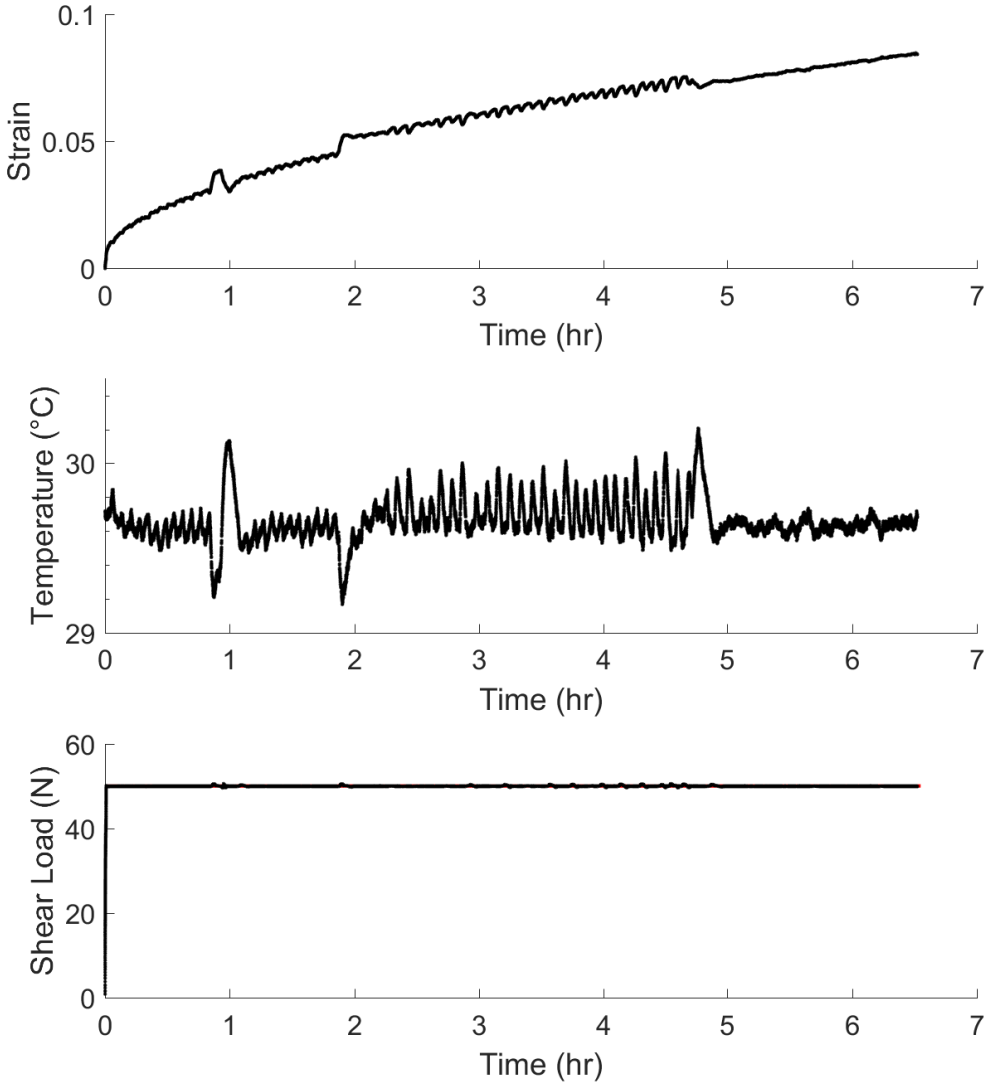

Figure 6.1. A creep test run with nominal parameters 50 N and 30°C. The load is within ±0.5 N of nominal and the temperature variation is less than ±0.5°C.

Several options exist to correct this issue. One option is to reduce the coefficient of thermal expansion by changing materials. Several candidate materials are listed in Table 6.1 below.

Table 6.1. Comparison of selected materials by coefficient of thermal expansion, and by elastic modulus.

Material	**CTE** (10^{-6} 1/K)	**Elastic Modulus** (GPa)
aluminum	22	69
carbon steel	12	200
stainless steel	10	200
tungsten carbide	5.5	>500
Invar	1.2	140
fused SiO_2	0.6	73

The capacitance sensor target must be electrically conductive, but is not a load bearing component. Therefore, stiffness is not an objective, only the coefficient of thermal expansion. Of the presented materials, fused SiO_2 has the lowest thermal expansion, but is not electrically conductive. This issue could perhaps be corrected by the use of a composite target, with a metal target bonded to a fused SiO_2 rod. A simpler option is to replace the aluminum target with an Invar target, which would both reduce thermal expansion and maintain electrical conductivity.

Reducing the thermal expansion of the two tester arms is a more difficult task. Unlike the capacitance sensor target, they are load bearing and stiffness is most certainly an objective. Candidate materials for replacement are stainless steel, Invar, and tungsten carbide. Of the three materials, Invar has the least thermal expansion, but also the smallest elastic modulus. On the other end of the spectrum, the elastic modulus of tungsten carbide is twice that of plain carbon steel, with half the thermal expansion. In the middle is stainless steel, which is equally stiff as plain carbon steel and expands $\sim$15% less for the same change in temperature. However, manufacturing costs for both stainless steel and tungsten carbide are significantly greater than plain carbon steel. In the case of pricing stainless steel parts, a common rule of thumb is three times as expensive as the equivalent steel part. For tungsten carbide, the manufacturing cost is at least two orders of magnitude higher than plain carbon steel.

Another solution is to simply move the capacitance sensor target outside the environmental chamber. The primary disadvantage here is the additional distance this solution would add between the capacitance sensor and the centerline of the tester. This distance acts as a lever arm, amplifying the effect of bending on the capacitance sensor measurement.

One last solution is software compensation. By determining an effective thermal expansion coefficient for the tester, the displacement measured by the capacitance sensor can be corrected. The correction can be either real-time within the LabVIEW control, or as post-processing of the data. The benefit of real time correction is that the corrected displacement can be used for closed-loop control.

6.1.2 The Actuator

One of the primary reasons the nano-precision tester outperforms the micro-precision tester is the design of the actuator. To put it simply, stepper-based actuators cannot offer the same level of precision as piezo-actuators. The NLS4 actuator used in the micro-precision tester has two fundamental issues that cannot be compensated for elsewhere in the design. The first issues is the noisy output of the actuator, which is due to the use of a stepper motor. Stepper motors cannot produce smooth velocity curves, which can be seen in Figure 3.3. The second issue is the backlash (Figure 2.6.) caused by the leadscrew, which causes difficulty in dynamic testing.

The most evident solution to these problems is to replace the NLS4 actuator. Three actuator designs fit this type of application:

1. a piezo-actuator
2. a DC motor/ballscrew based stage
3. a linear motor based stage

A piezo-actuator is certainly the most precise option, but no options exist that can match the range and load capacity of the current actuator.

The second option is to replace the offending sub-components individually. Stepper motors are commonly used due to their high precision to cost ratio, but other motor options

exist. The same is true for trapezoidal leadscrews. An actuator using a DC motor coupled to a ballscrew would likely mitigate both issues. This type of actuator can be found with similar dimensions and capacity as the NLS4, making the physical replacement fairly straightforward.

A third option is a linear motor actuator, which operates on the principle of a traditional electric motor, only unrolled into a straight line. This would simultaneously eliminate both noise and backlash problems. However, linear motors are less power-dense than stepper motors, and it is somewhat challenging to find a linear motor with the same load capacity for the same overall dimension.

All options presented offer some complications. At minimum, each solution requires significant time investment. PID tuning, manufacturing new fixtures, and software efforts would be required to integrate a new actuator into the current setup. Additionally, the cost-benefit ratio must be considered. It is possible that the efforts made to replace the micro-precision tester's actuator would not significantly increase the reliability of the data.

6.2 Recommendations for the Nano-Precision Tester

While the nano-precision mechanical tester is capable of tests, there is still significant room for improvement. This section proposes solutions to two gaps in the current tester design, namely the capability of multi-temperature testing, and validation in a similar manner to that of the micro-precision tester.

6.2.1 Multi-Temperature Testing

One of the larger deficiencies is the capability of multi-temperature testing, which is required for generating a complete constitutive model. An environmental chamber similar to that of the micro-precision tester is one solution to this issue. Another solution is to use a setup similar to that of Wiese et al. [17], [18]. They place a thick-film resistive heater between the sample and tester. A PT100 temperature sensor adjacent to the heater is used to implement closed-loop control. With this setup, temperatures up to 150°C were tested.

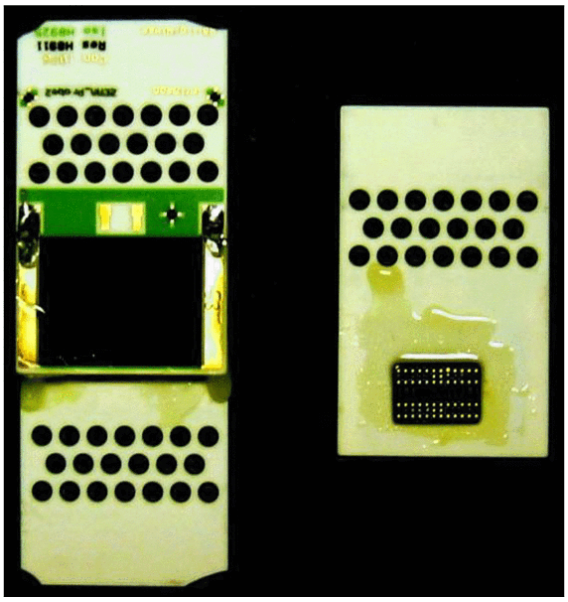

(a) The resistive heater and a ceramic substrate (left) and the specimen epoxied to another ceramic substrate (right).

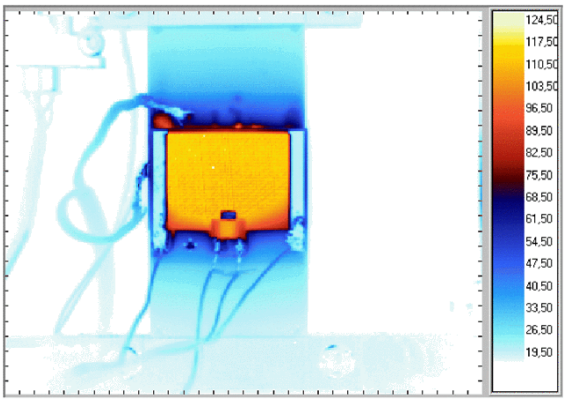

(b) An infrared image of the local heating. The temperature scale is in Celsius.

Figure 6.2. Thick-film heating apparatus. Images reproduced from [17], [18].

6.2.2 Validation

A final concern is validation of the nano-precision tester. It is possible to do this in the same manner as the micro-precision tester. In order to perform a similar validation procedure on the load cell, an adjustable fixture would need to be manufactured to install the higher precision load cell where the sample would sit. A proposed set of fixtures are shown in Figure 6.3.

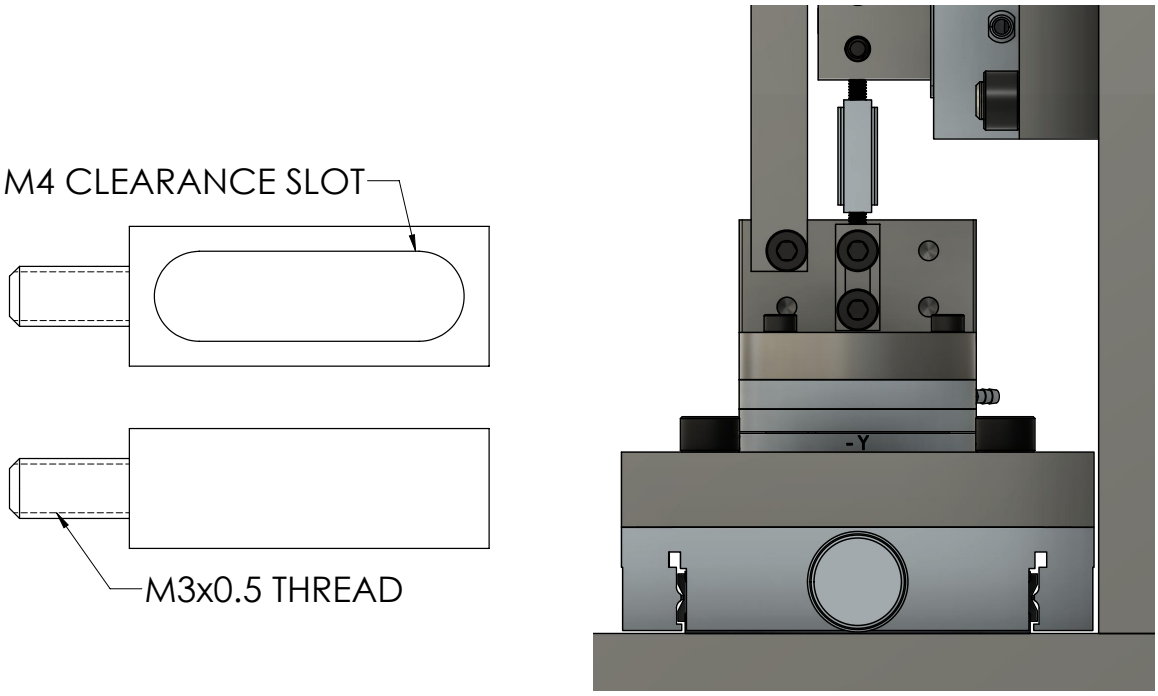

Figure 6.3. Proposed setup for validation of the load cell. Adjustable fixtures would be used to hold the validation load cell in the place of the sample.

For validation of the nano-precision tester by tensile test, a similar issue presents itself for fixturing the tensile sample. A proposed solution is presented in Figure 6.4. Additionally, note the sample would need to be very compliant, so would need a small cross section.

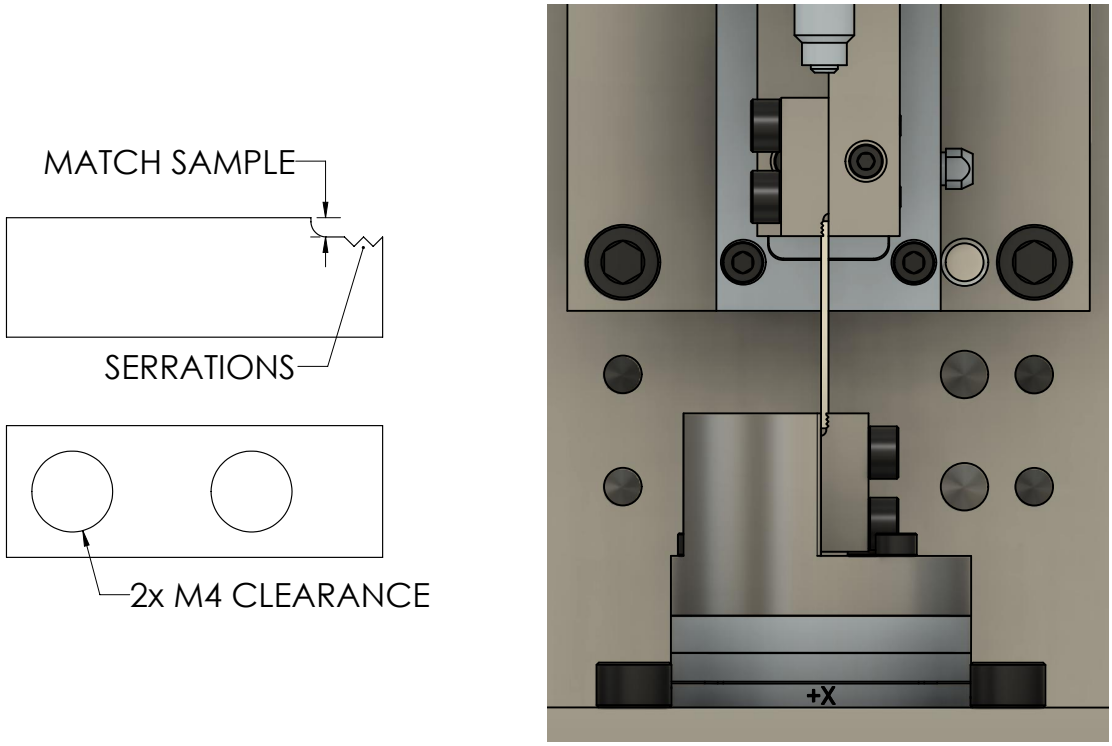

Figure 6.4. Proposed setup for validation by tensile test on an aluminum sample. The aluminum sample is clamped by two jaws, one on the actuator side, and one on the load cell side. Note the capacitance sensor target is hidden to better see the setup.

Serrated jaws are proposed because the clamping method used for validation of the micro-precision tester is thought to slip. It is possible that serrations may produce yielding at the extremities of the sample, introducing more issues than they solve.

REFERENCES

[1] R. Darveaux and K. Banerji, "Constitutive relations for tin-based solder joints," *IEEE Transactions on Components, Hybrids, and Manufacturing Technology*, vol. 15, no. 6, pp. 1013–1024, 1992. DOI: 10.1109/33.206925.

[2] S. Wiese, A. Schubert, H. Walter, R. Dukek, F. Feustel, E. Meusel, and B. Michel, "Constitutive behaviour of lead-free solders vs. lead-containing solders-experiments on bulk specimens and flip-chip joints," in *2001 Proceedings. 51st Electronic Components and Technology Conference (Cat. No.01CH37220)*, 2001, pp. 890–902. DOI: 10.1109/ECTC.2001.927900.

[3] H. Ma, J. Suhling, P. Lall, and M. Bozack, "Effects of aging on the stress-strain and creep behaviors of lead free solders," in *Thermal and Thermomechanical Proceedings 10th Intersociety Conference on Phenomena in Electronics Systems, 2006. ITHERM 2006.*, 2006, pp. 961–976. DOI: 10.1109/ITHERM.2006.1645450.

[4] D. Chan, G. Subbarayan, and L. Nguyen, "Maximum-Entropy Principle for Modeling Damage and Fracture in Solder Joints," *Journal of Electronic Materials*, vol. 41, no. 2, pp. 398–411, 2012. DOI: 10.1007/s11664-011-1804-9.

[5] D. K. Chan, "A maximum entropy fracture model for low and high strain-rate fracture in SnAgCu alloys," Ph.D. dissertation, Purdue University, West Lafayette, 2012.

[6] T. Dale, Y. Singh, I. Bernander, G. Subbarayan, C. Handwerker, S. Peng, and B. Glasauer, "Fatigue Life of Sn3.0Ag0.5Cu Solder Alloys Under Combined Shear and Compressive Loads," in *Proceedings of the ASME 2019 International Technical Conference and Exhibition on Packaging and Integration of Electronic and Photonic Microsystems*, 2019, V001T01A007. DOI: 10.1115/IPACK2019-6507.

[7] D. Bhate, D. Chan, G. Subbarayan, and T. C. Chiu, "Solder interconnection specimen design and test control procedure for valid constitutive modeling of solder alloys," in *Thermal and Thermomechanical Proceedings 10th Intersociety Conference on Phenomena in Electronics Systems, 2006. ITHERM 2006.*, 2006, pp. 977–983. DOI: 10.1109/ITHERM.2006.1645451.

[8] D. Bhate, D. Chan, G. Subbarayan, T. C. Chiu, V. Gupta, and D. R. Edwards, "Constitutive Behavior of Sn3.8Ag0.7Cu and Sn3.0Ag0.5Cu Alloys at Creep and Low Strain Rate Regimes," *IEEE Transactions on Components and Packaging Technologies*, vol. 31, no. 3, pp. 622–633, 2008. DOI: 10.1109/TCAPT.2008.2001165.

[9] K. Mysore, G. Subbarayan, V. Gupta, and R. Zhang, "Constitutive and Aging Behavior of Sn3.0Ag0.5Cu Solder Alloy," *IEEE Transactions on Electronics Packaging Manufacturing*, vol. 32, no. 4, pp. 221–232, 2009. DOI: 10.1109/TEPM.2009.2024119.

[10] H. Kuhn and D. Medlin, Eds., *Mechanical Testing and Evaluation*. ASM International, 2000, ISBN: 978-1-62708-176-4. DOI: 10.31399/asm.hb.v08.9781627081764.

[11] *Producer/Consumer Architecture in LabVIEW*, National Instruments, 2021. [Online]. Available: https://www.ni.com/en-us/support/documentation/supplemental/21/producer-consumer-architecture-in-labview0.html.

[12] *CPL190/CPL290 User's Guide*, M015-9450.021, Lion Precision, 2019. [Online]. Available: https://www.lionprecision.com/wp-content/uploads/2019/04/CPL190-290-USER-MANUAL.pdf.

[13] *F/T Sensor Data Acquisition (DAQ) Systems*, 9620-05-DAQ, ATI Industrial Automation, 2000. [Online]. Available: https://www.ati-ia.com/app_content/documents/9620-05-DAQ.pdf.

[14] *Vibration Measurement; Vibration sensors; Measuring Vibration Precisely*, LA05-0020, Lion Precision, 2013. [Online]. Available: https://www.lionprecision.com/vibration-measurement-vibration-sensors-measuring-vibration-precisely/.

[15] J. Lemaitre, *A Course on Damage Mechanics*, 2nd ed. Springer Berlin Heidelberg, 1996, ISBN: 978-3-540-60980-3. [Online]. Available: https://books.google.com/books?id=Gc9RAAAAMAAJ.

[16] R. Budynas and J. Nisbett, *Shigley's Mechanical Engineering Design*, 10th ed. McGraw-Hill Education, 2015, ISBN: 978-0073398204.

[17] S. Wiese, M. Röllig, M. Mueller, S. Rzepka, K. Nocke, C. Luhmann, F. Kraemer, K. Meier, and K. Wolter, "The Influence of Size and Composition on the Creep of SnAgCu Solder Joints," in *2006 1st Electronic Systemintegration Technology Conference*, vol. 2, 2006, pp. 912–925. DOI: 10.1109/ESTC.2006.280120.

[18] M. Röllig, S. Wiese, K. Meier, and K. Wolter, "Creep Measurements of 200 µm - 400 µm Solder Joints," in *2007 International Conference on Thermal, Mechanical and Multi-Physics Simulation Experiments in Microelectronics and Micro-Systems. EuroSime 2007*, 2007, pp. 1–9. DOI: 10.1109/ESIME.2007.359938.

[19] *F/T Sensor: Gamma*, ATI Industrial Automation, 2000. [Online]. Available: https://www.ati-ia.com/products/ft/ft_models.aspx?id=Gamma.

[20] *NLS4 Series Precision Linear Stage*, Newmark Systems, 2020. [Online]. Available: https://www.newmarksystems.com/linear-positioners/nls4-series/.

[21] *BM17.51*, Newport Corporation, 2020. [Online]. Available: https://www.newport.com/p/BM17.51.

[22] *M-UMR8.51*, Newport Corporation, 2020. [Online]. Available: https://www.newport.com/p/M-UMR8.51.

[23] J. Hokanson. (2010). "TDMS Reader," [Online]. Available: https://www.mathworks.com/matlabcentral/fileexchange/30023-tdms-reader?s_tid=mwa_osa_a.

[24] *F/T Sensor: Mini40*, ATI Industrial Automation, 2007. [Online]. Available: https://www.ati-ia.com/products/ft/ft_models.aspx?id=Mini40.

[25] *P-753 LISA Linear Actuator and Stage*, PI USA (Physik Instrumente), 2020. [Online]. Available: https://www.pi-usa.us/en/products/piezo-flexure-nanopositioners/x-linear-piezo-flexure-nanopositioning-stages/p-753-lisa-linear-actuator-stage-200900/.

A. THE MICRO-PRECISION MECHANICAL TESTER

A.1 General Operating Procedure

1. Start the LabVIEW program, enter operator name and sample ID into the information prompt.

2. Flip the `Testing` switch to ON. The tester will now be running a monitor test which samples data, but does not command the actuator.

3. Bolt in removable glue fixtures.

   (a) Tighten bolts lightly.

   (b) Adjust manual stage so that the fixture faces touch.

   (c) Tighten the bolts fully while squeezing the fixtures together. This ensures parallelism.

4. Adjust the manual stage until the sample barely fits into the gap.

5. Zero the load cell. At this point, no additional weight will be placed on the load cell and the two halves of the tester are not in contact.

6. Holding the sample with tweezers, place glue on both sides.

7. Lift the load cell side at the manual stage and place the sample on the bottom fixture.

8. Begin a sample protect test. This commands to the motor to hold a 0 N shear load (F_z).

9. Adjust the manual stage until the glue load (F_x) is $\sim$1 N.

10. Move the heat chamber into position and set the heater to the desired temperature.

11. Wait for the temperature to reach steady-state.

12. Adjust the manual stage until the glue load (F_x) is 0-1 N (again).

13. Adjust the capacitance sensor target, then zero the capacitance sensor.

    - For uni-directional tests (monotonic and creep), adjust the target so that the sensor is in the lower 10% of its range.
    - For bi-directional tests (fatigue), adjust the target so that the sensor is in the center of its range.

14. Load the desired test parameters, PID vales, and stopping conditions, then and start the test.

A.2 General Post-Processing Procedure

Test data is saved to `~\test data\sample ID\data.txt` where `~` is the folder of the micro-precision tester. The name of the data file contains the sample ID, the date, the type of test, and the parameter used for closed-loop control. The data is formatted as a tab-delimited text file, which can be imported into any program for post-processing.

A.3 List of Components

Table A.1. List of manufactured components in the micro-precision tester.

Component	Vendor	Part Number	Quantity
01_MC	manufactured in-house	n/a	1
02_MC			1
03_MC			1
04_MC			1
05_MC			1
06_MC			1
07_MC			1
08_MC			8
09_MC			1
10_MC			1
11_MC			1
12_MC			2
13_MC			1

Table A.2. List of purchased components.

Component	Vendor	Part Number	Quantity
load cell	ATI Industrial Automation, Inc		
transducer		9105-TIF-GAMMA	1
driver		9105-IFPS-1	1
capacitance sensor	Lion Precision		
driver		CPL190	1
probe		C4-2.0-2.0	1
stepper actuator	Newmark Systems		
stage		NLS4-2-11	1
controller		NSC-A1	1
manual stage	Newport Corporation		
stage		M-UMR8.51	2
micrometer head		BM17.51	1
lock		CL12-51	2
PCIe DAQ	NI (National Instruments)	PCIe-6323	1
thermocouple DAQ	NI (National Instruments)	9210	1
optical table	Thorlabs, Inc.	T46HK	1
bolts	McMaster-Carr		
M3 x 0.5 - 8 mm		91290A113	8
M4 x 0.7 - 8 mm		91290A140	8
M4 x 0.7 - 16 mm		91290A154	8
M6 x 1.0 - 15 mm		91290A320	18
M6 x 1.0 - 20 mm		91290A326	4
M6 x 1.0 - 25 mm		91290A330	7
1/4"-20 - 1 in		91251A542	10
dowel pins	McMaster-Carr		
1/8" x 1/2"		98381A471	6

Table A.3. List of components in the environmental chamber.

Component	Vendor	Part Number	Quantity
heater core			1
tungsten heating element	ZIRCAR Ceramics	DX2161-1	1
aluminum tube	McMaster-Carr	9056K84	1
wide temperature range fan	Mouser Electronics	978-9GT0912P1M001	1
duct	McMaster-Carr	55125K79	2
tube clamps	McMaster-Carr	5312K13	4
driver			
process controller	Omega	CN77344-C2	1
solid state relay	Engineering	SSRL240DC10	1
15 A fuse		FRN15	1

A.4 Manufacturing Drawings

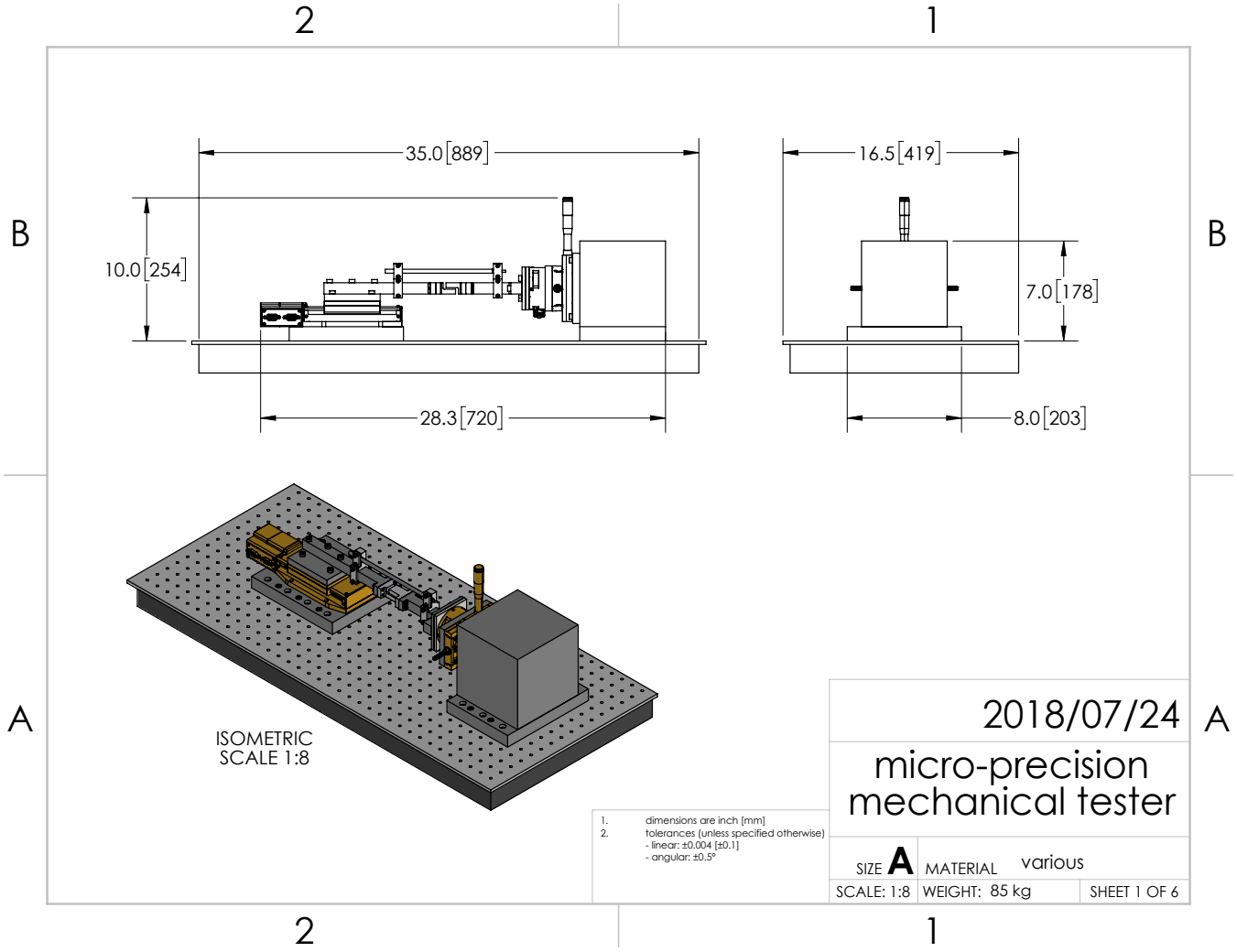

Figure A.1. Assembly drawing with selected dimensions.

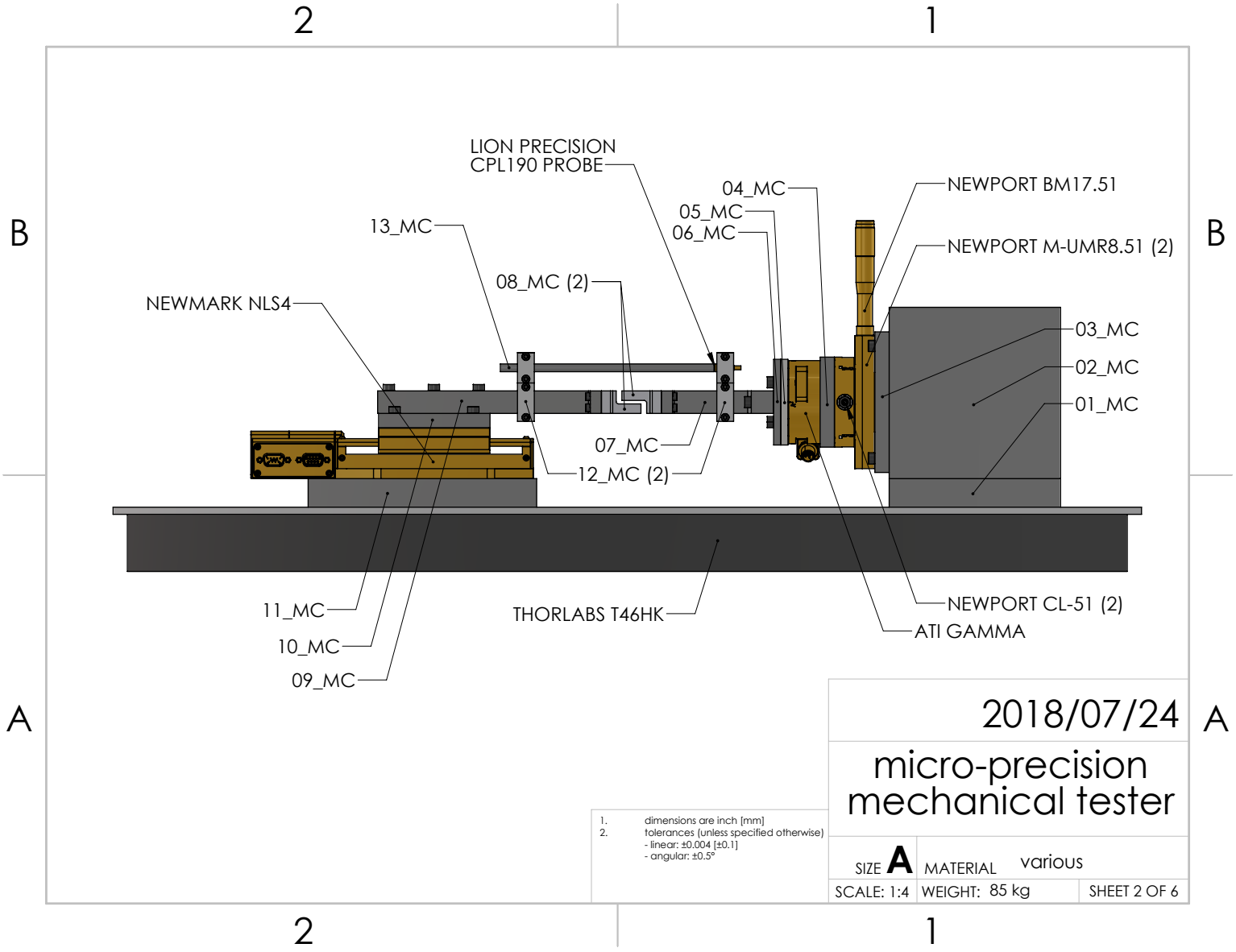

Figure A.2. Isometric assembly drawing with labels for each component.

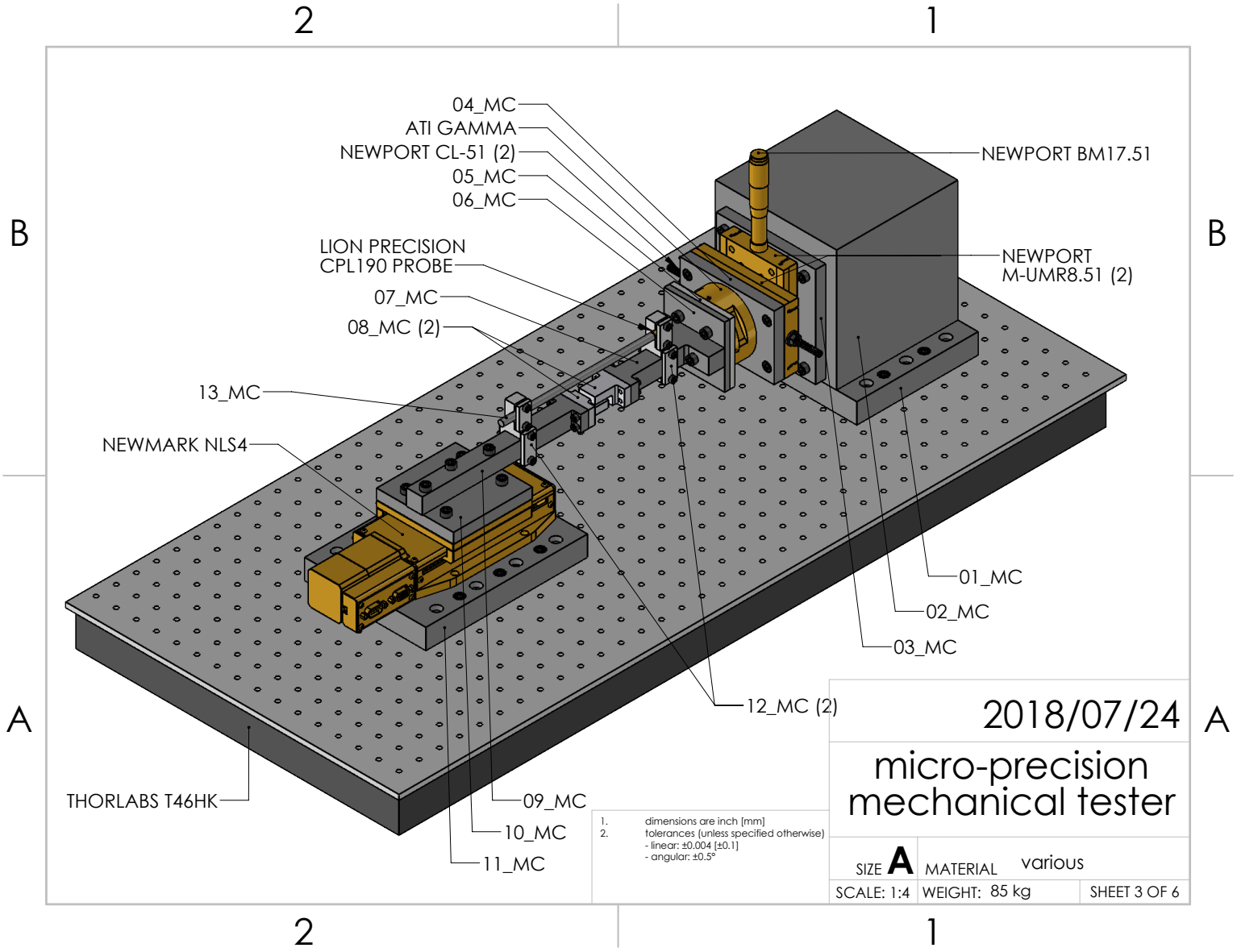

Figure A.3. Front-view assembly drawing with labels for each component.

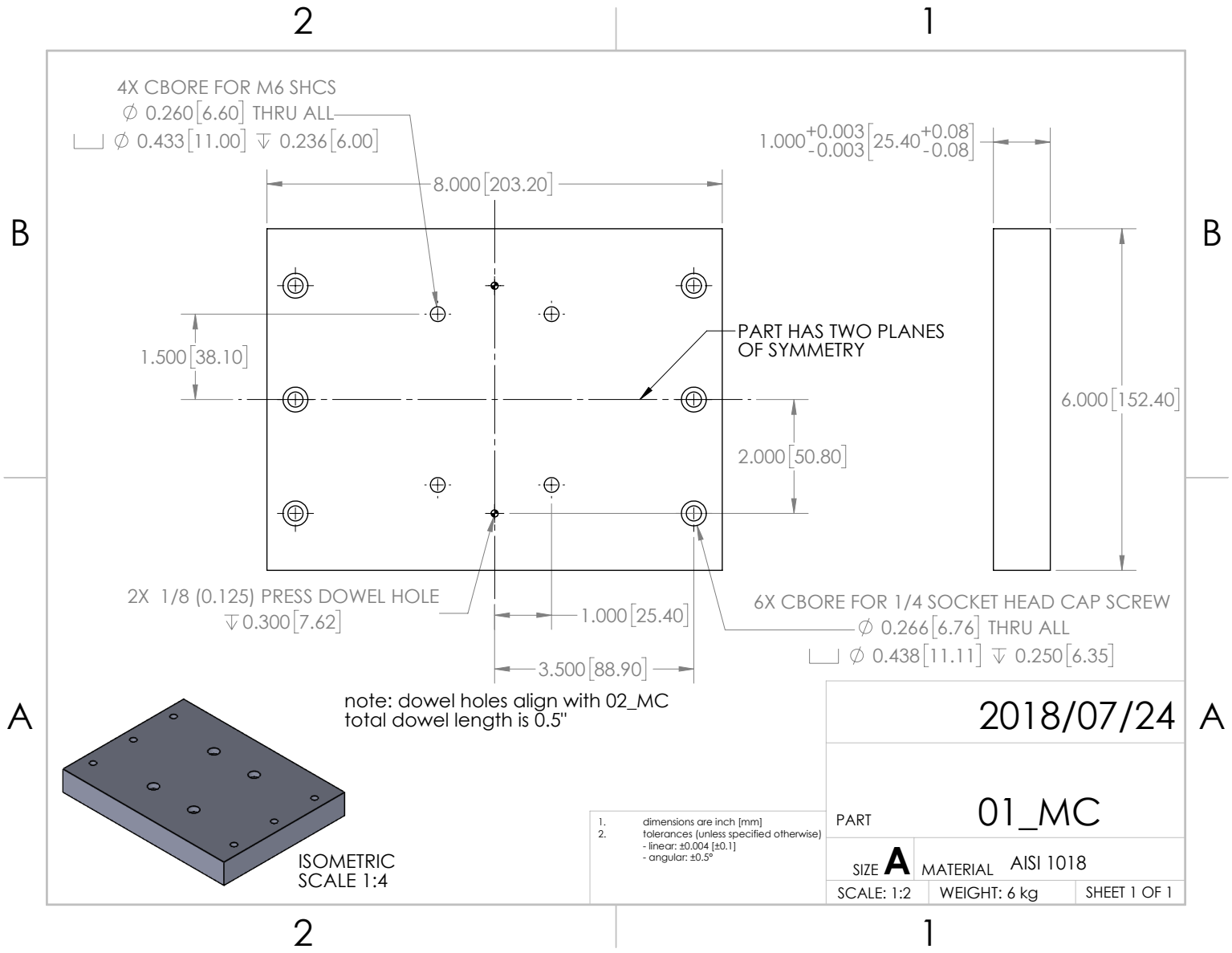

Figure A.4. Base plate for mounting the load cell side to the optical table.

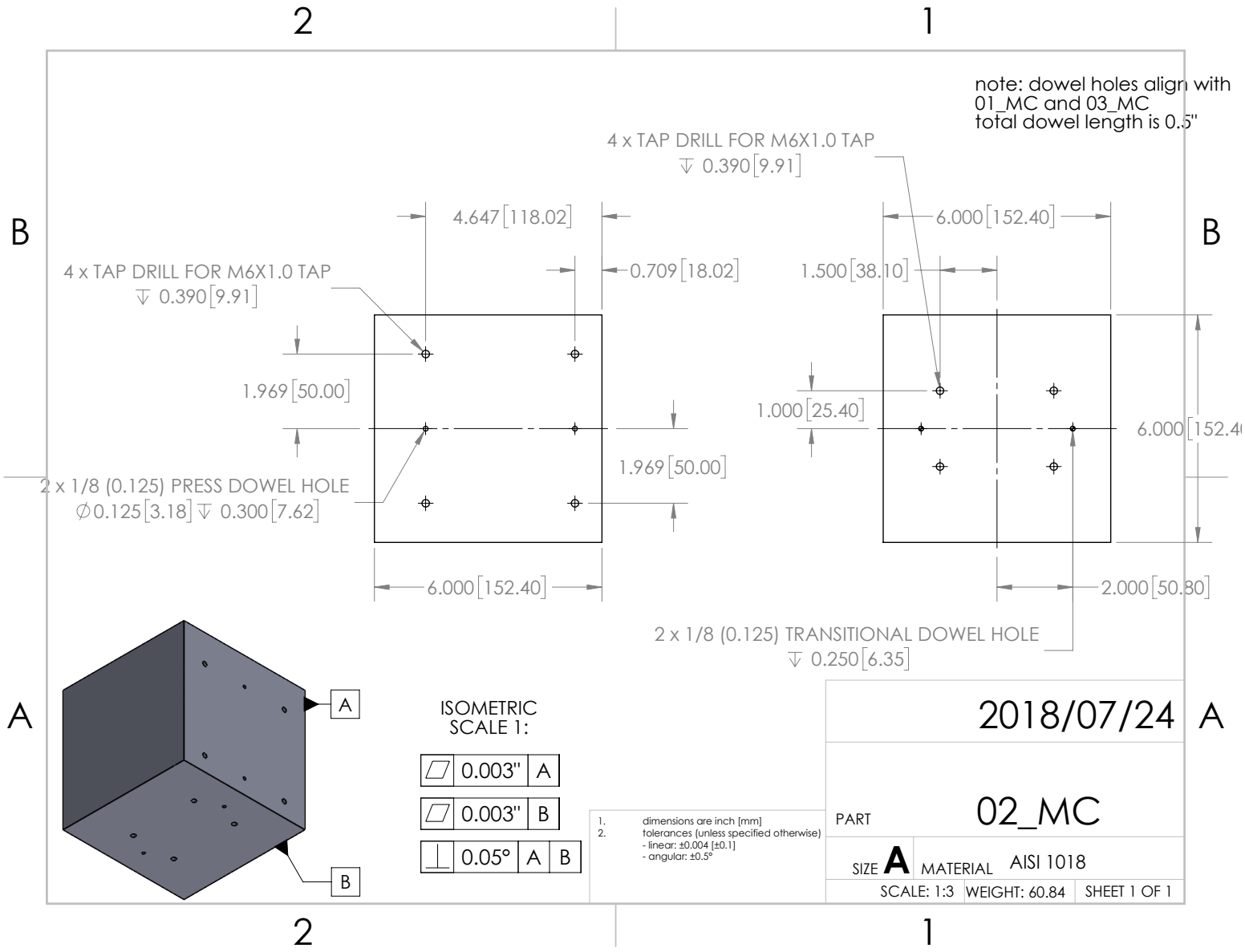

Figure A.5. Angle plate supporting the load cell side.

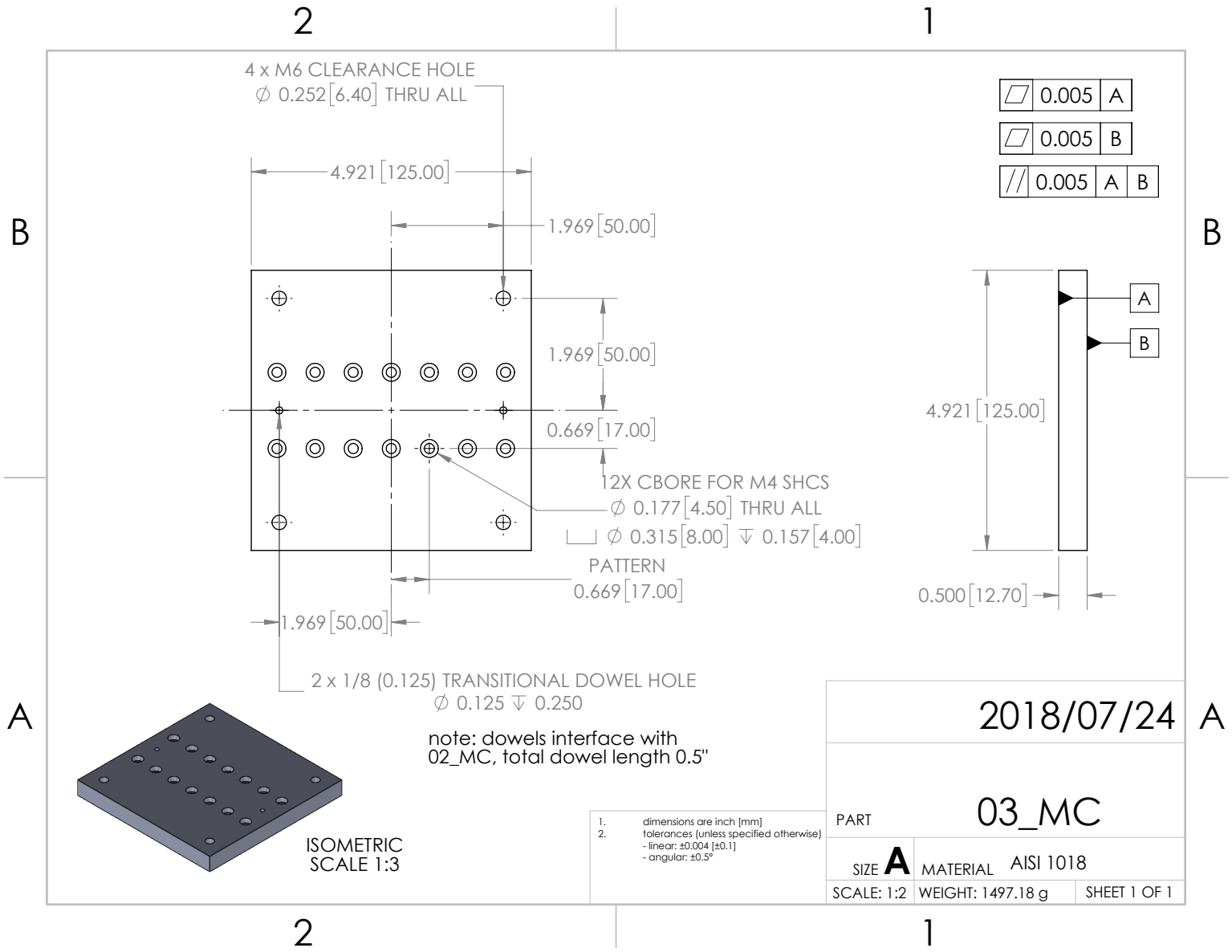

Figure A.6. Fixture plate for mounting the manual stages to the angle plate (02_MC).

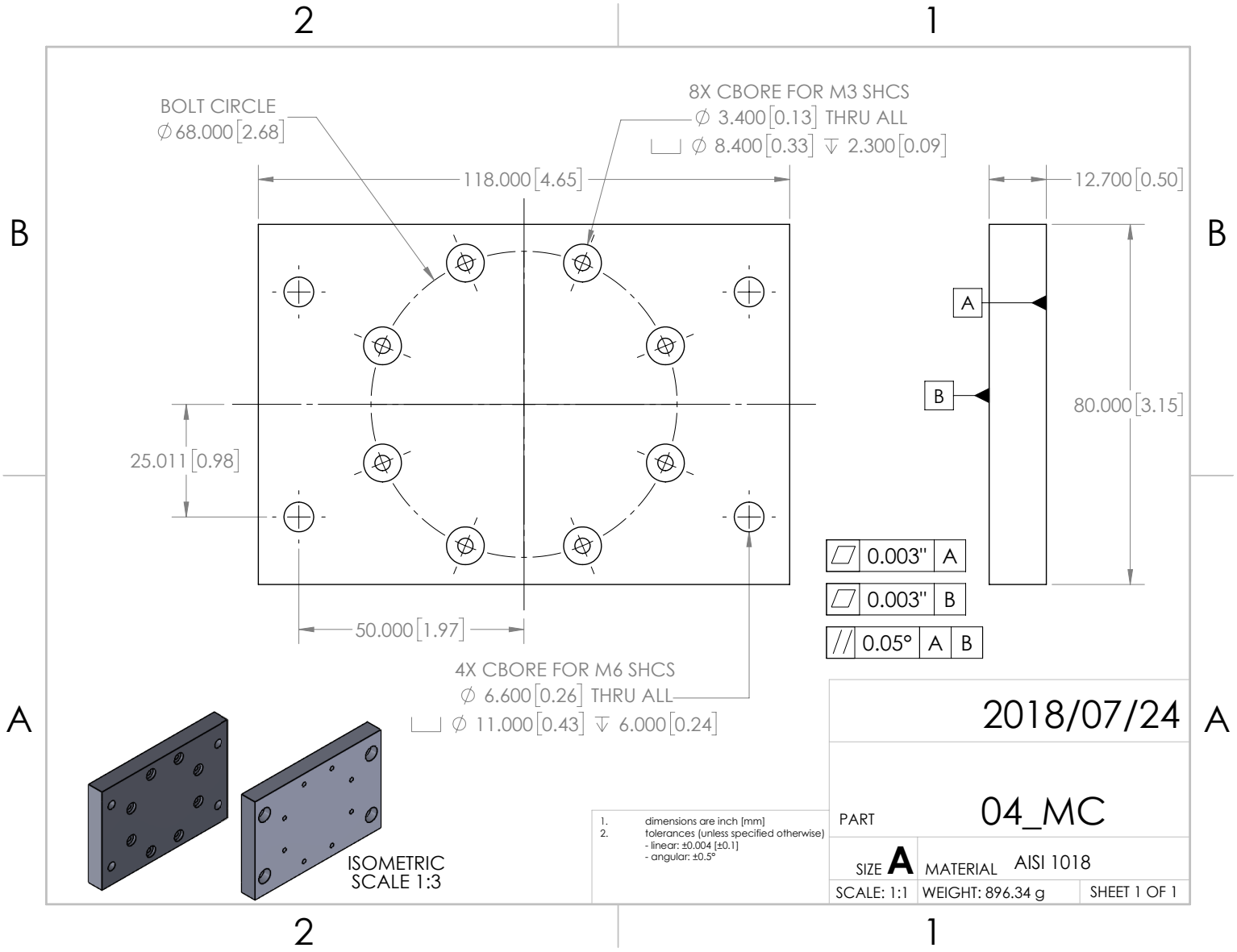

Figure A.7. Fixture plate for mounting the load cell to the manual stages.

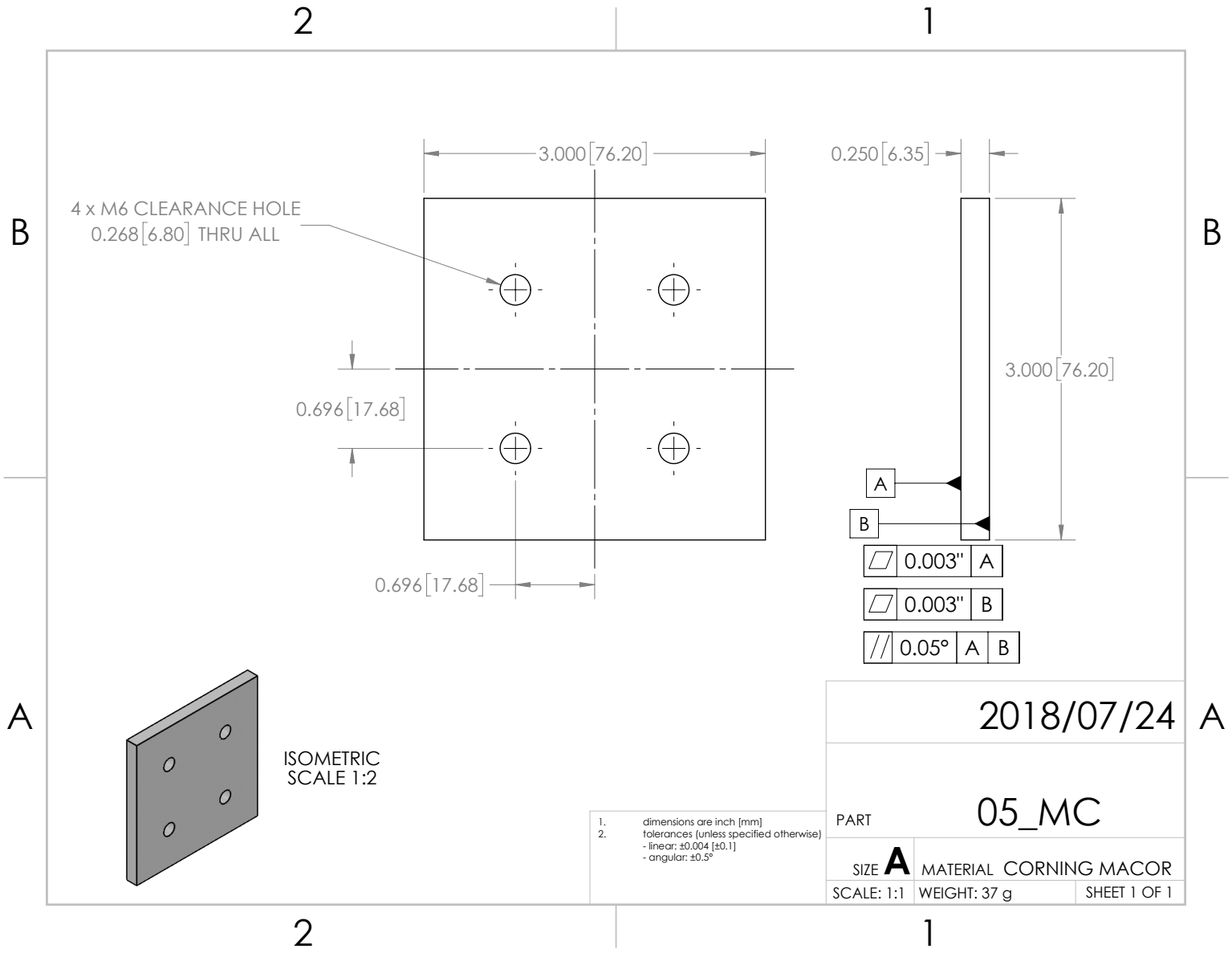

Figure A.8. Ceramic plate providing thermal insulation to the load cell.

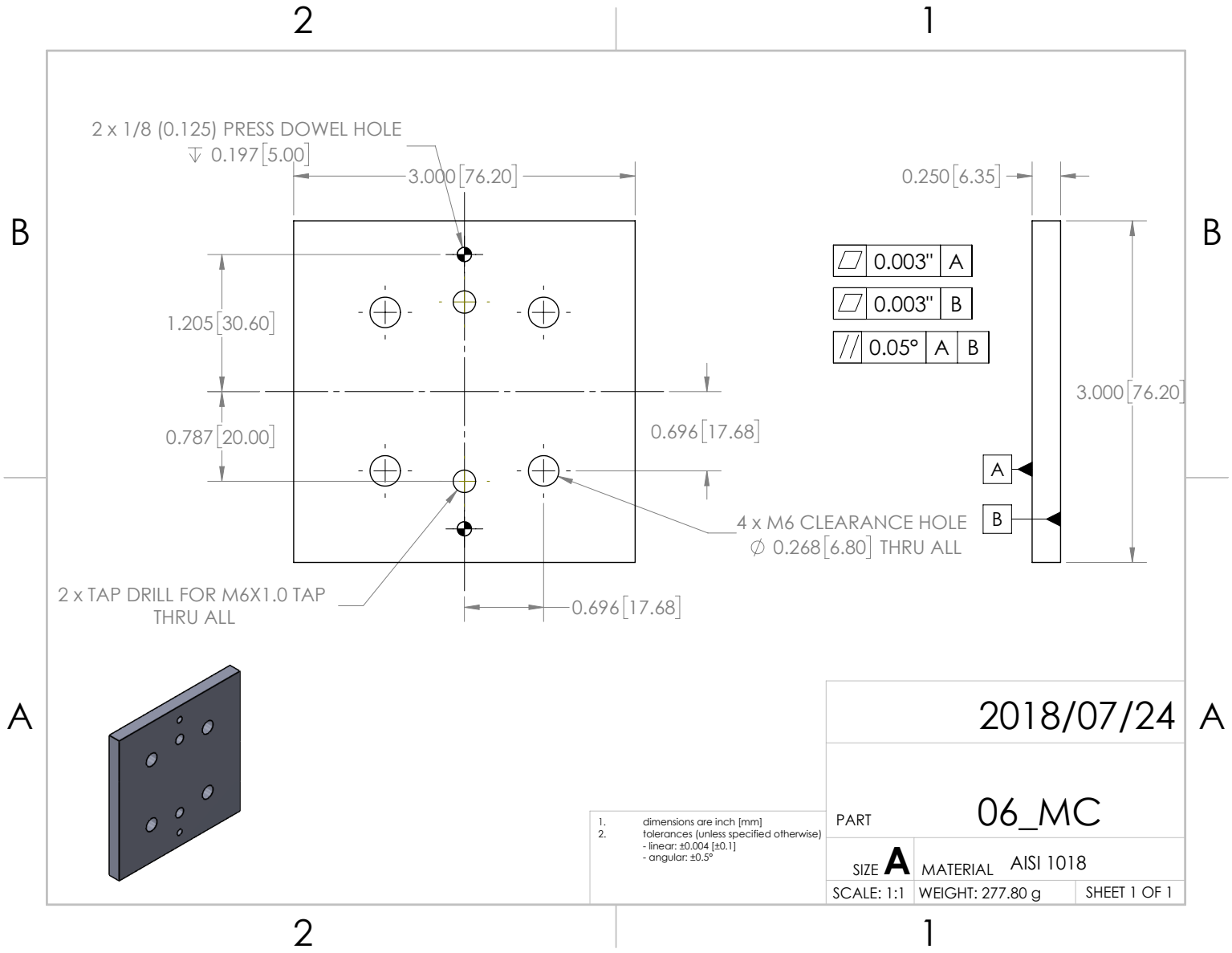

Figure A.9. Fixture plate for mounting the fixture arm (07_MC) to the load cell.

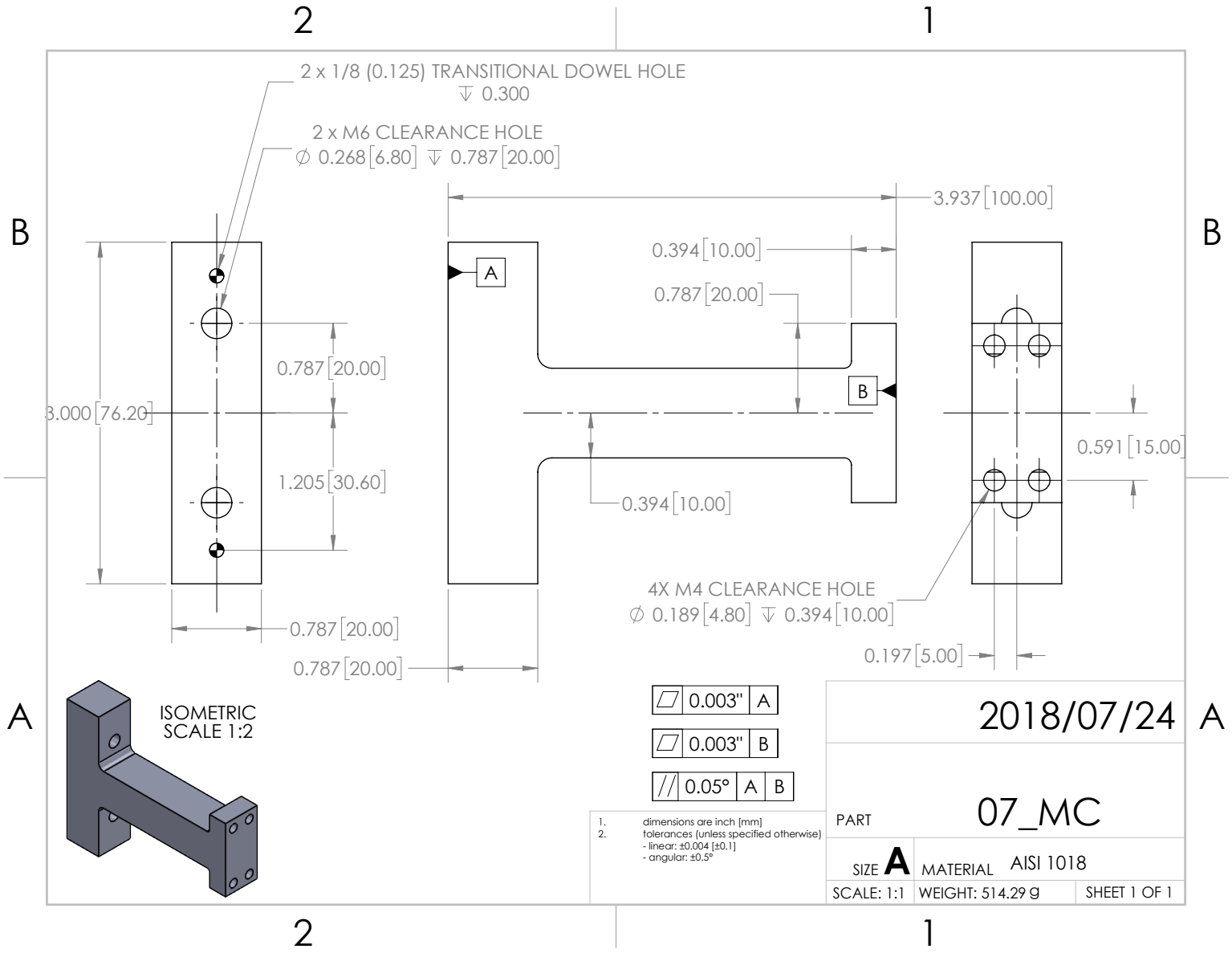

Figure A.10. Fixture arm for mounting both a sample fixture (08_MC) and the capacitance sensor clamp (13_MC).

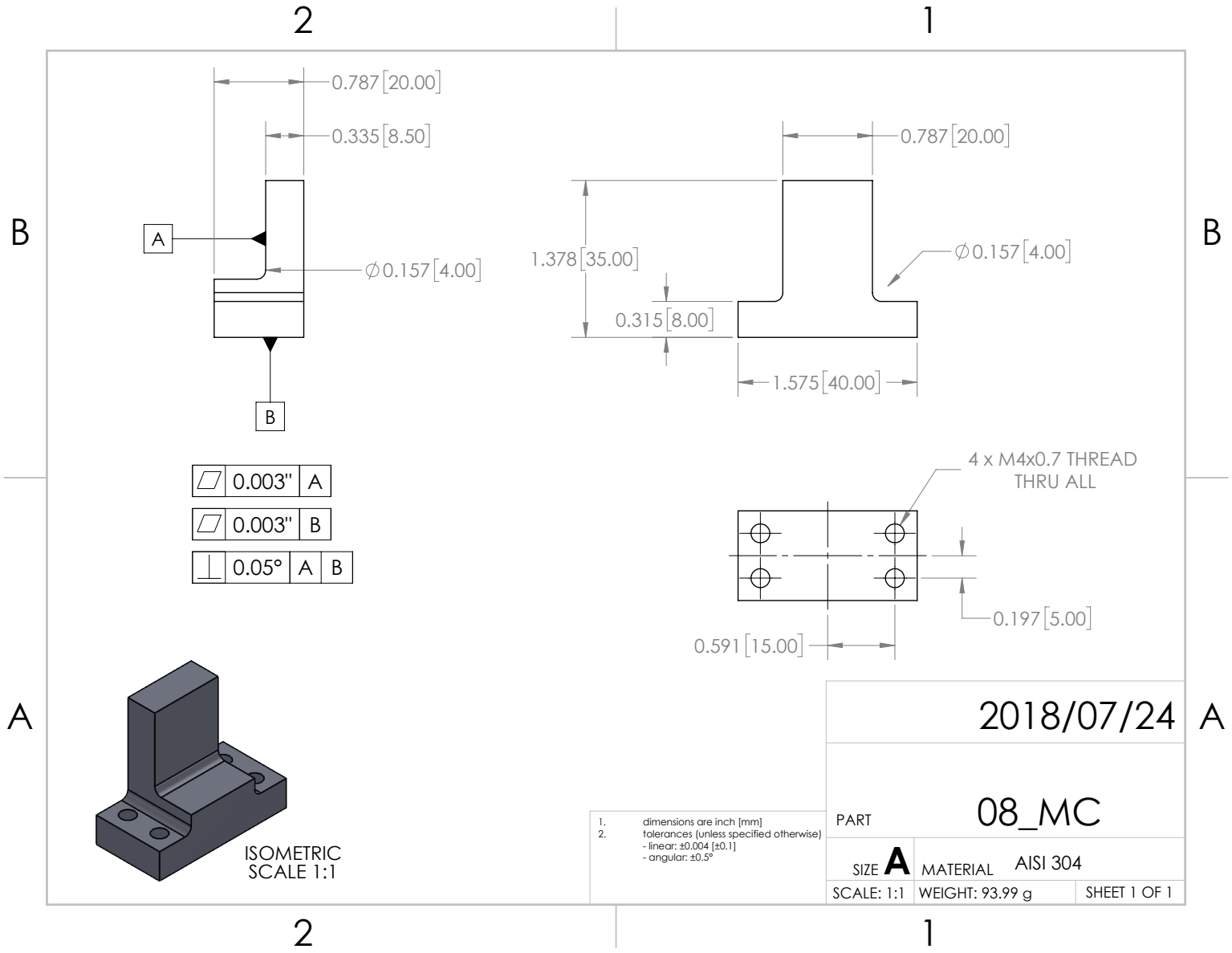

Figure A.11. Removable sample fixtures, for gluing samples into the tester.

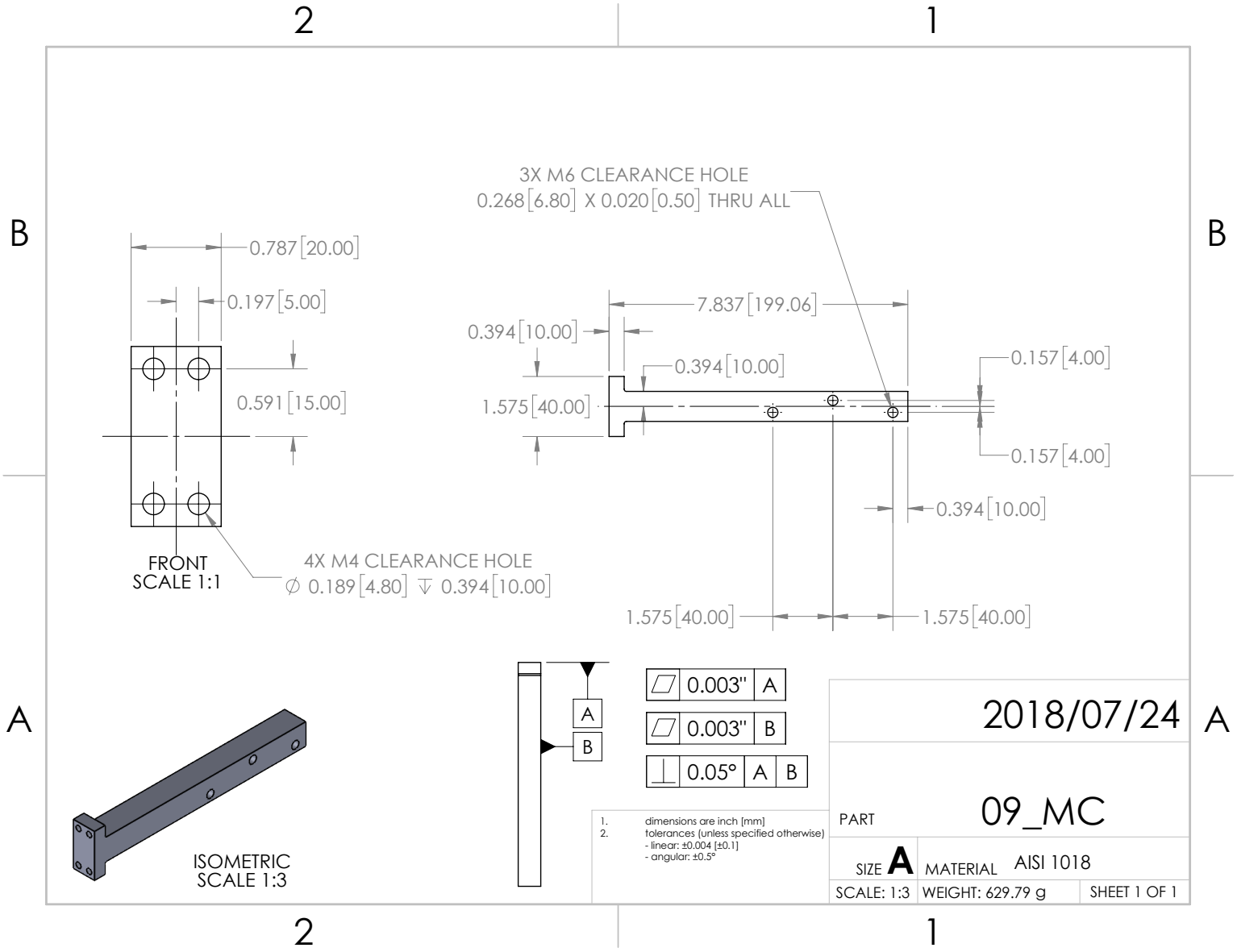

Figure A.12. Fixture arm for mounting both a sample fixture (08_MC) and the clamp for the capacitance sensor target (13_MC).

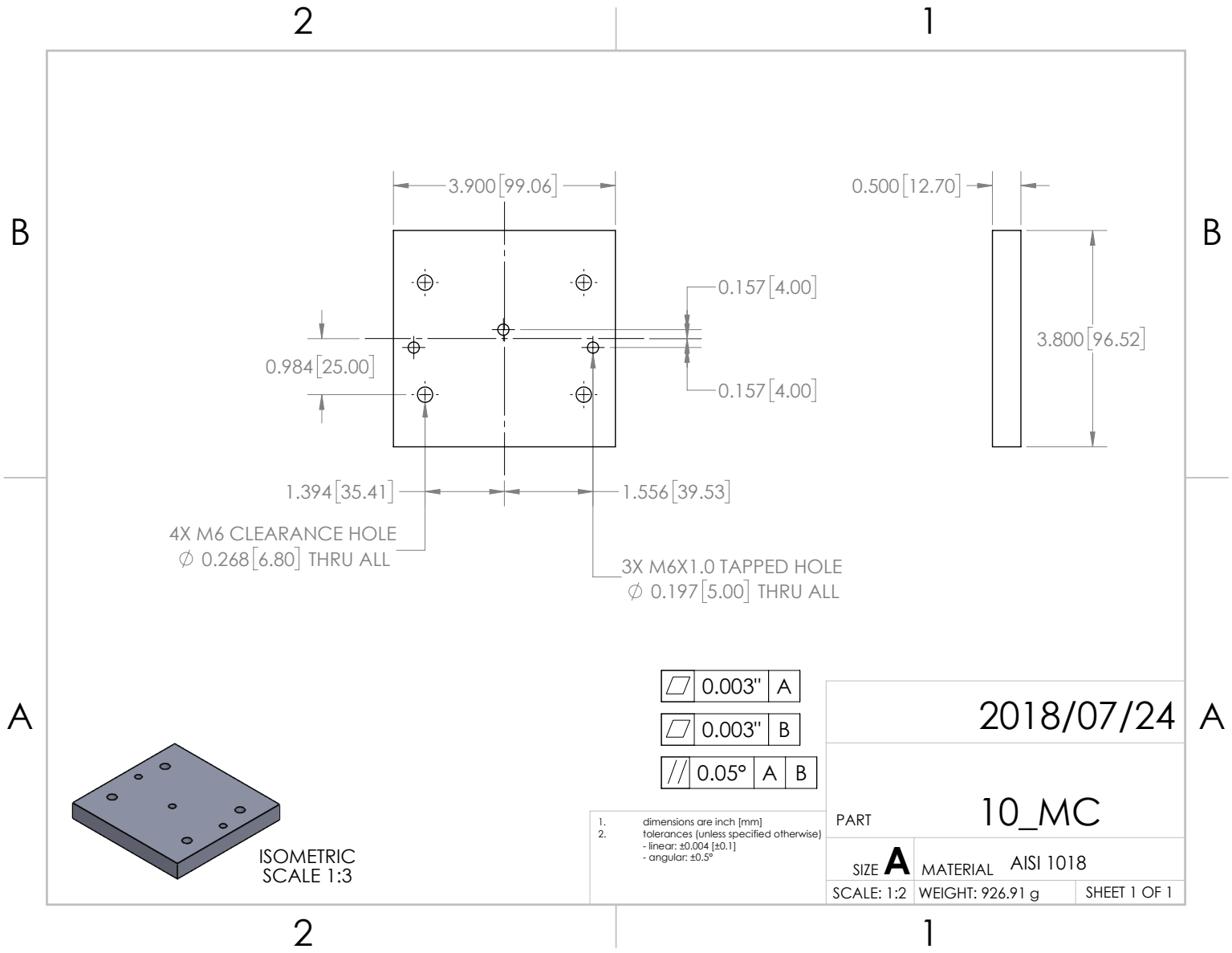

Figure A.13. Fixture plate between the fixture arm (09_MC) and the actuator.

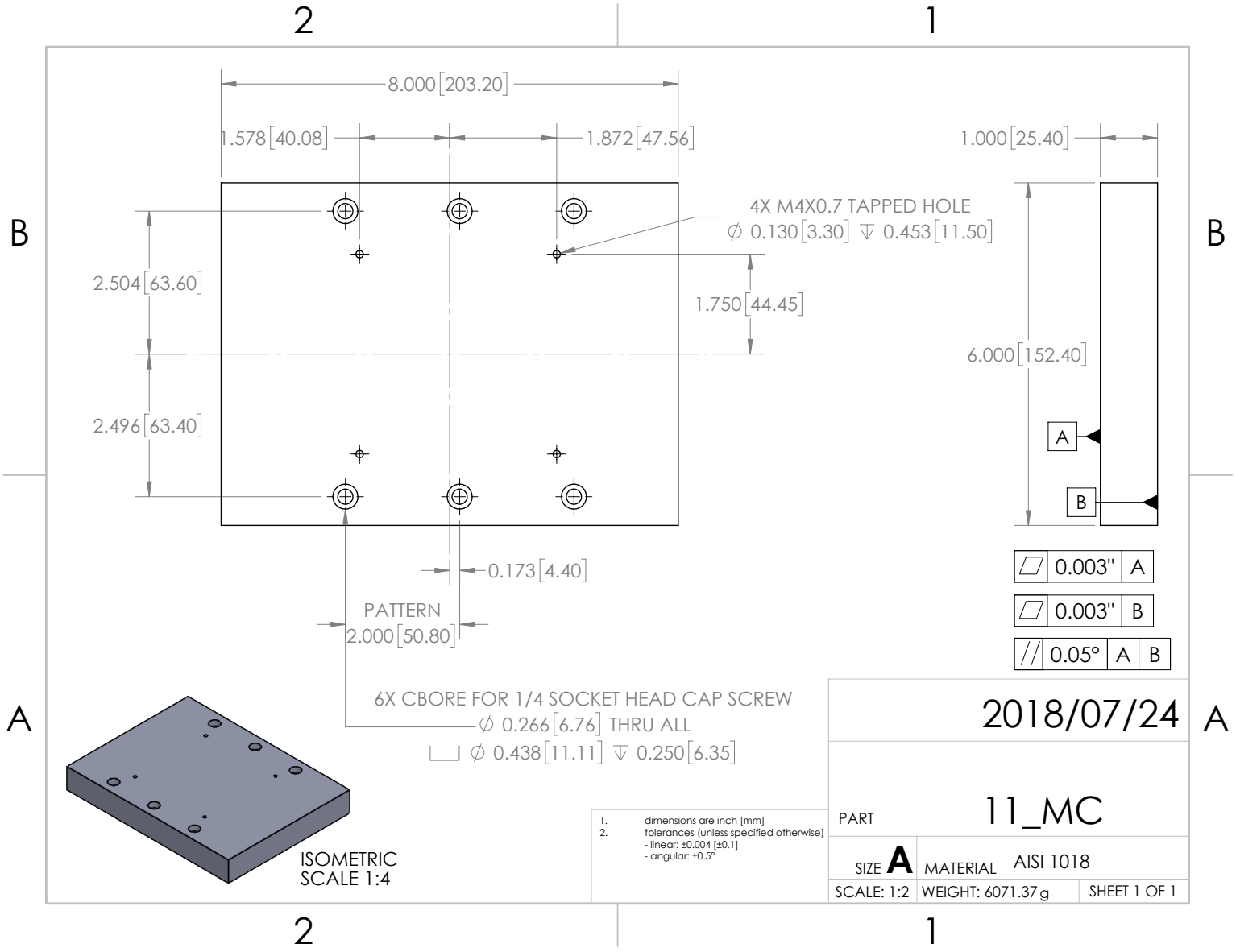

100

Figure A.14. Base plate for mounting the actuator to the optical table.

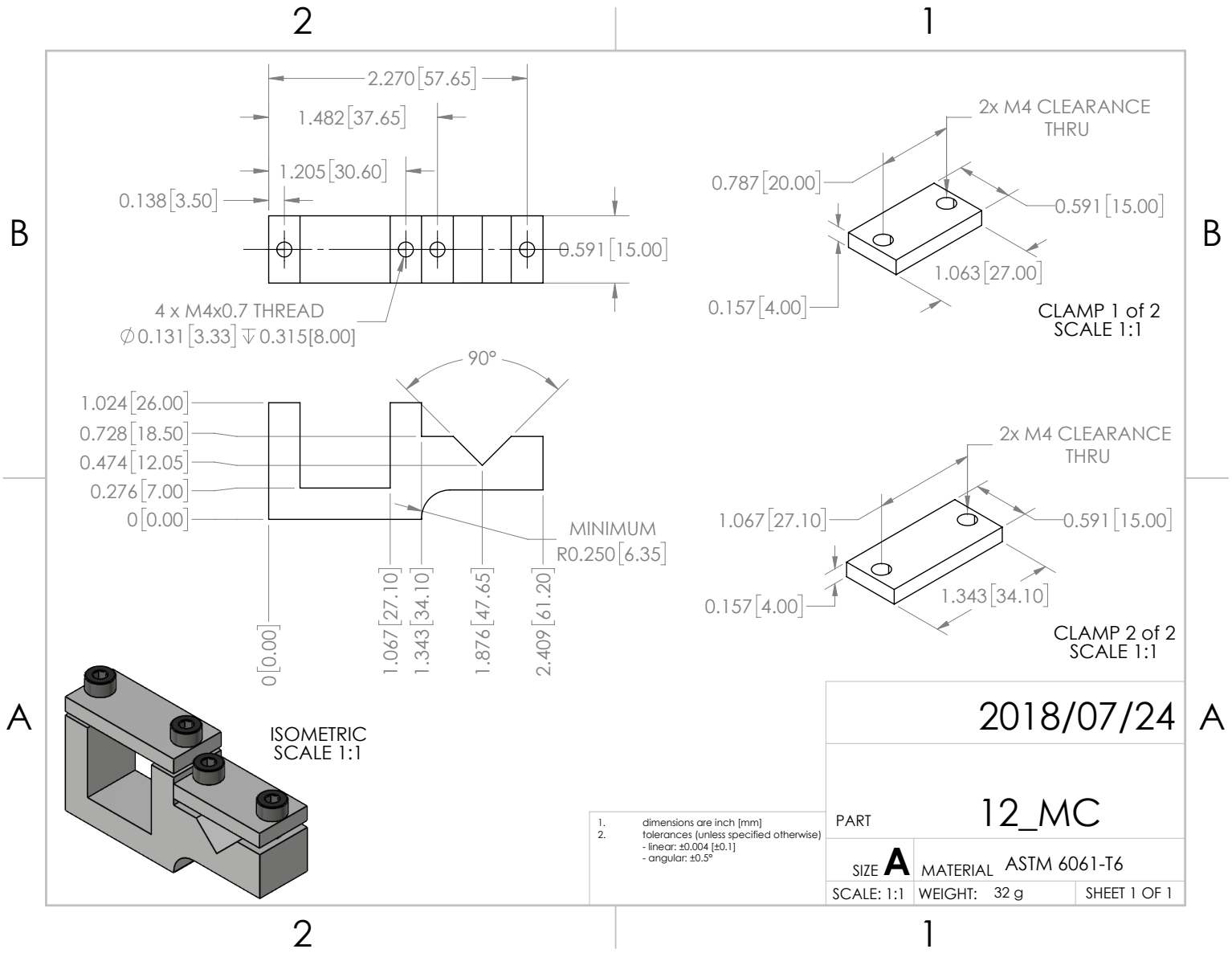

Figure A.15. Fixture assembly for clamping the capacitance sensor and target (13_MC).

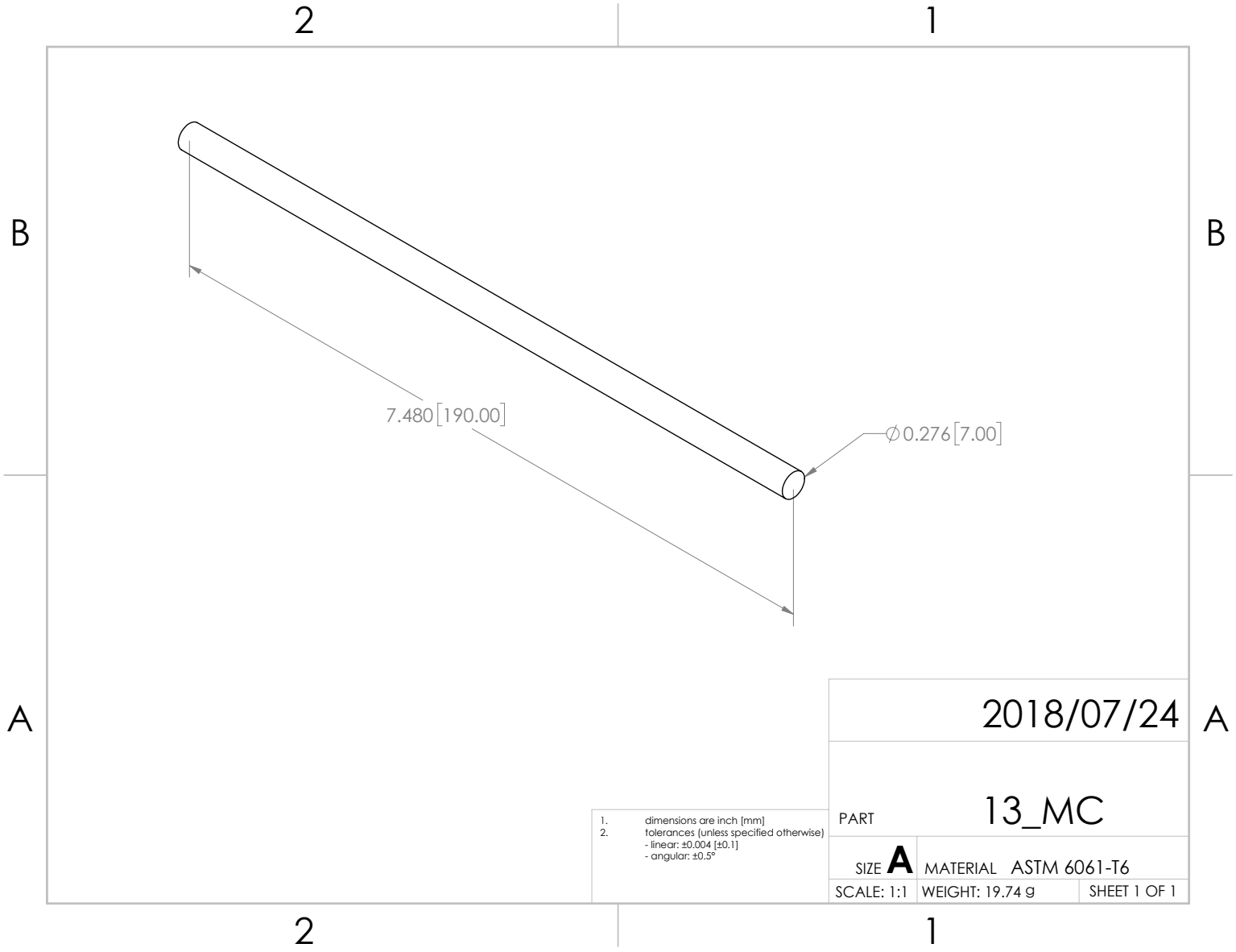

Figure A.16. Target for the capacitance sensor.

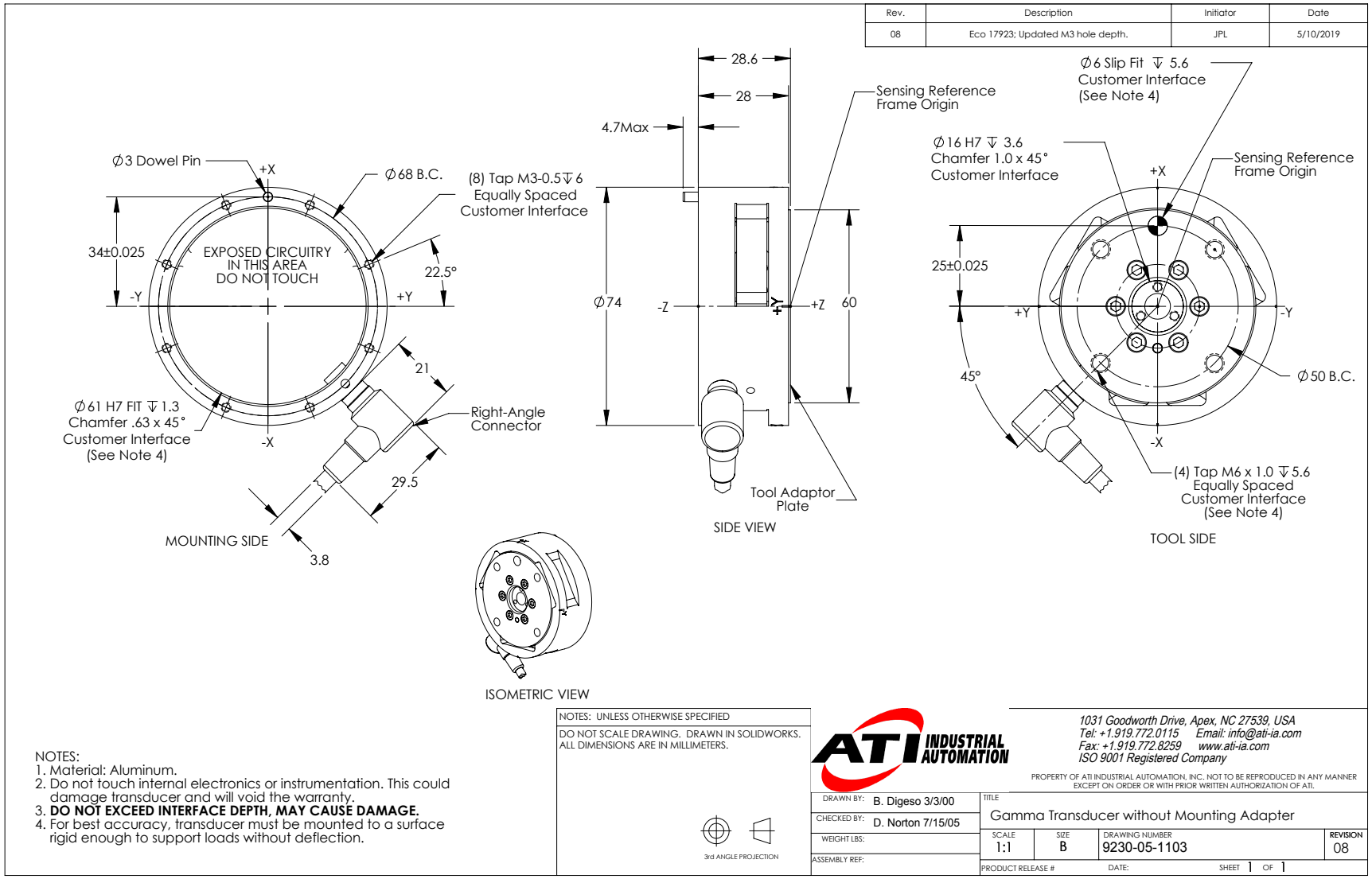

Figure A.17. 6-axis load cell, manufacturer part number 9105TIFGAMMA. Drawing courtesy of ATI Industrial Automation, Inc [19].

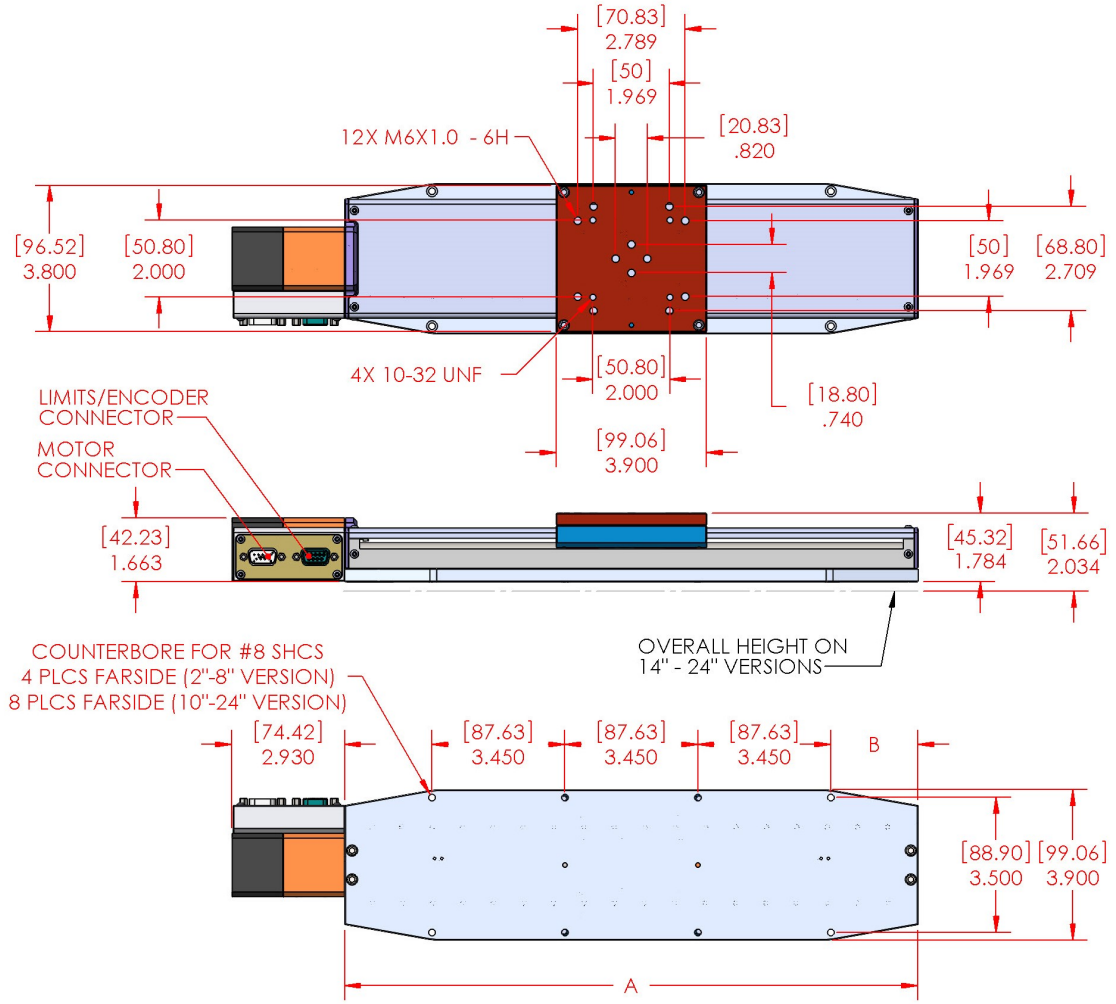

TRAVEL	DIM "A"	DIM "B"
2	[176] 6.950	[44.45] 1.750
4	[225.43] 8.875	[68.90] 2.713
6	[276.23] 10.875	[94.30] 3.713
8	[327.03] 12.875	[119.70] 4.713
10	[377.83] 14.875	[57.47] 2.263
12	[428.63] 16.875	[82.87] 3.263
14	[479.43] 18.875	[108.27] 4.263
16	[530.23] 20.875	[133.67] 5.263
20	[631.83] 24.875	[184.47] 7.263
24	[733.43] 28.875	[235.27] 9.263

Figure A.18. Stepper motor actuated linear stage, manufacturer part number NLS4211. Drawing courtesy of Newmark Systems [20].

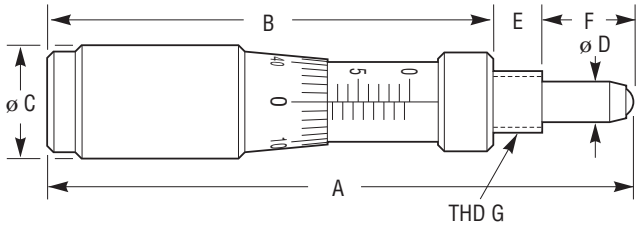

Dimensions [in. (mm)]									Thread
Model	**A**	**B** Min	**B** Max	**C**	**D**	**E**	**F** Min	**F** Max	**G**
BM11.5	1.36 (34.5)	1.00 (25.5)	1.20 (30.5)	0.43 (11)	0.16 (4)	0.13 (3.2)	0.03 (0.8)	0.23 (5.8)	M6 x 0.50
BM11.10	2.01 (51)	1.40 (35.5)	1.79 (45.5)	0.43 (11)	0.16 (4)	0.19 (4.7)	0.03 (0.8)	0.43 (10.8)	M6 x 0.50
BM11.16	2.24 (57)	1.40 (35.5)	2.03 (51.5)	0.43 (11)	0.16 (4)	0.19 (4.7)	0.03 (0.8)	0.66 (16.8)	M6 x 0.50
BM11.25	3.00 (76.2)	1.81 (46)	2.80 (71)	0.43 (11)	0.16 (4)	0.19 (4.7)	0.02 (0.5)	0.98 (25)	M6 x 0.50
BM17.25	3.25 (82.5)	1.95 (49.5)	2.93 (74.5)	0.67 (17)	0.28 (7.2)	0.28 (7.2)	0.03 (0.8)	1.01 (25.8)	M12 x 0.50
BM17.51	5.43 (138)	3.04 (77.1)	5.04 (128.1)	0.67 (17)	0.28 (7.2)	0.28 (7.2)	0.09 (2.4)	2.10 (53.4)	M12 x 0.50
BM25.40	4.92 (125)	2.72 (69)	4.29 (109)	0.98 (25)	0.31 (8)	0.57 (14.5)	0.12 (3)	1.69 (43)	M18 x 1.00
BM25.63	6.79 (172.5)	3.70 (94)	6.18 (157)	0.98 (25)	0.31 (8)	0.57 (14.5)	0.04 (1)	2.52 (64)	M18 x 1.00
BM32.80	8.35 (212)	4.17 (106)	7.32 (186)	1.26 (32)	0.47 (12)	0.94 (24)	0.08 (2)	3.23 (82)	M22 x 1.00

Newport

Figure A.19. Adjustment screw for manual stage, manufacturer part number BM17.51. Drawing courtesy of Newport Corporation [21].

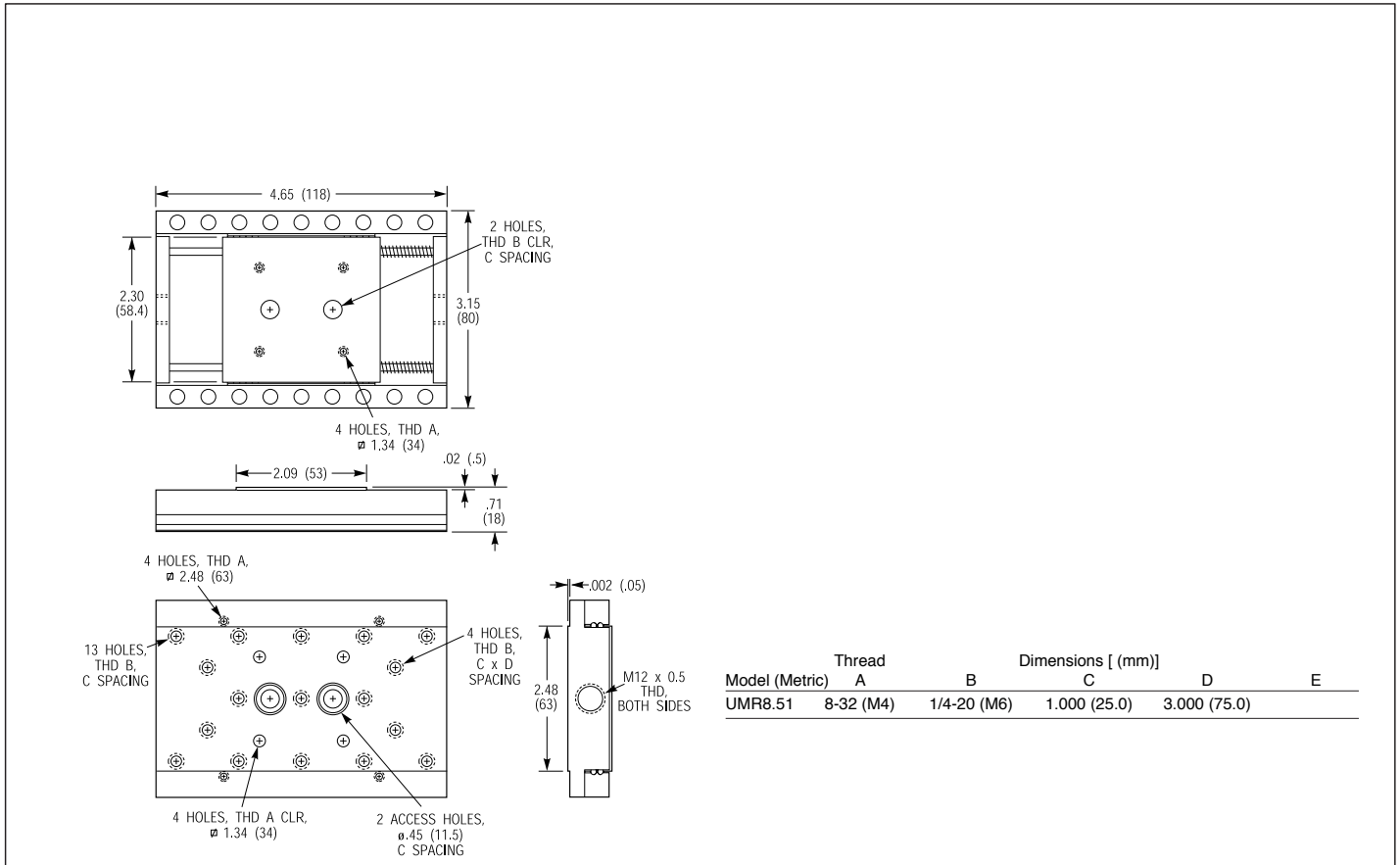

	Thread	Dimensions [(mm)]			
Model (Metric)	A	B	C	D	E
UMR8.51	8-32 (M4)	1/4-20 (M6)	1.000 (25.0)	3.000 (75.0)	

Figure A.20. Manual linear stage, manufacturer part number MUMR8.51. Drawing courtesy of Newport Corporation [22].

A.5 Operator's Manual 90ish % finished

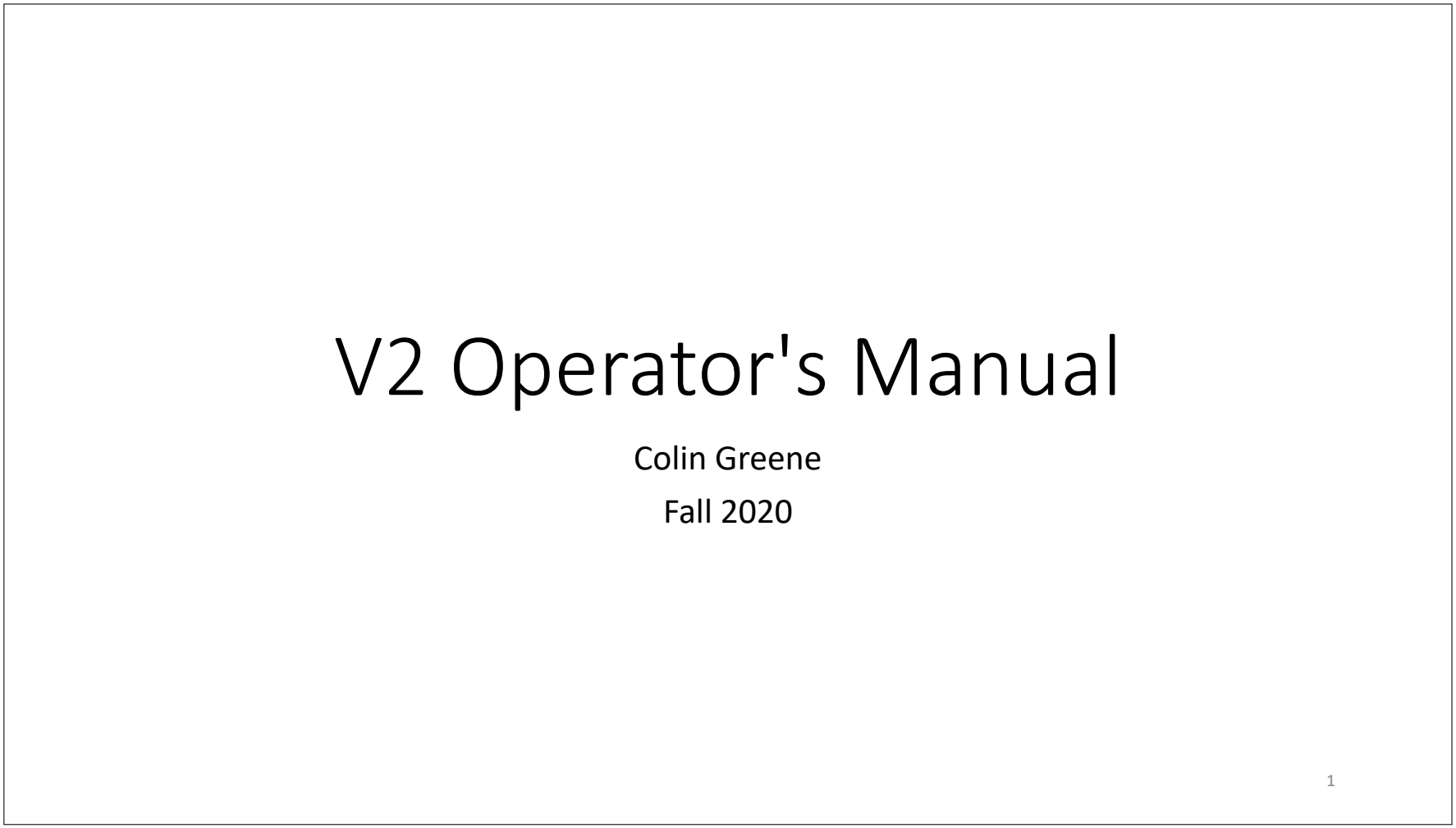

Figure A.21. The micro-precision tester operator's manual, which includes instructions for all tasks associated with testing a solder sample.

This manual is intended to give instructions on every procedure used to test a solder sample in the second micro-precision mechanical tester (V2).

The first page of each section presents the instructions without much detail.

The following pages elaborate on steps that may require more detail.

Table of Contents

LabVIEW Overview

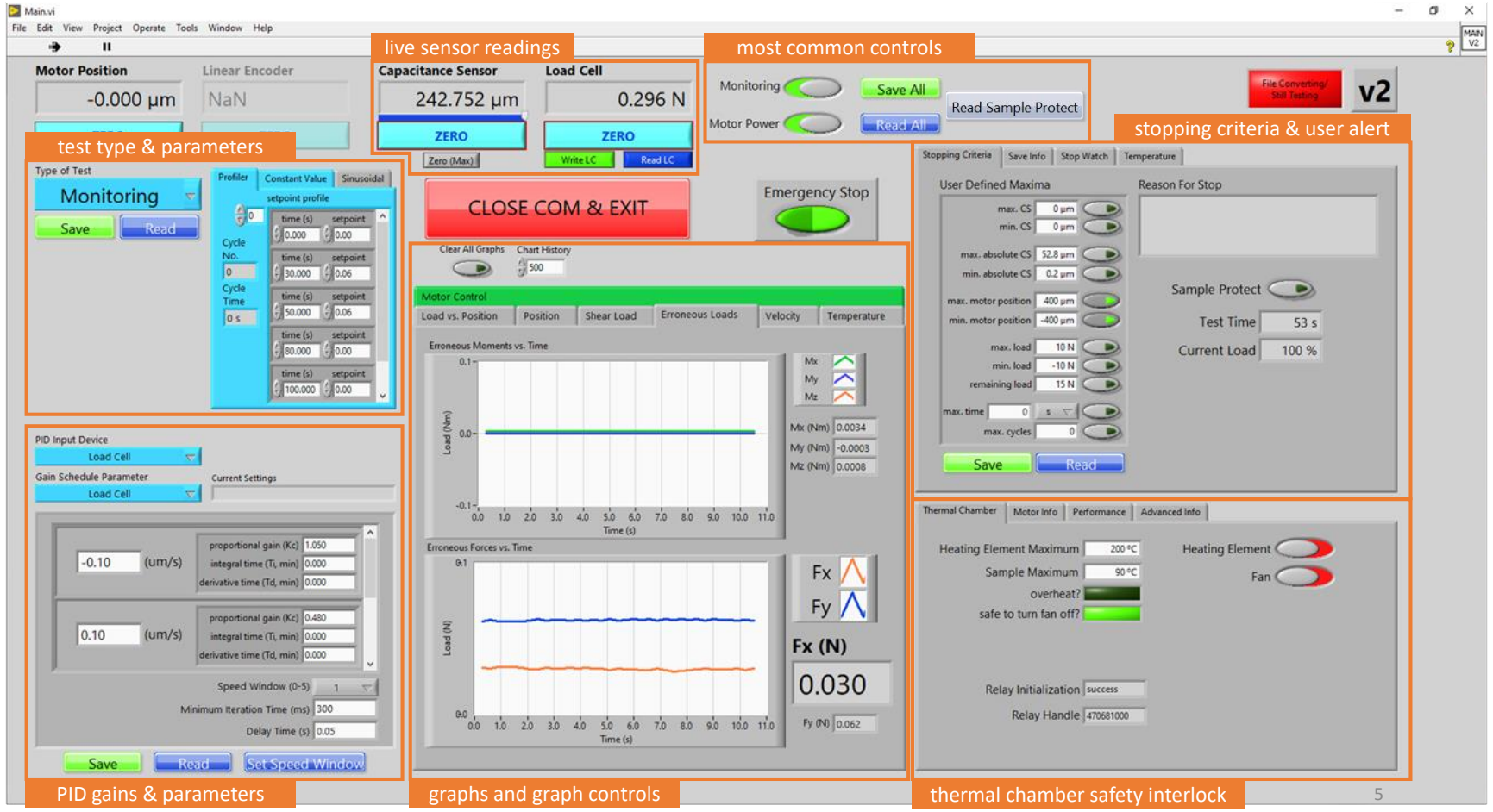
live sensor readings
most common controls
test type & parameters
stopping criteria & user alert
PID gains & parameters
graphs and graph controls
thermal chamber safety interlock
Motor Position
-0.000 µm
Linear Encoder
NaN
Capacitance Sensor
242.752 µm
ZERO
Zero (Max)
Load Cell
0.296 N
ZERO
Write LC
Read LC
Monitoring
Motor Power
Save All
Read All
Read Sample Protect
File Converting/ Still Testing
v2
CLOSE COM & EXIT
Emergency Stop
Type of Test
Monitoring
Save
Read
Profiler
Constant Value
Sinusoidal
setpoint profile
Cycle No.
Cycle Time
Clear All Graphs
Chart History
Motor Control
Load vs. Position
Position
Shear Load
Erroneous Loads
Velocity
Temperature
Erroneous Moments vs. Time
Mx
My
Mz
Mx (Nm) 0.0034
My (Nm) -0.0003
Mz (Nm) 0.0008
Load (Nm)
Time (s)
Erroneous Forces vs. Time
Fx
Fy
Fx (N)
0.030
Fy (N) 0.062
Load (N)
Time (s)
Stopping Criteria
Save Info
Stop Watch
Temperature
User Defined Maxima
max. CS 0 µm
min. CS 0 µm
max. absolute CS 52.8 µm
min. absolute CS 0.2 µm
max. motor position 400 µm
min. motor position -400 µm
max. load 10 N
min. load -10 N
remaining load 15 N
max. time 0 s
max. cycles 0
Save
Read
Reason For Stop
Sample Protect
Test Time 53 s
Current Load 100 %
PID Input Device
Load Cell
Gain Schedule Parameter
Load Cell
Current Settings
-0.10 (um/s)
proportional gain (Kc) 1.050
integral time (Ti, min) 0.000
derivative time (Td, min) 0.000
0.10 (um/s)
proportional gain (Kc) 0.480
integral time (Ti, min) 0.000
derivative time (Td, min) 0.000
Speed Window (0-5) 1
Minimum Iteration Time (ms) 300
Delay Time (s) 0.05
Save
Read
Set Speed Window
Thermal Chamber
Motor Info
Performance
Advanced Info
Heating Element Maximum 200 °C
Sample Maximum 90 °C
overheat?
safe to turn fan off?
Heating Element
Fan
Relay Initialization success
Relay Handle 470681000
5

Setting Up a Test: Overview

1. Start LabVIEW
2. Bolt in removable glue fixtures
3. Pre-set sample gap
4. **Zero load cell**
5. Hold sample with tweezers and place glue on sample
6. Lift load cell side and place sample on bottom fixture
7. Start glue test
8. Move the heat chamber into position
9. Turn on heater
10. Wait for temperature to reach steady-state
11. Adjust glue load to ~0.5 N

1. Start LabVIEW

a. Start the LabVIEW program (button in the top left)

b. Enter information in the popup window
   - Select your name
   - Type in the sample ID

c. Begin monitoring
   - The program defaults to a monitoring test

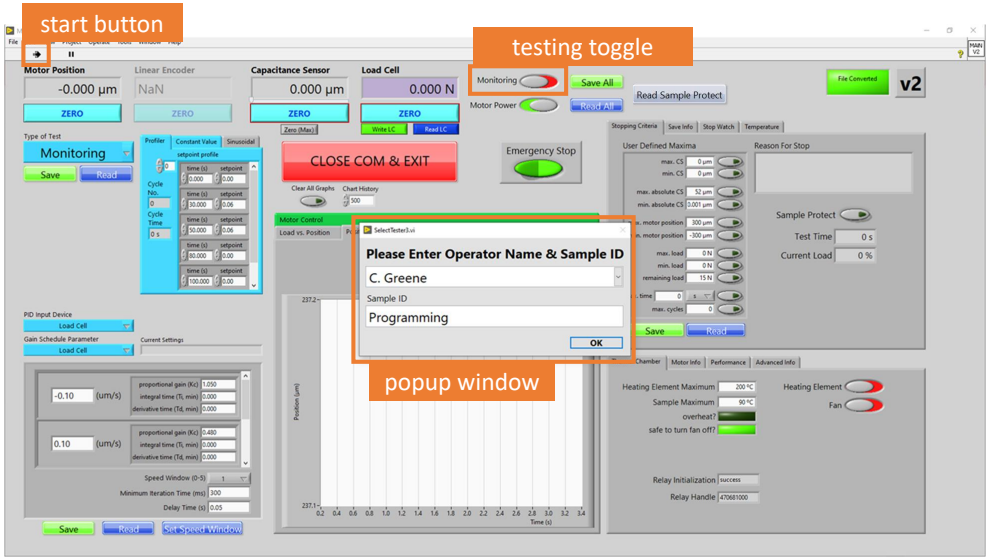

2. Bolt in removable glue fixtures

a. Tighten bolts lightly
b. Adjust manual stage to bring the glue fixtures close
c. Simultaneously squeeze the fixtures and fully tighten all bolts (this is to ensure parallelism of the glue fixture faces)

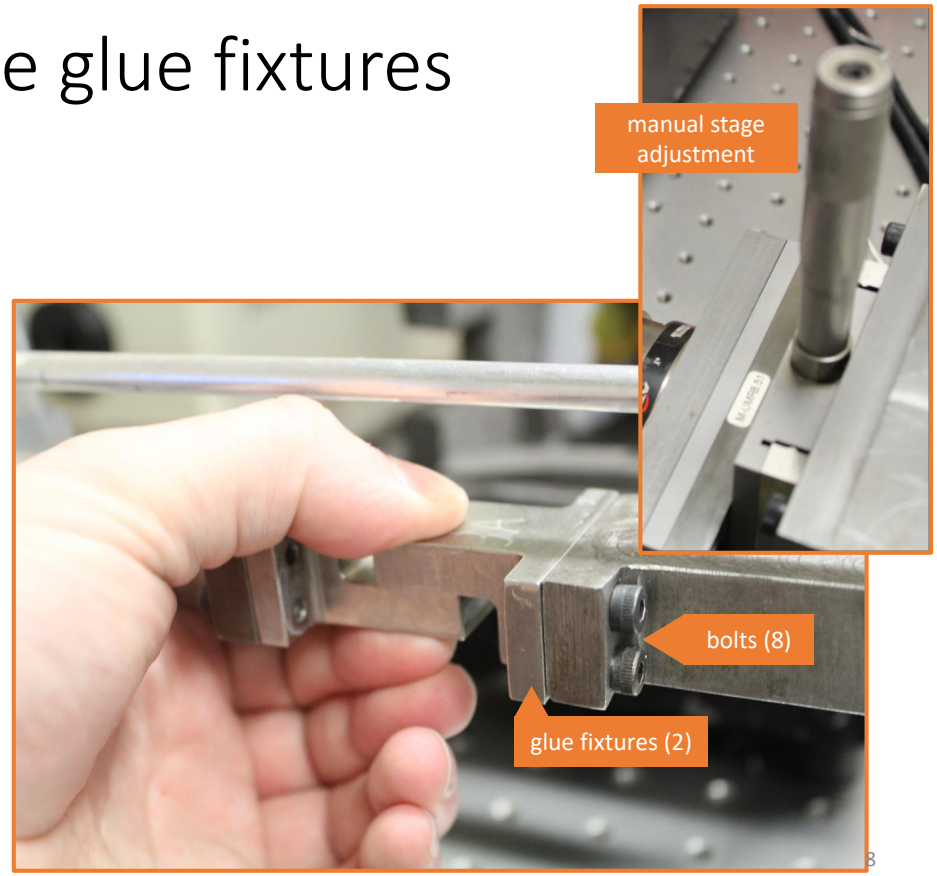

3. Pre-set sample gap

- Increase gap until the sample barely fits (a slight amount of friction will be felt)
- Do not decrease the gap with the sample inside, so as not to crush the sample

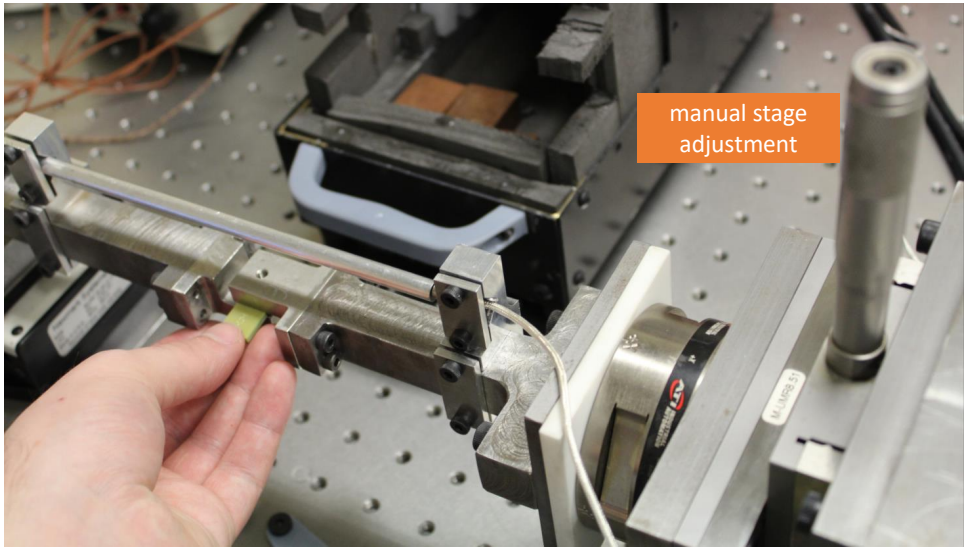

4. Zero load cell

- `ZERO` will zero the load cell and write to file
  - `write LC` will also write the zero to file
  - `read LC` will read the last written zero

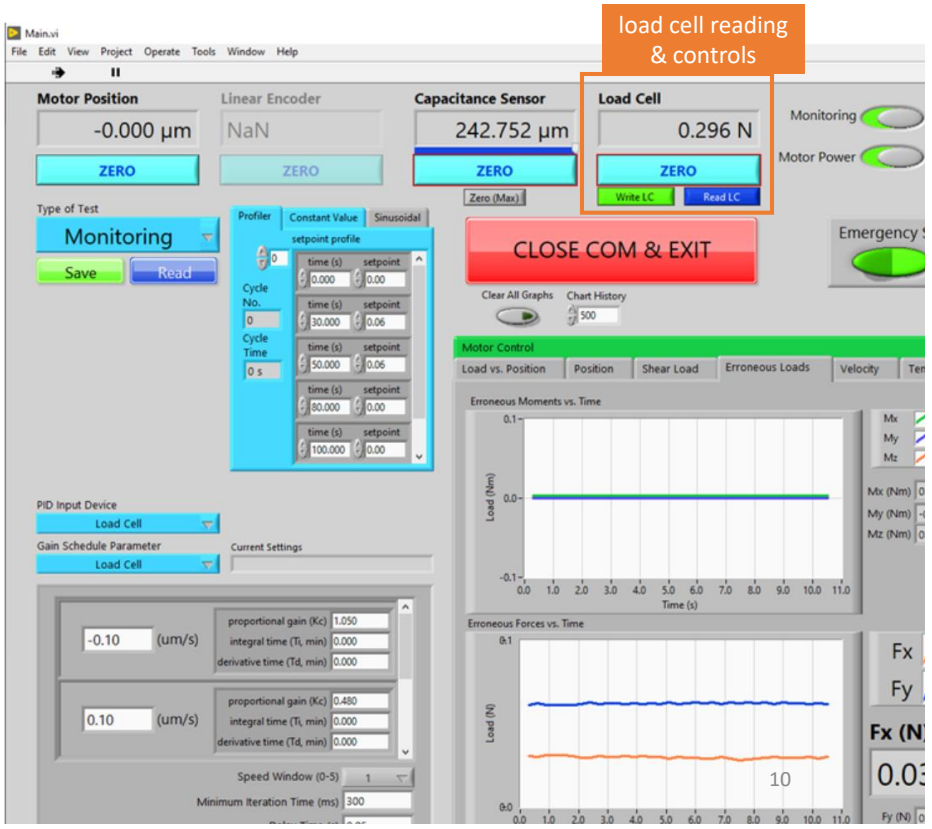

5. Hold sample with tweezers and place glue on sample

- Reverse tweezers recommended
- Only a small amount of glue is needed
- Use the glue with the purple cap, it cures more quickly

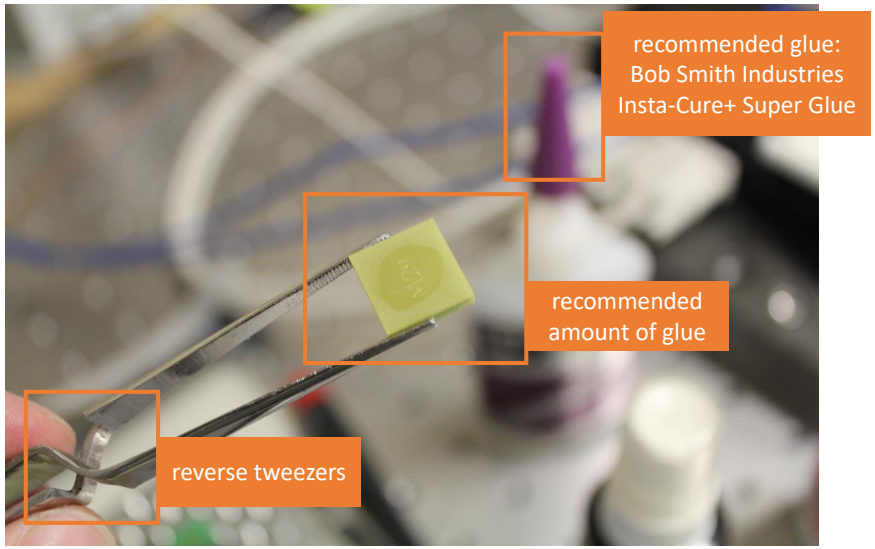

5. Lift load cell side and place sample on bottom fixture

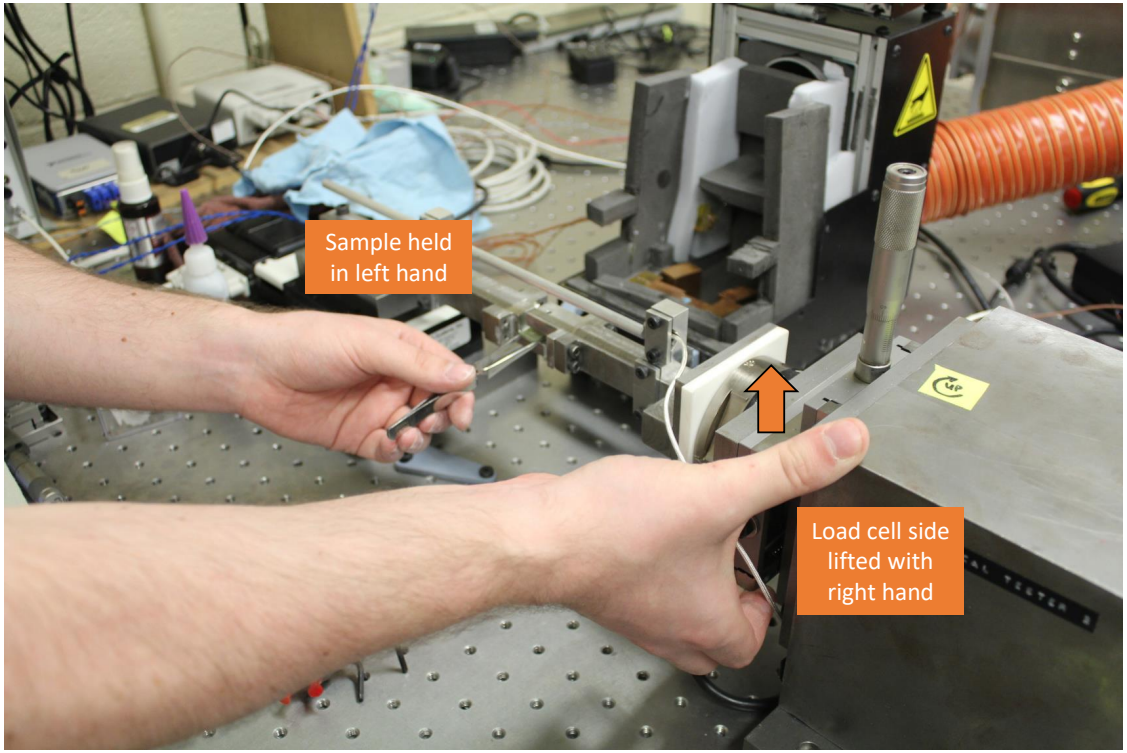

7. Run sample protect test

a. Set `Testing` switch to off

b. Press `Read Sample Protect`

   a. This loads the sample protect test parameters

c. Restart test

d. Let the glue spread for ~1 min (2-5N)

e. Reduce Fx to 0.2-1N after glue spreads thin

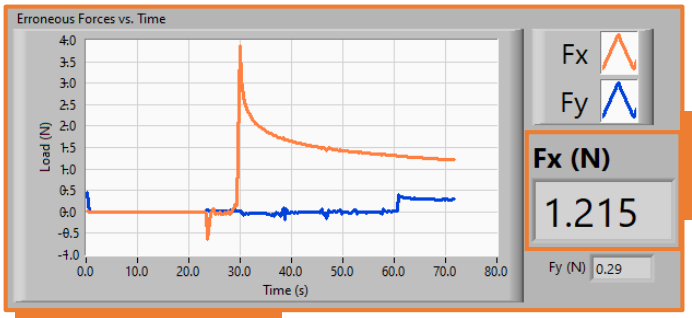

Fx is the compressive force on the glue

the glue spreading thin will look similar to this

8. Move the heat chamber into position

- Slide the chamber into position
- The chamber should not contact the tester. Contact will be visible on the erroneous forces plot.

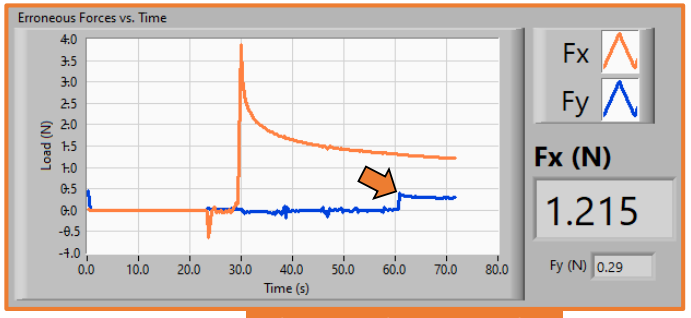

bumping the tester with the heating chamber will be visible on the plot

9. Turn on heater

a. in LabVIEW, turn on fan and heating element

b. on the heater control box, flip switch labeled `PID` on

c. set correct setpoint
   - press `MENU` once
   - press `MIN` to move between digits
   - press `MAX` to change the digit
   - press `MIN` twice to reset the controller with new setpoint

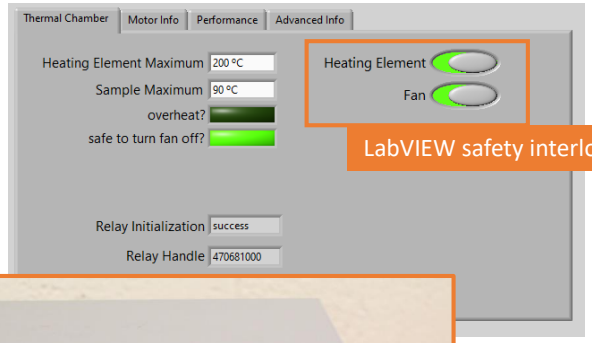

LabVIEW safety interlocks

heater control box

10. Wait for temperature to reach steady-state

- Recommend minimum
  - 30min for 30°C test
  - 60min for 75°C test

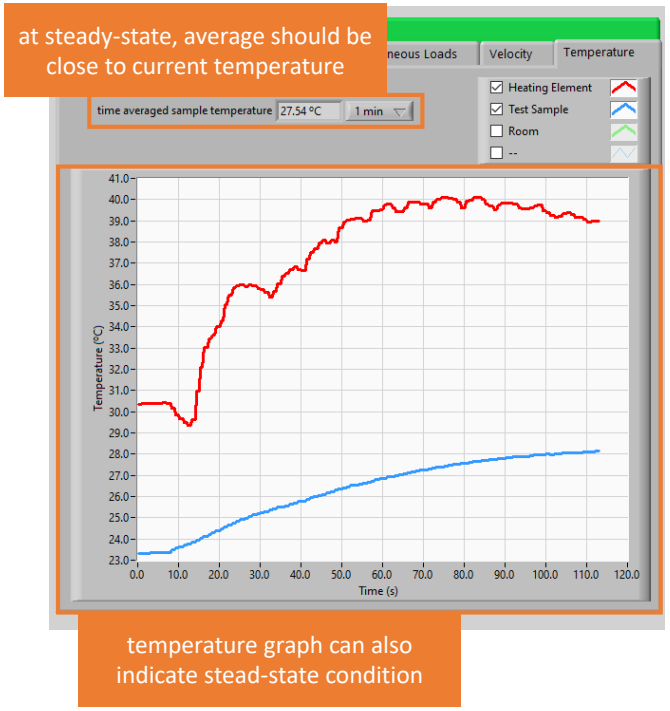

11. Adjust glue load (Fx) to ~0.5 N

- While heating, the glue load usually drifts, so we correct it before starting the test

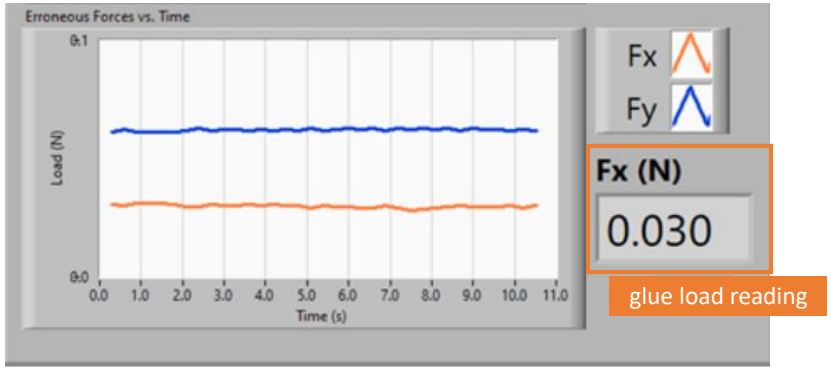

Running a Test: Overview

0. Set up test
1. Adjust capacitance sensor
2. Load appropriate test profile
3. Start test
4. Request alert (if desired)
5. PID tune as required

1. Adjust capacitance sensor

- Adjust aluminum target while watching CS reading
  (this gets easier with practice)
  - Creep/monotonic: ~10-20 µm (lower 10% of range)
  - Fatigue: ~100 µm (50% range)
- Tighten bolts *moderately*
  - Do not undertighten and try to be consistent between bolts

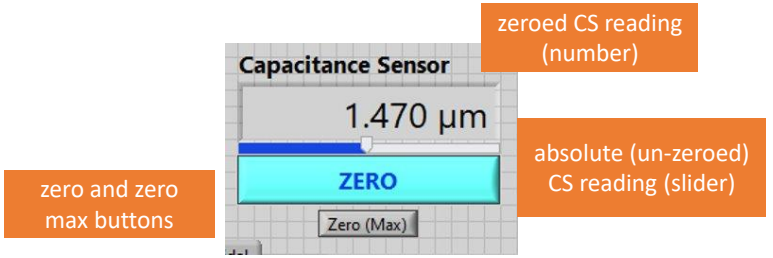

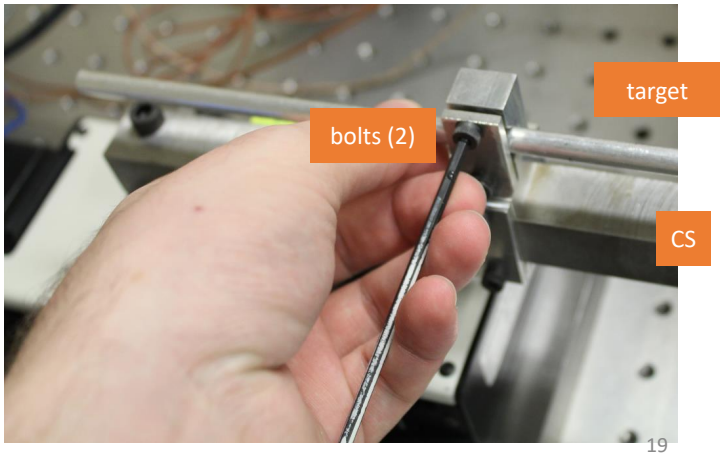

2. Load appropriate test profile
3. Start test

a. Press the `Read All` button
   - This is a shortcut for pressing the `read` buttons for test type, PID, and stopping criteria individually
   - Alternatively, load each individually

b. Toggle `Testing` slider to start test
   - Tests automatically turn off when using any `read` button

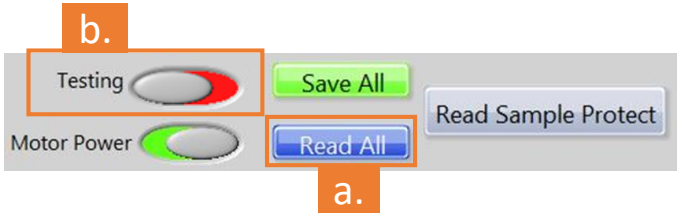

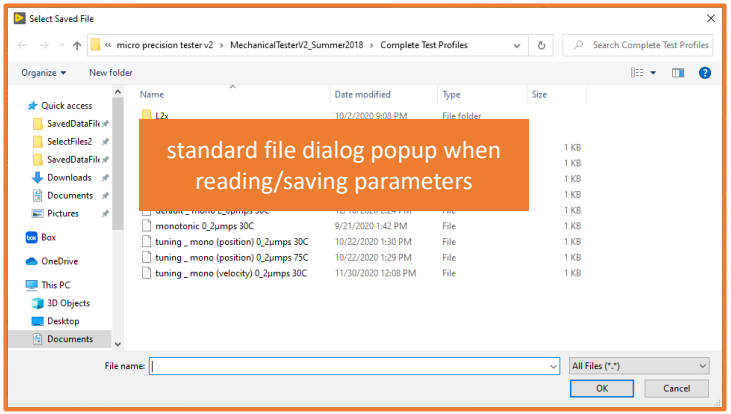

4. Request alert (if desired)

5. PID tune as required

- Request a text alert for when the test ends, if desired
  - To send alerts, the setting 'Less secure account access' for hidaclabs@gmail.com must be turned on.
- See the PID tuning section for instructions on how to PID tune and what constitutes a good test

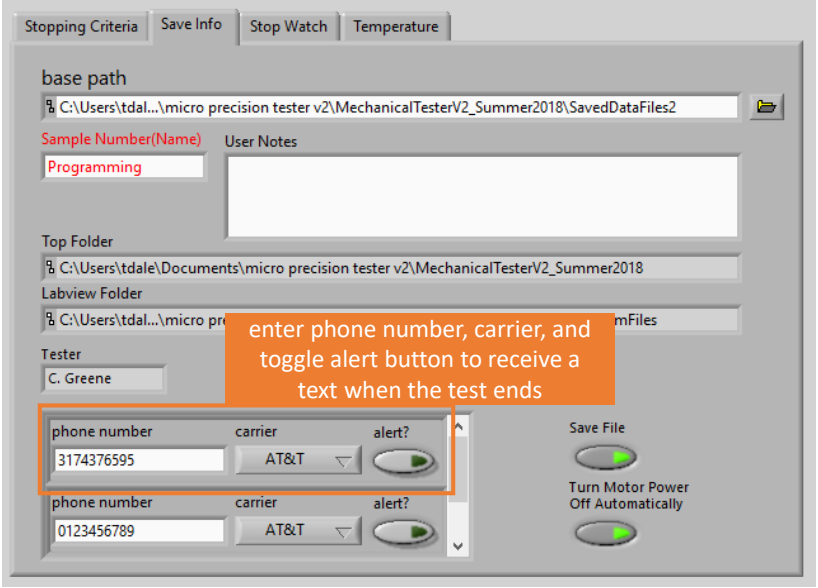

Ending a Test: Overview

0. A stopping criteria has been met and tester is running a 'sample protect' test
1. Check if sample is at room temperature and load is near zero
2. Optionally, preserve sample with glue
3. Wait for glue to cure
4. Remove sample
5. End test
6. Close LabVIEW program
7. De-glue

0. A stopping criteria has been met and tester is running a 'sample protect' test

- A 'sample protect' test is simply a creep test with a setpoint of 0 N.

  This is to prevent additional damage to the sample.

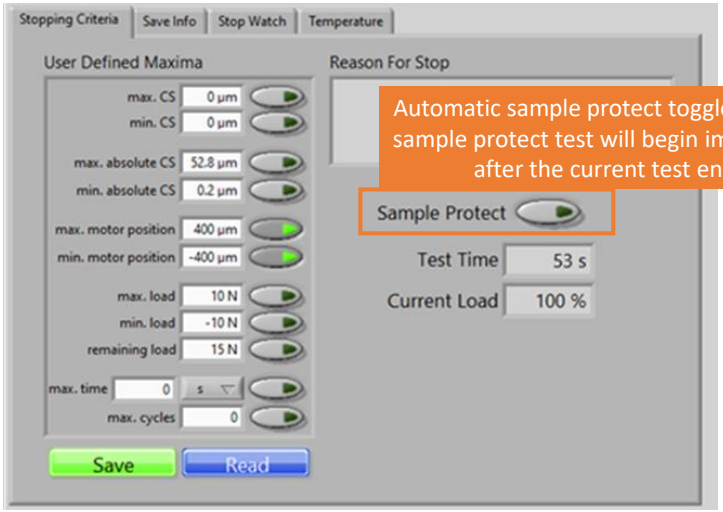

2. Optionally, preserve sample with glue
3. Wait for glue to cure
4. Remove sample

This step is only required if preserving sample for SEM or other type of additional analysis.

a. Cover table area with cloth
b. Spray sample with accelerator
c. Glue fixtures together
   - The goal is to prevent unscrewing forces from further damaging sample
d. Wait for glue to cure
   - 10-20 min recommended
e. Unscrew bolts and remove glue fixtures & sample together

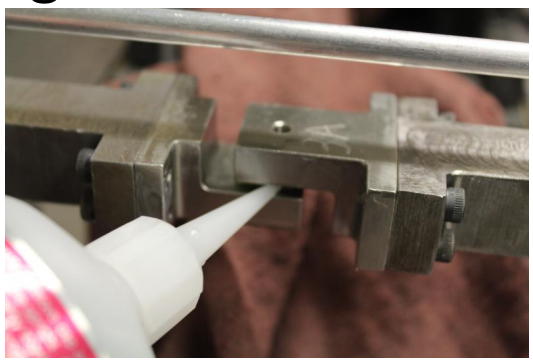

steps a-c

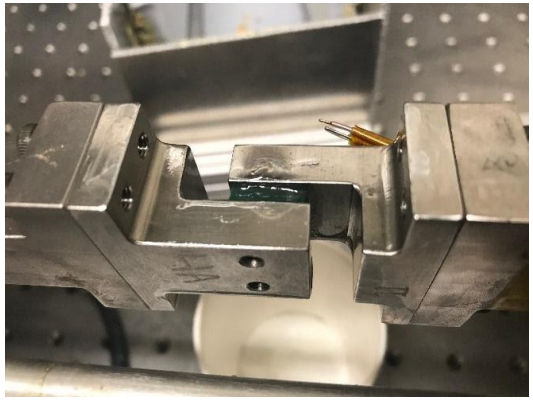

fixtures glued together

5. End test
6. Close LabVIEW program

a. End test

b. Close LabVIEW program
   - Press `CLOSE COM & EXIT`
   - If the heater is unsafe to shut off, the program will not close
   - If the test data has not been recorded, the program will give an 'are you sure?' Prompt

7. De-glue

a. Dissolve glue with acetone
   - Recommend 20-24 hr
b. Rinse with alcohol
   - Recommend an hour
c. Let alcohol evaporate

- Note: be extra careful when preserving samples, so as not to introduce additional damage

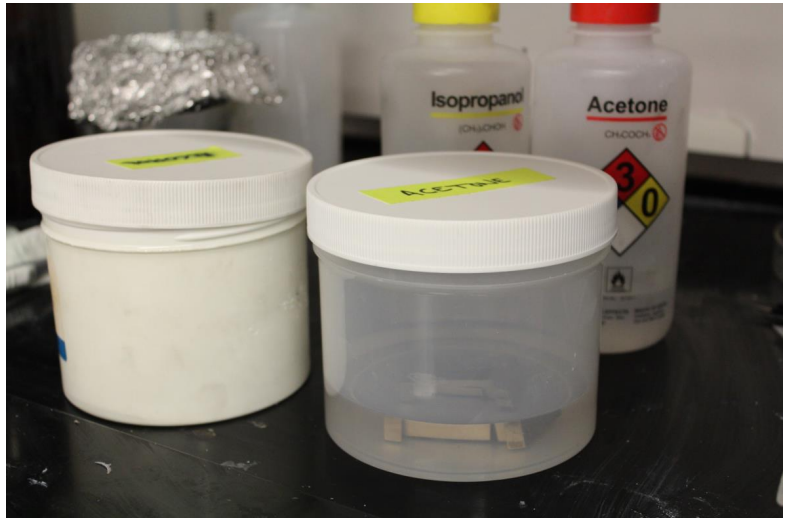

PID Tuning

PID Tuning: Monotonic

- I have had good luck with Kc in the range of 5-20
- In my opinion, 0.02 µm/s is too slow to do on this tester, stick with >= 0.2 µm/s
- Red lines shown in plots should be considered the goal

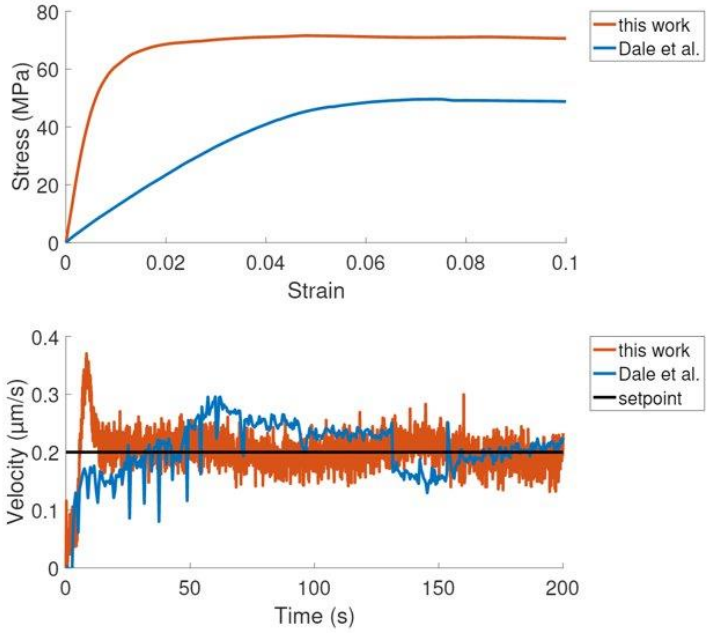

PID Tuning: Creep

- Creep tests are well tuned, unlikely to require further tuning
- Red line should be considered the goal
- Essentially, PID can keep the load within a ‘deadband’ where the motor is off

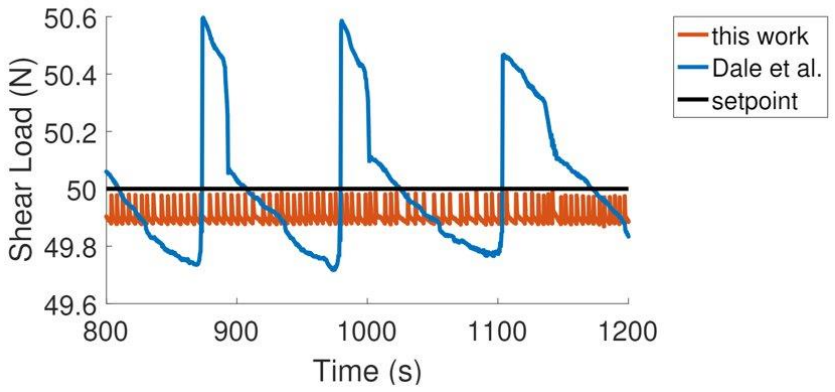

PID Tuning: Fatigue

Gain Schedule Theory:

- High gain at change from rise to dwell/dwell to fall to compensate for motor backlash
- Higher initial gain, while joint is strong and stiff
- Lower gain applied after joint begins to yield (how much to lower usually requires tweaking, especially when changing composition and temperature)
- Integral and derivative gains are a waste of both time and effort

PID Tuning: Fatigue

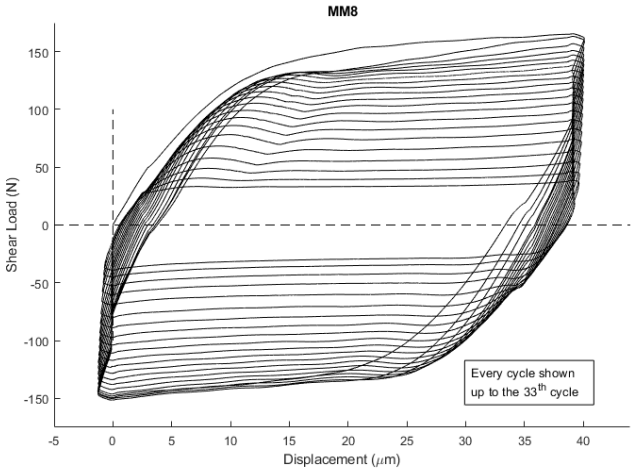

A well-tuned test

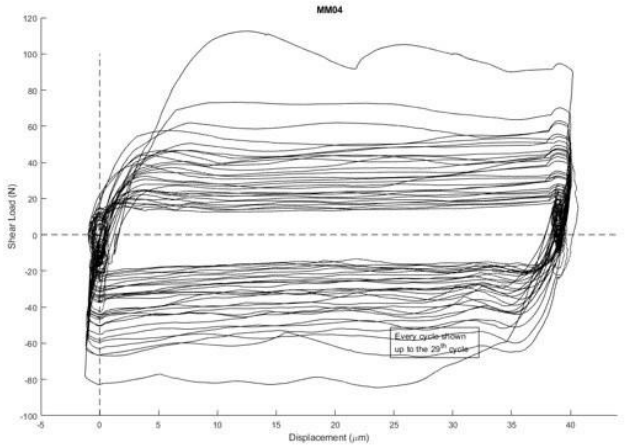

A poorly-tuned test,
especially the first cycle

PID Tuning: Fatigue

Looking at the well-tuned test's displacement profile, note

- Non-zero error, that is, perfection is not needed
- Overshoot, again, perfection not needed
- CS does not intersect setpoint line

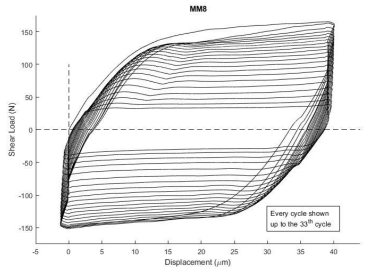

PID Tuning: Fatigue - Ramp

- High initial gain
- Cutover to lower secondary gain
- Very important to never cross setpoint line to ensure no backlash

Tunable parameters:

- Cutover time
- Secondary gain

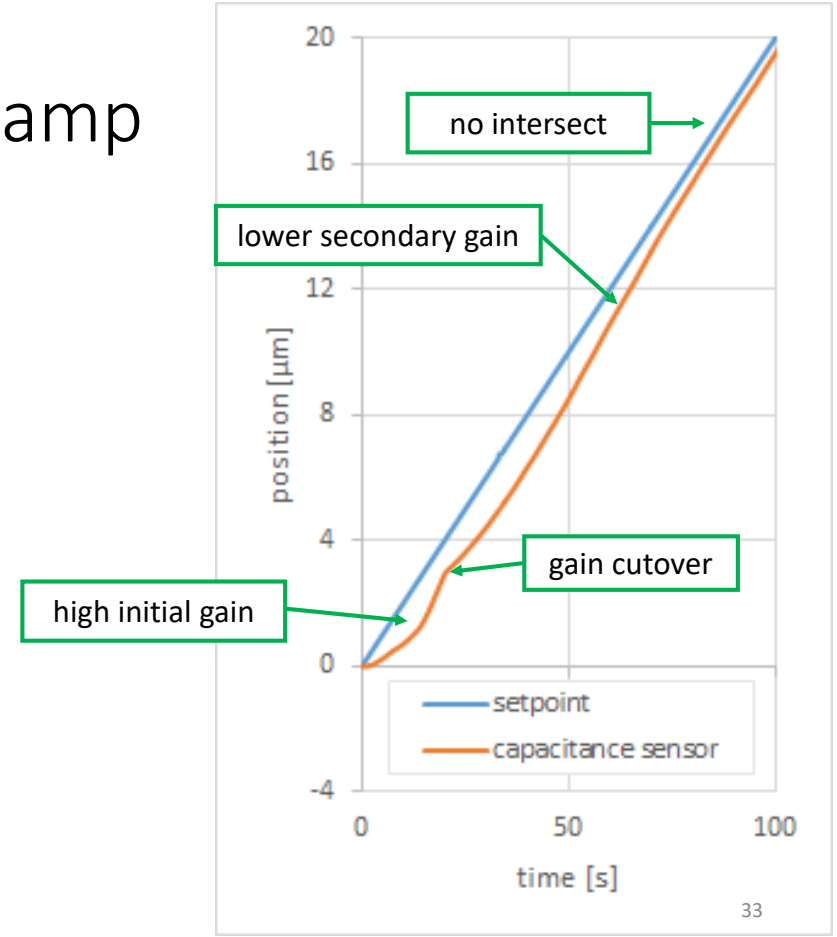

PID Tuning: Fatigue - Dwell

- High initial gain
- Cutover to lower secondary gain
- Very important to never cross setpoint line to ensure no backlash

Tunable parameters:

- Cutover time
- Secondary gain

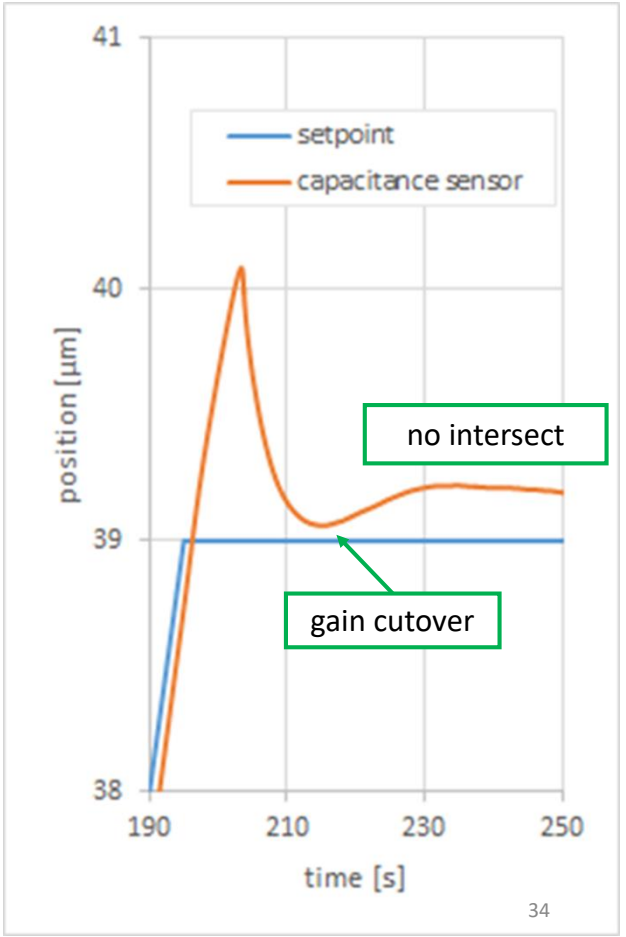

Labelling Samples

Labelling Samples: Overview

1. Determine the sample numbers to etch
2. Put on PPE (safety glasses, hearing protection)
3. Etch both sides of the sample (setting 2 is plenty)
4. Place samples back in storage

diamond tipped engraving tool

safety glasses

hearing protection

Aging Samples

Aging Samples: Overview

1. Preheat the oven
2. Select samples to age
3. Record the sample ids
4. Place the samples in the oven
5. After the correct duration has be reached, turn off the oven
6. Wait at least an hour for the samples to cool

1. Preheat the oven

To set the desired temperature on the oven:

a. Press `STOP`, `RUN`, then `MAN`
b. Press `4/VALUE` to until `SETPOINT` appears in the top display
c. Press `EDIT` to edit the setpoint
d. Use the number pad to enter the desired temperature
e. Press `ENTER` to confirm
f. Flip the `POWER` switch to on

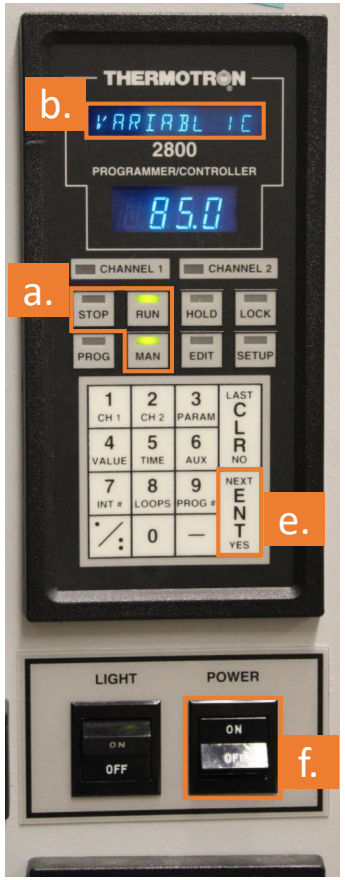

Aging Samples: Tips

- Place the samples on an aluminum plate to make the task of taking the samples in and out of the oven easier

- Do not handle hot objects without heat resistant gloves. Do not handle hot objects for longer than a few seconds.

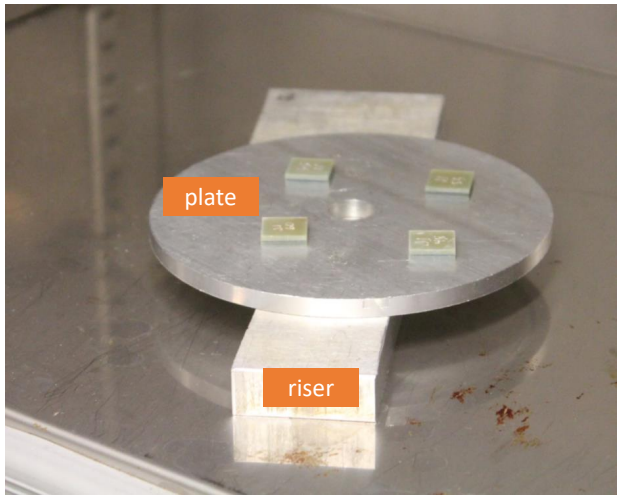

Miscellaneous Tasks

Adjusting the Z Gap

- Over the course of many tests, the "z gap" between the left and right halves of the tester increases until it cannot fit a sample
- To fix this, jog the stage back into position using the `Motor Control` tab
- Start the tester, set `Target` to +1000µm, and press `Move`
- Repeat as necessary
- At the end of this procedure, `zero` the motor position

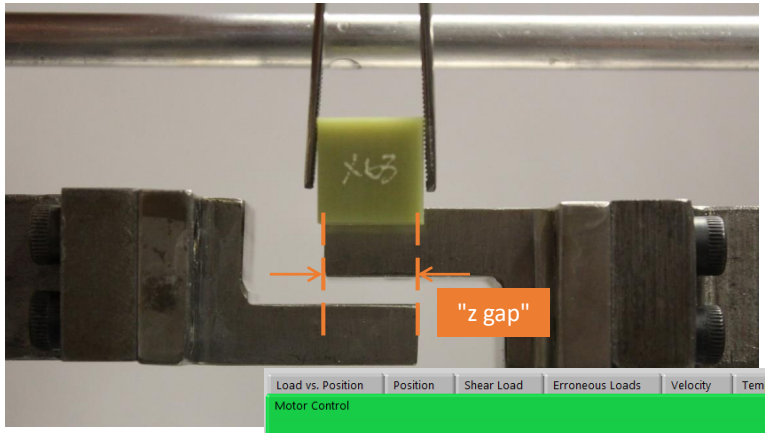

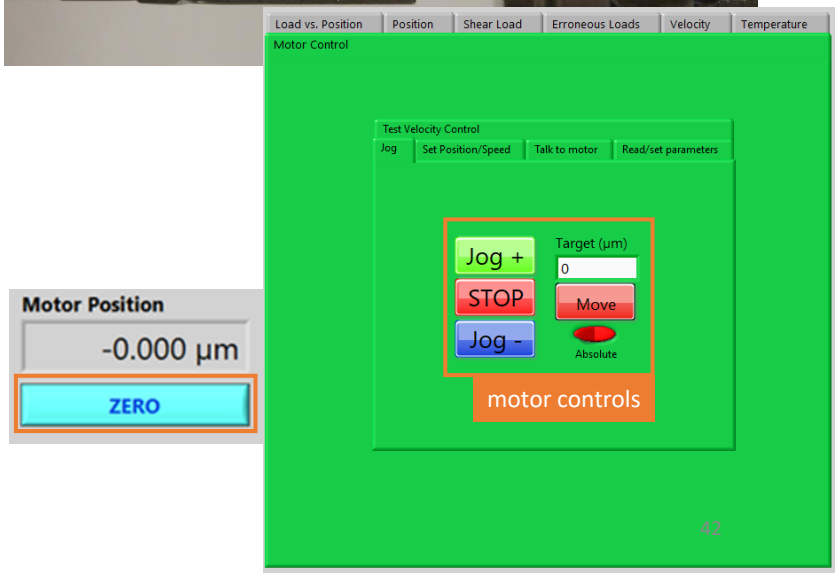

B. THE NANO-PRECISION MECHANICAL TESTER

B.1 General Operating Procedure

1. Start the LabVIEW program.
2. Fill in the information prompt. LabVIEW will give the user a prompt that asks for
   - operator information
   - sample ID
   - test parameters

   After this point, the program will enter a monitor state, where all the sensors are monitored, but no automatic commands are sent to the actuator.
3. Glue the sample to the first fixture. Wait at least 2 minutes for the glue to cure.
4. Attach the glue fixture (with sample) to the load cell with two M4 bolts.
5. If not installed, attach the capacitance sensor target to the load cell with an M4 bolt.
6. Zero the load cell. At this point, no additional dead weight will be placed on the load cell and the actuator side is not in contact with the load cell side.
7. Back the manual stage by $\sim$1 mm.
8. Apply glue to the exposed side of the sample.
9. Attach the second glue fixture to the actuator with two M4 bolts.
10. Using the manual stage's adjustment micrometer, bring the sample in contact with the second glue fixture. The glue load is F_y, which should be around 1 N.

11. Wait at least 10 minutes for the glue to cure.

12. Adjust the stage micrometer until the glue load is near 0 N, then lock the manual stage. This process may take some fiddling.

13. Manually jog the actuator in 0.01 µm increments until F_z is near zero.

14. Zero the capacitance sensor.

15. Start the test.

Additional notes:

For uni-directional tests, begin with the actuator at the bottom of its travel (0 µm). This is the default behavior of the LabVIEW program.

For bi-directional tests, such as cyclic loading, begin with the actuator near the center of travel. This adjustment must occur before step 10.

B.2 General Post-Processing Procedure

Test data is saved in `~\test data\sample ID\data.tdms` where `~` is the folder of the nano-precision tester. The name of the data file contains the sample ID, test type, and the date the data was recorded. The data is saved in National Instrument's `.tdms` file format. LabVIEW can natively manipulate this data but Hokanson's TDMS Reader is used to import the data into MATLAB [23].

After the test, LabVIEW will launch MATLAB, which will in turn load the data. The data will be stored in a struct with a format shown in Figure B.1. The data is divided into monitor, test, and sample protect data, where the test data contains the relevant data and the monitor and sample protect data serve to validate that the sample was tested correctly.

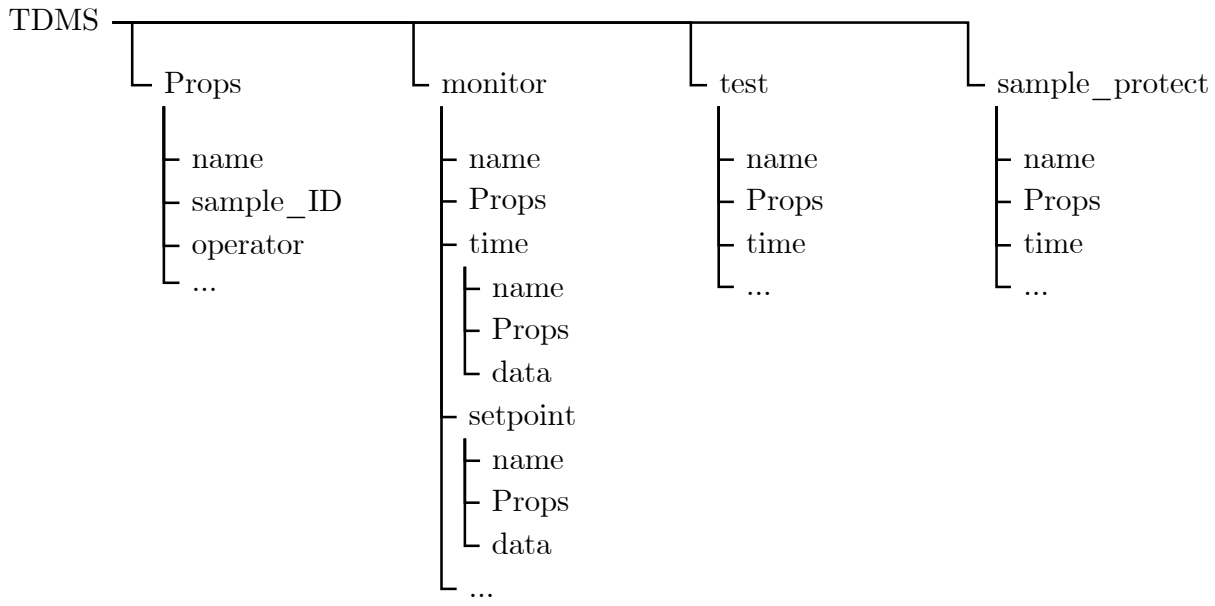

Figure B.1. The TDMS data structure used by the nano-precision tester.

Property sub-fields `X.Props` contain information about the field `X`. The `TDMS.Props` field contains the properties that apply globally, such as `operator` and `sample_ID`. Properties that apply to a specific test are stored in that test, e.g. `TDMS.sample_protect.Props`. Properties that apply to a single channel, such as dimensional units, are stored in `TDMS.test.channel.Props`

The sampled data is stored in the `.channel.data` field. For example, `TDMS.test.time.data` contains a vector of all sampling times and the MATLAB command `plot(TDMS.test.time.data, TDMS.test.Fz.data)` would plot load over time for the test.

B.3 List of Components

Table B.1. List of manufactured components.

Component	Vendor	Part Number	Quantity
CS MOUNT	manufactured in-house	n/a	1
CS TARGET			1
GLUE MOUNT			2
H BASE			1
LOAD MOUNT			1
LOAD RISER			1
STAGE MOUNT			1
STAGE RISER			1
V BASE			1

Table B.2. List of purchased components.

Component	Vendor	Part Number	Quantity
load cell			
transducer	ATI Industrial Automation, Inc	9105-TW-MINI40-E-1.8	1
driver		9105-IFPS-1	1
capacitance sensor			
driver	Lion Precision	CPL490	1
probe		2G-C8-1.2-E1-2.0	1
pizeo-actuator			
stage	PI USA (Physik Instrumente)	P-753.3CD	1
controller		E-625.CR	1
manual stage			
stage	Newport Corporation	M-UMR8.51	1
micrometer head		BM17.51	1
lock		CL12-51	1
optical table	Thorlabs, Inc.	T46HK	1
PCI DAQ	NI (National Instruments)	PCI-6220	2
thermocouple DAQ	NI (National Instruments)	NI-9211	1
bolts			
M2.5 x 0.45 - 8 mm	McMaster-Carr	91290A101	3
M2.5 x 0.45 - 20 mm		91290A108	3
M3 x 0.5 - 12 mm		91290A117	8
M4 x 0.7 - 16 mm		91290A154	4
M6 x 1.0 - 10 mm		91290A316	2
M6 x 1.0 - 20 mm		91290A326	8
M12 x 1.75 - 80 mm		91290A636	5
dowel pins			
1/4" x 1/2"	McMaster-Carr	98381A537	4
1/4" x 2"		98381A550	2

B.4 Manufacturing Drawings

The following appendix contains manufacturing drawings for the nano-precision tester. These are limited dimension drawings and do not necessarily contain all information required for manufacturing.

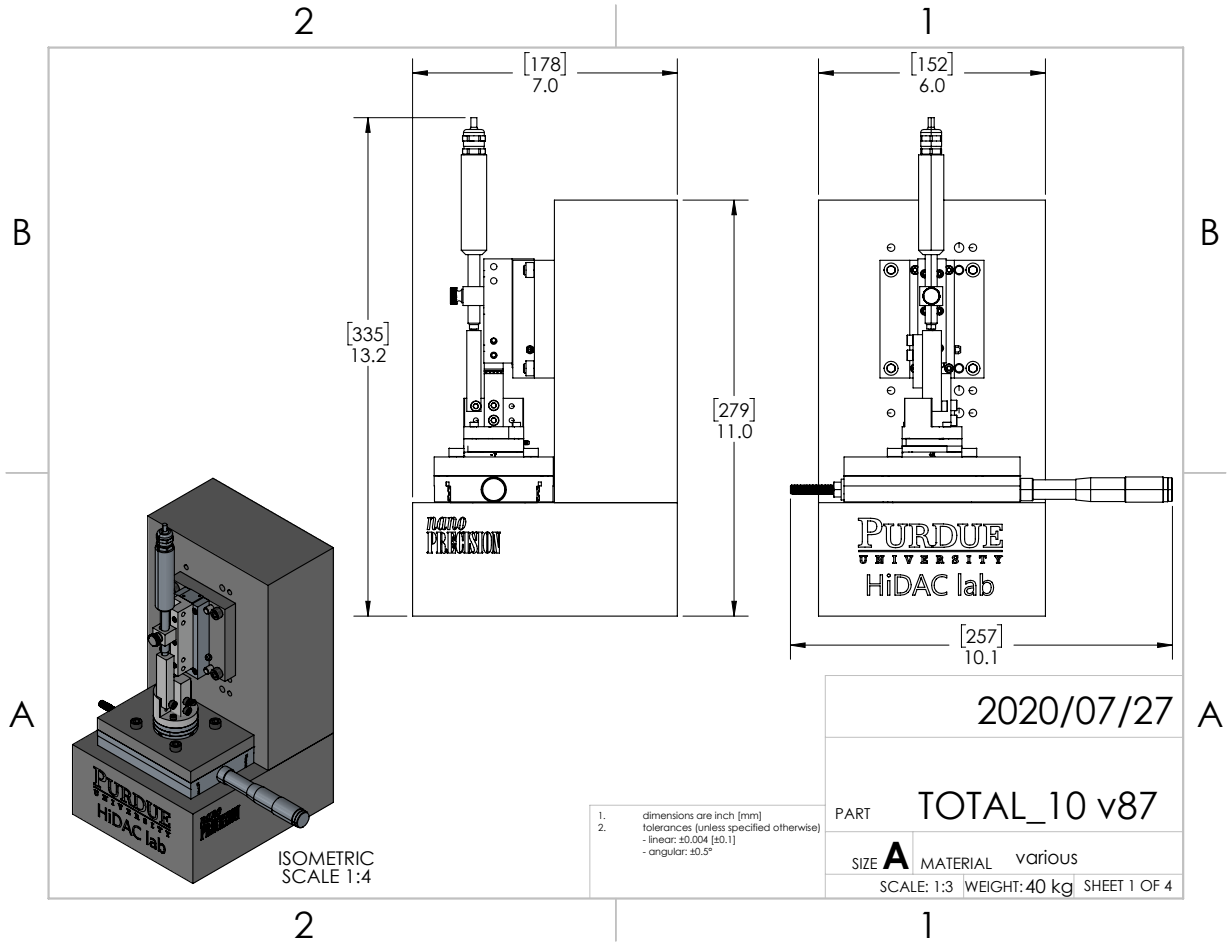

Figure B.2. Assembly drawing with selected dimensions.

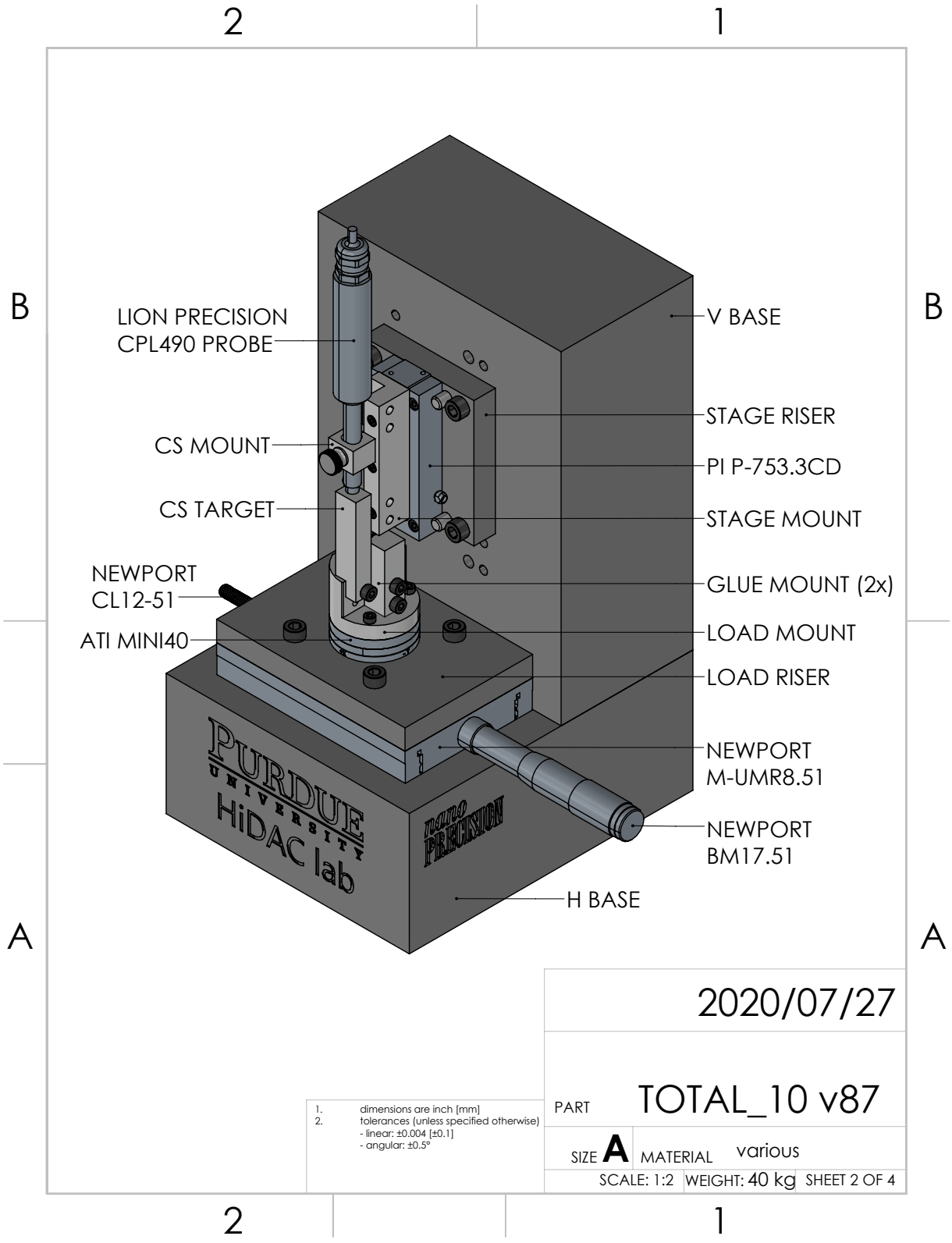

Figure B.3. Isometric assembly drawing with labels for each component.

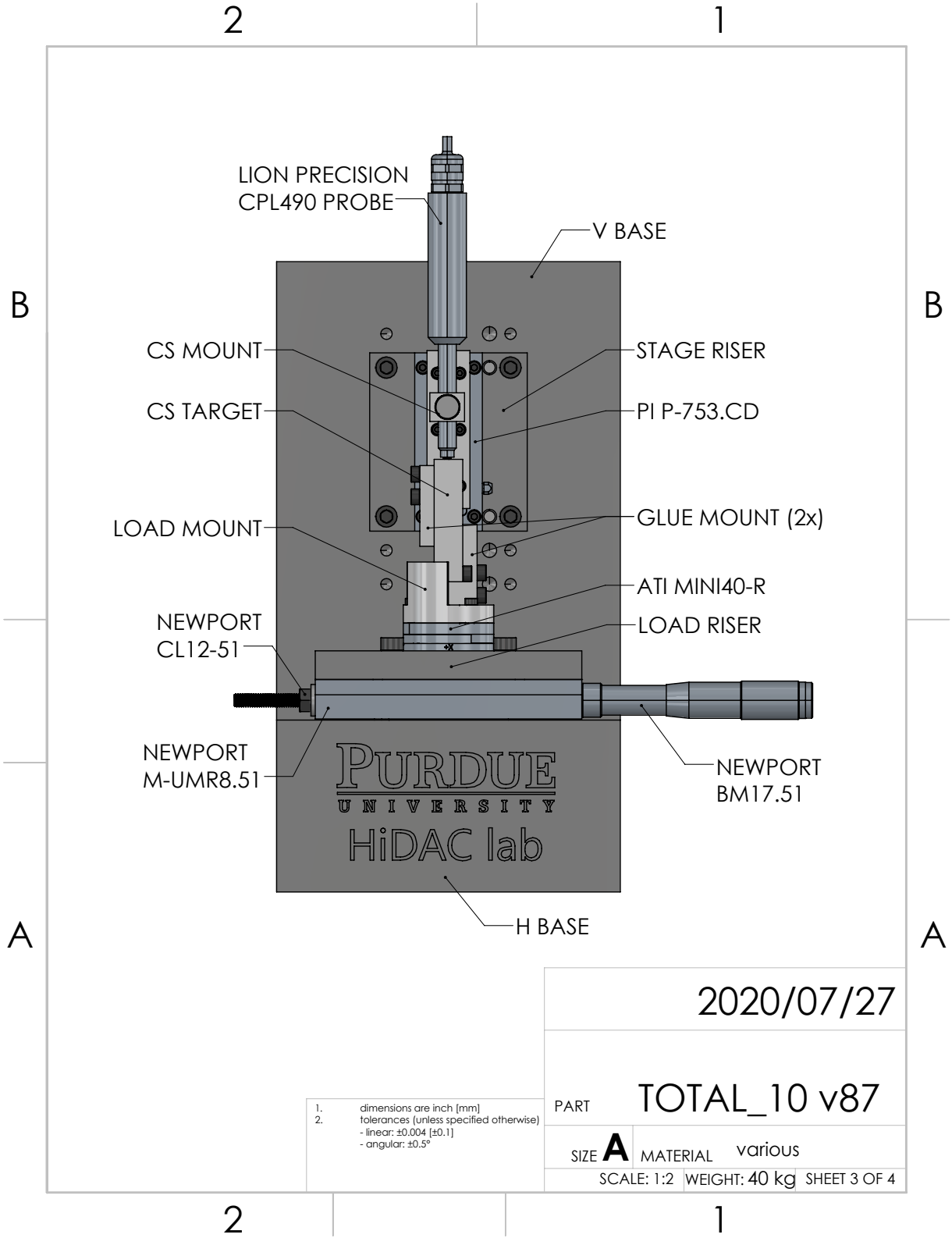

Figure B.4. Front-view assembly drawing with labels for each component.

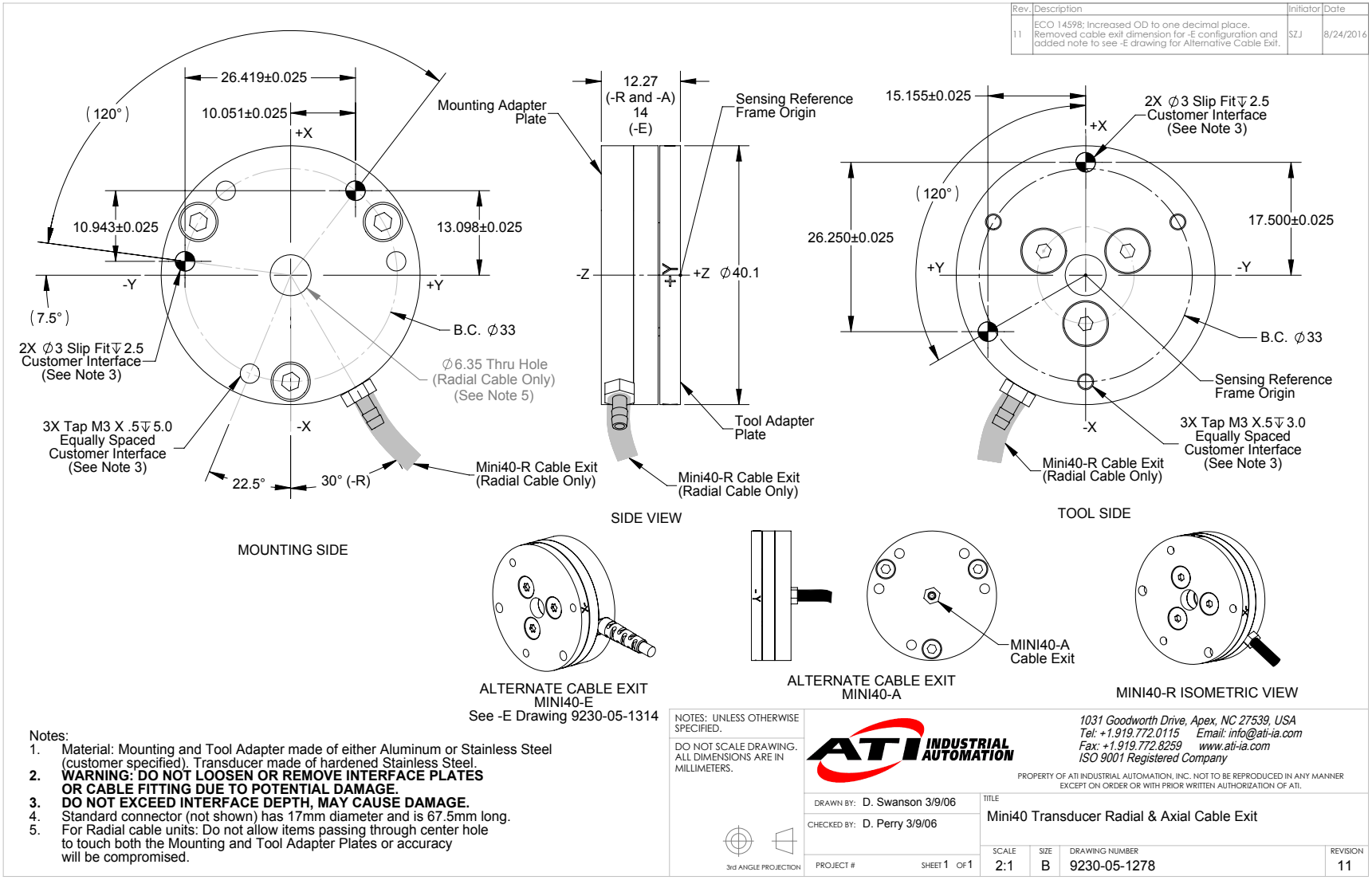

Figure B.5. 6-axis load cell, manufacturer part number 9105TWMini40R. Drawing courtesy of ATI Industrial Automation, Inc [24].

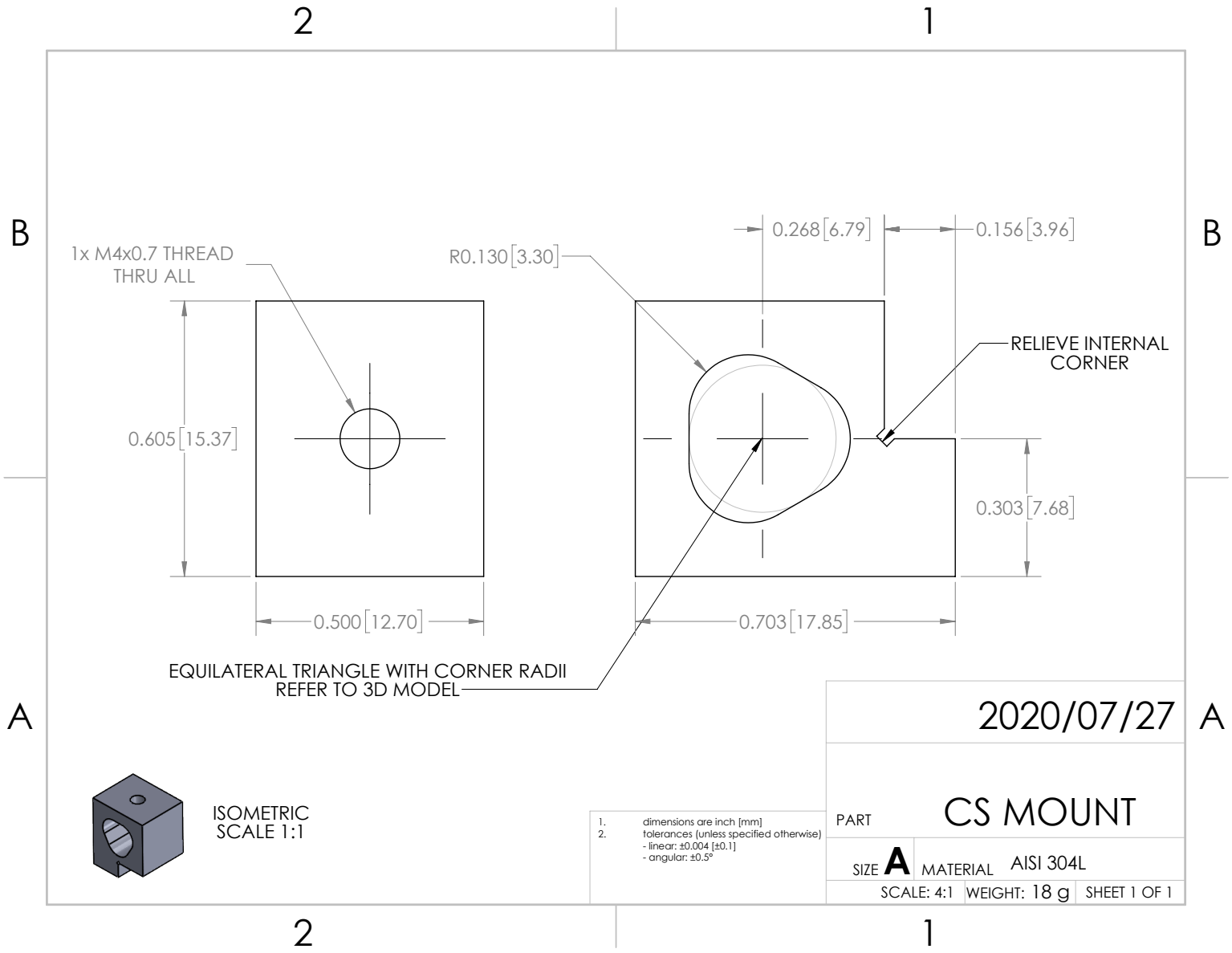

Figure B.6. Capacitance sensor mounting fixture.

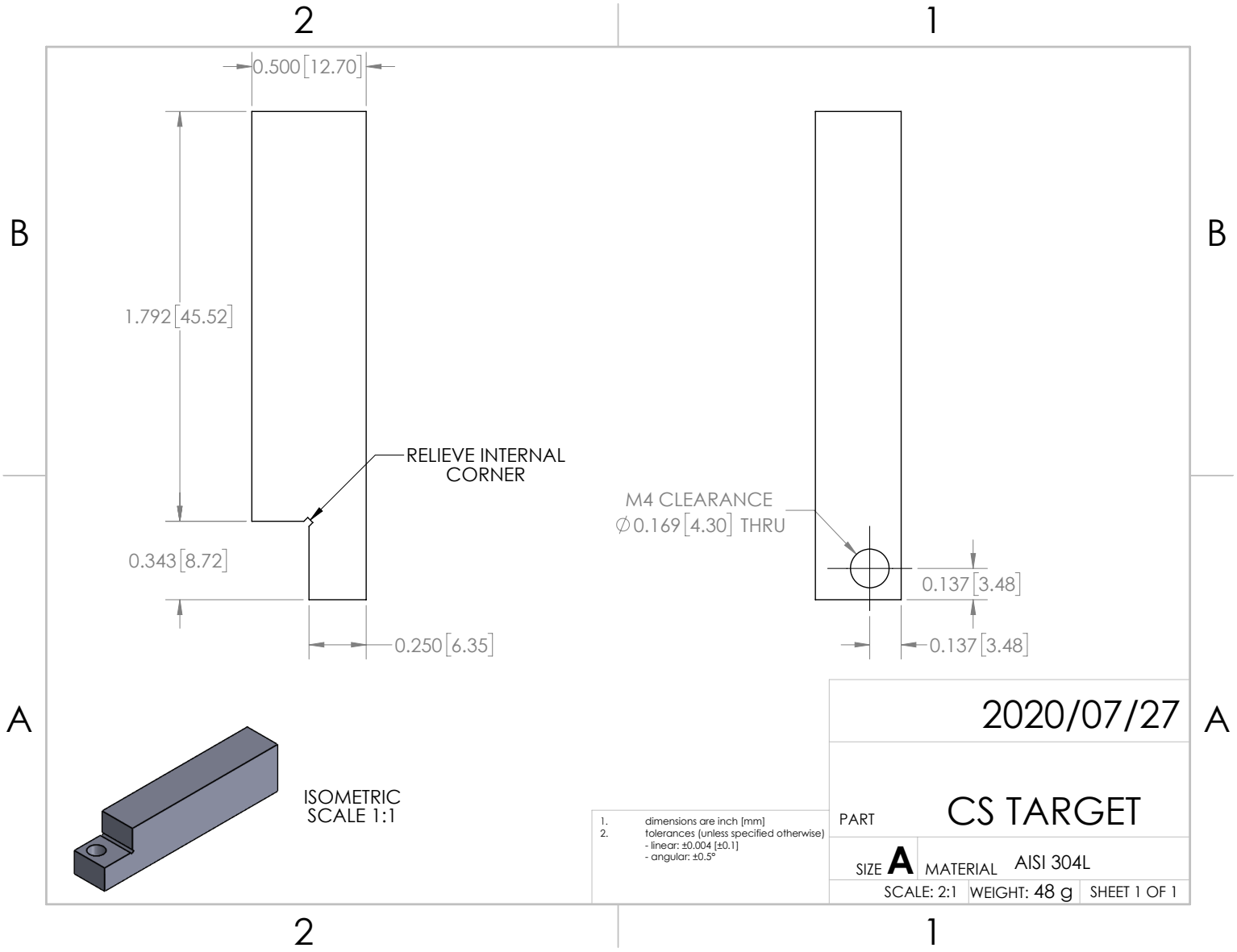

Figure B.7. Capacitance sensor target.

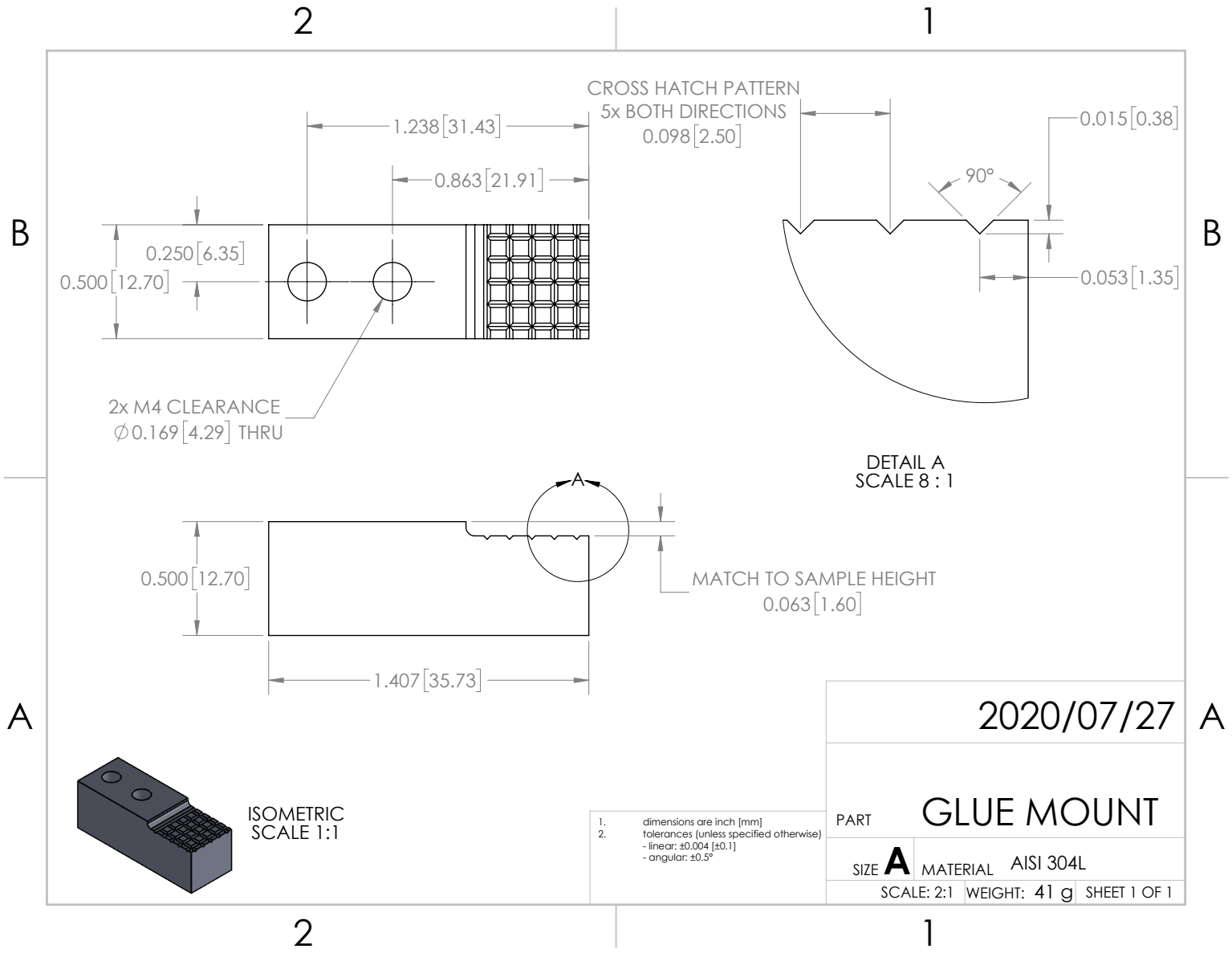

Figure B.8. Removable glue fixture for attaching samples.

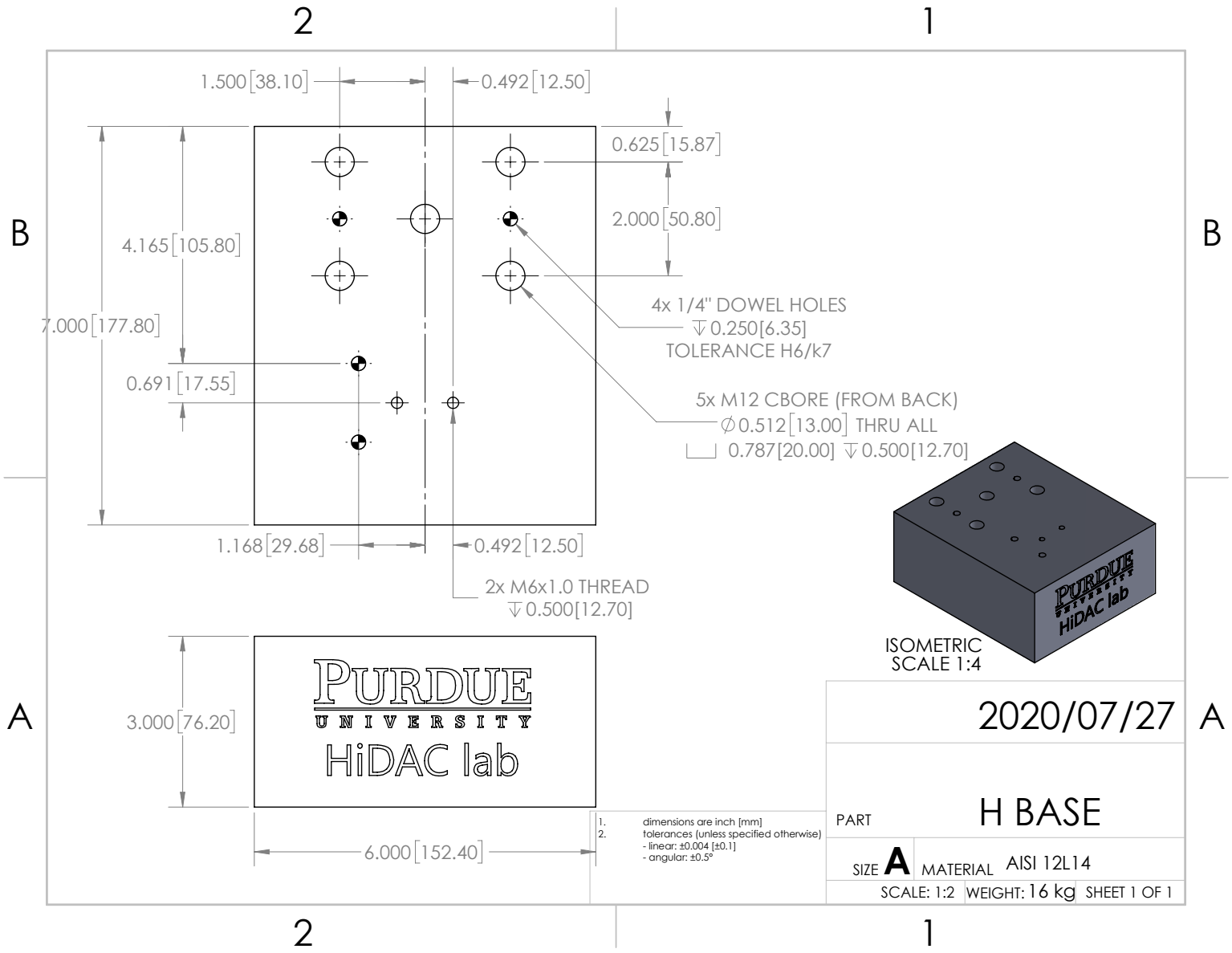

Figure B.9. One of two components that form the base of the tester.

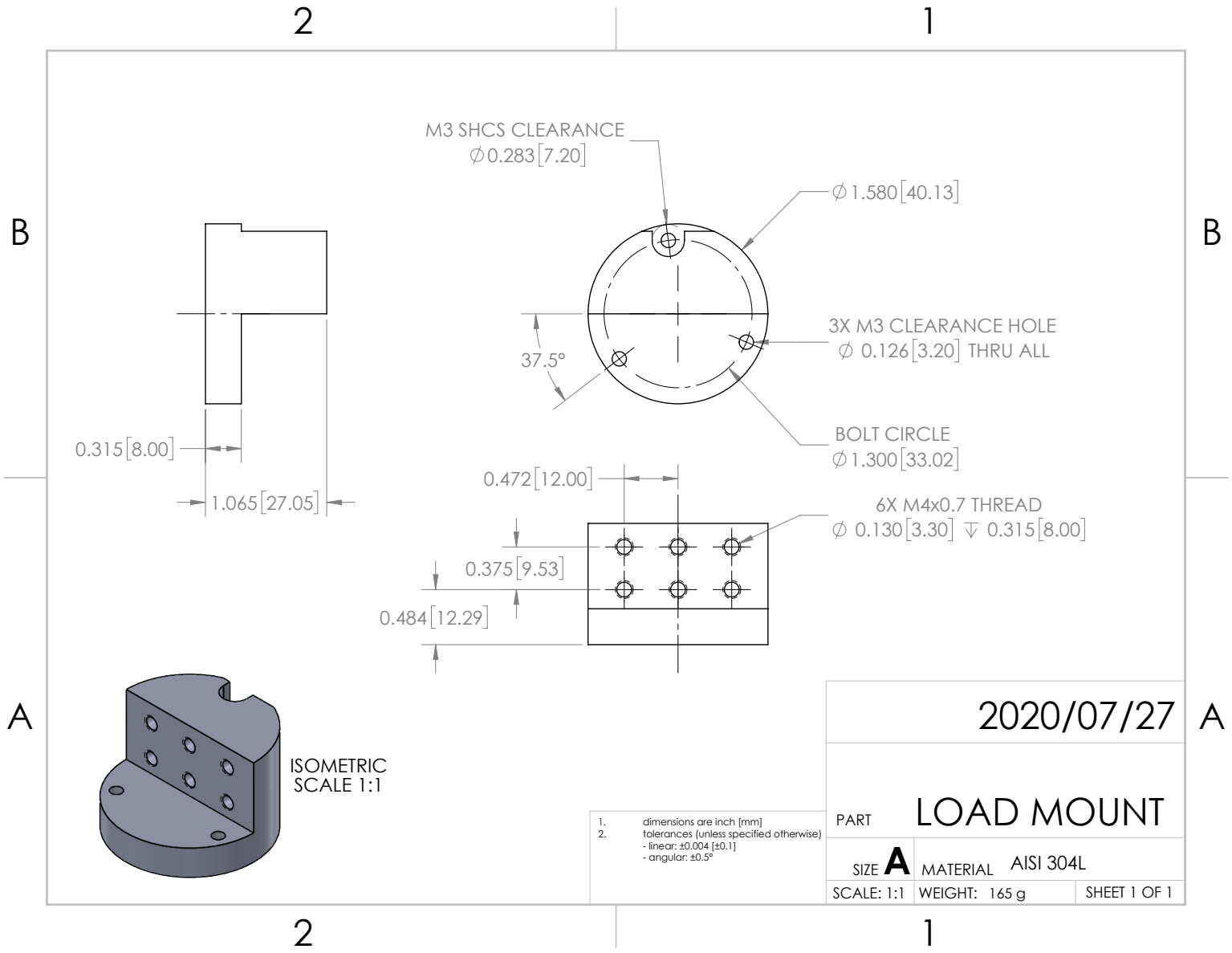

Figure B.10. Mounting fixture for bolting the lower glue fixture to the load cell.

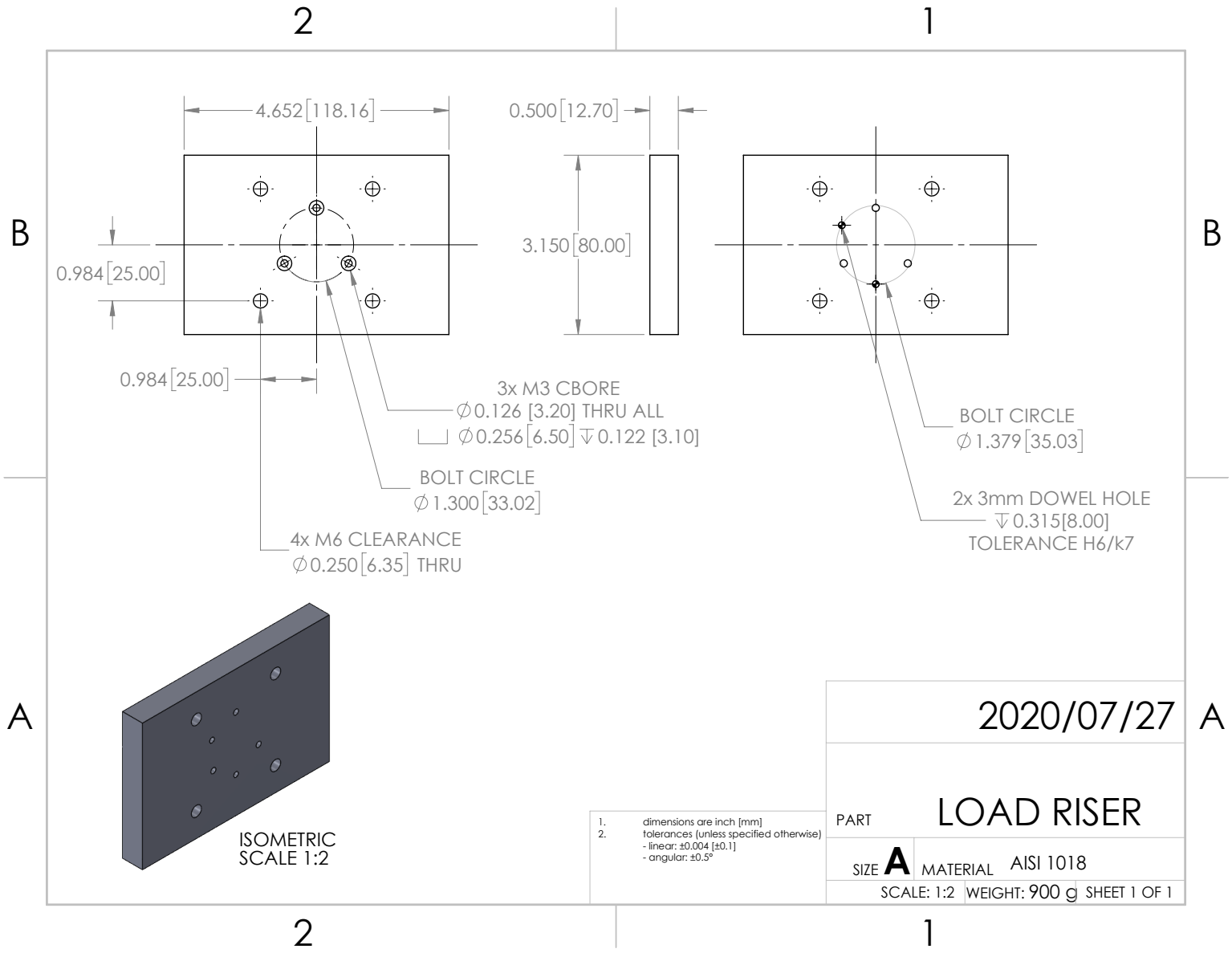

Figure B.11. Mounting plate attaching the load cell to the manual stage.

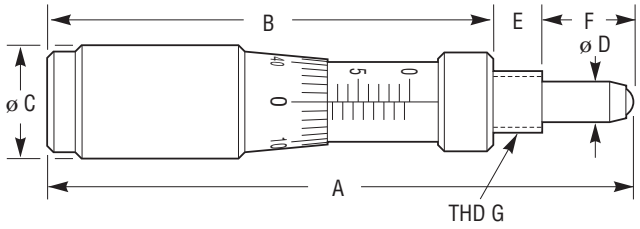

Dimensions [in. (mm)]									Thread
Model	**A**	**B Min**	**B Max**	**C**	**D**	**E**	**F Min**	**F Max**	**G**
BM11.5	1.36 (34.5)	1.00 (25.5)	1.20 (30.5)	0.43 (11)	0.16 (4)	0.13 (3.2)	0.03 (0.8)	0.23 (5.8)	M6 x 0.50
BM11.10	2.01 (51)	1.40 (35.5)	1.79 (45.5)	0.43 (11)	0.16 (4)	0.19 (4.7)	0.03 (0.8)	0.43 (10.8)	M6 x 0.50
BM11.16	2.24 (57)	1.40 (35.5)	2.03 (51.5)	0.43 (11)	0.16 (4)	0.19 (4.7)	0.03 (0.8)	0.66 (16.8)	M6 x 0.50
BM11.25	3.00 (76.2)	1.81 (46)	2.80 (71)	0.43 (11)	0.16 (4)	0.19 (4.7)	0.02 (0.5)	0.98 (25)	M6 x 0.50
BM17.25	3.25 (82.5)	1.95 (49.5)	2.93 (74.5)	0.67 (17)	0.28 (7.2)	0.28 (7.2)	0.03 (0.8)	1.01 (25.8)	M12 x 0.50
BM17.51	5.43 (138)	3.04 (77.1)	5.04 (128.1)	0.67 (17)	0.28 (7.2)	0.28 (7.2)	0.09 (2.4)	2.10 (53.4)	M12 x 0.50
BM25.40	4.92 (125)	2.72 (69)	4.29 (109)	0.98 (25)	0.31 (8)	0.57 (14.5)	0.12 (3)	1.69 (43)	M18 x 1.00
BM25.63	6.79 (172.5)	3.70 (94)	6.18 (157)	0.98 (25)	0.31 (8)	0.57 (14.5)	0.04 (1)	2.52 (64)	M18 x 1.00
BM32.80	8.35 (212)	4.17 (106)	7.32 (186)	1.26 (32)	0.47 (12)	0.94 (24)	0.08 (2)	3.23 (82)	M22 x 1.00

Newport

Figure B.12. Adjustment screw for manual stage, manufacturer part number BM17.51. Drawing courtesy of Newport Corporation [21].

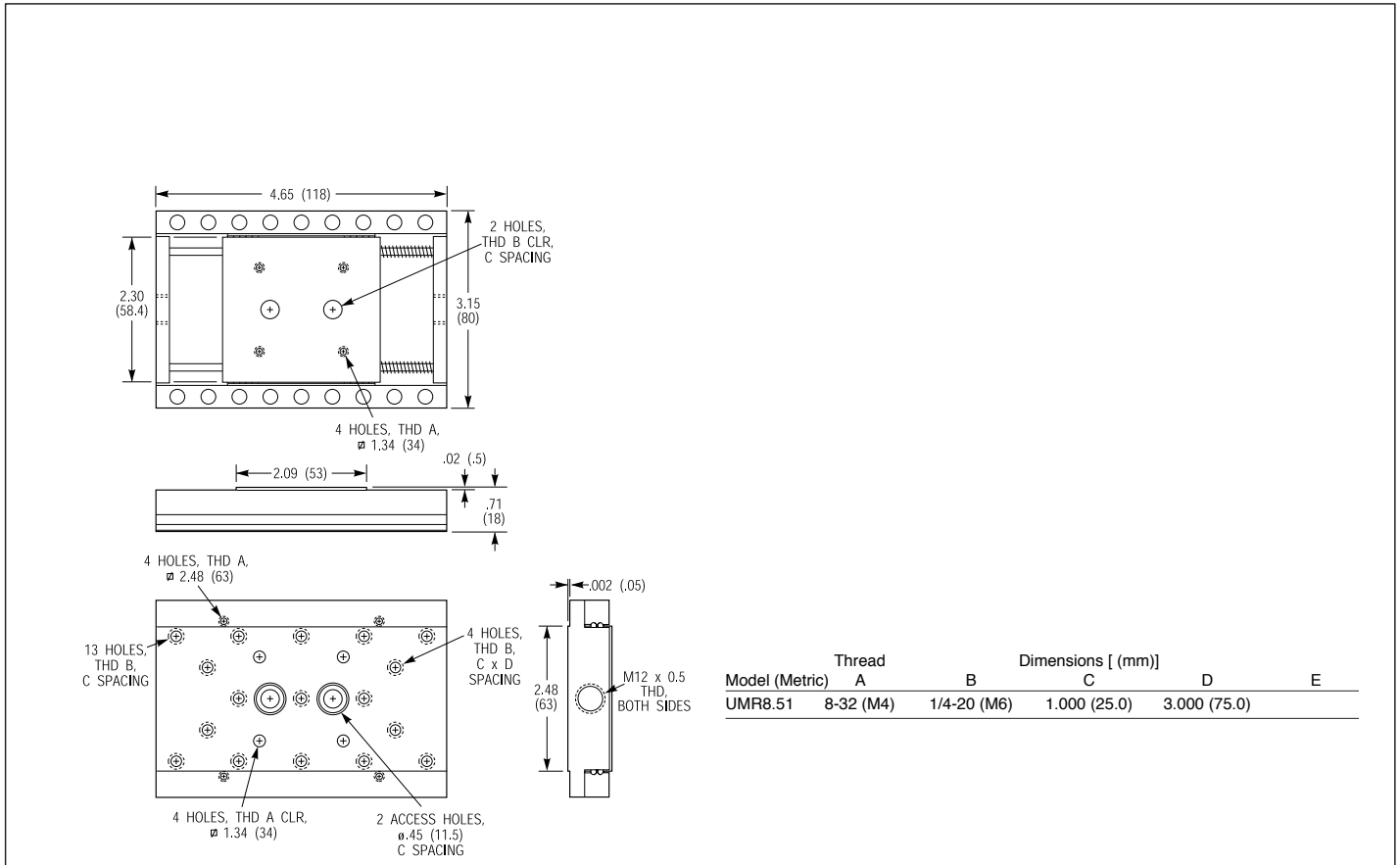

	Thread	Dimensions [(mm)]			
Model (Metric)	A	B	C	D	E
UMR8.51	8-32 (M4)	1/4-20 (M6)	1.000 (25.0)	3.000 (75.0)	

Figure B.13. Manual linear stage, manufacturer part number MUMR8.51. Drawing courtesy of Newport Corporation [22].

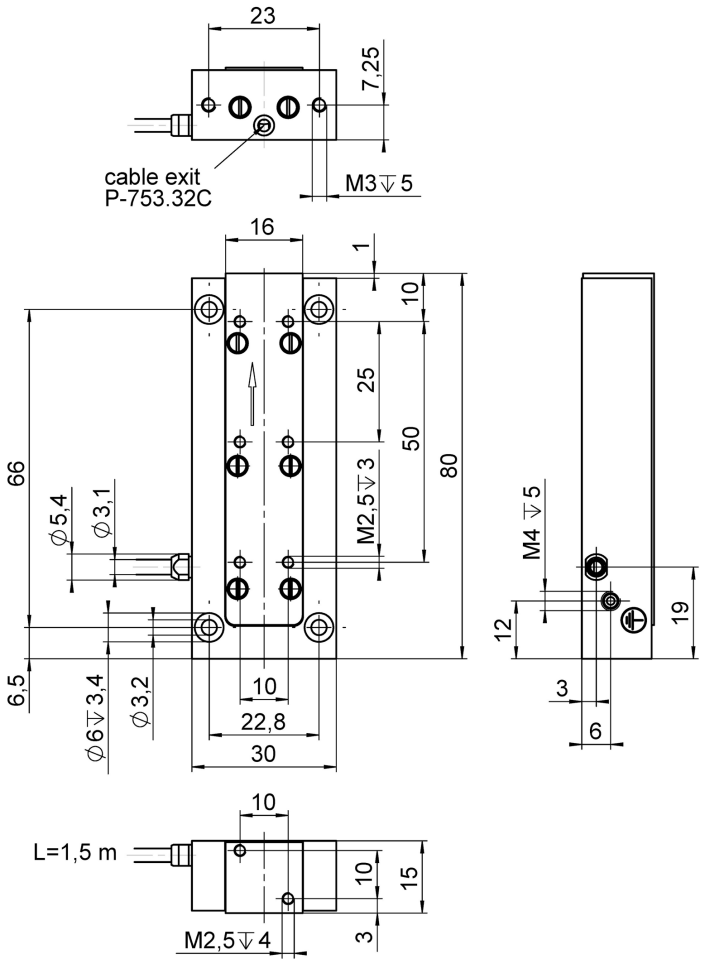

P-753.3, dimensions in mm. Max. torque at the M2.5 threads: 0.3 Nm.

Figure B.14. Piezoacutated linear stage, manufacturer part number P-753.3CD. Drawing courtesy of PI USA (Physik Instrumente) [25].

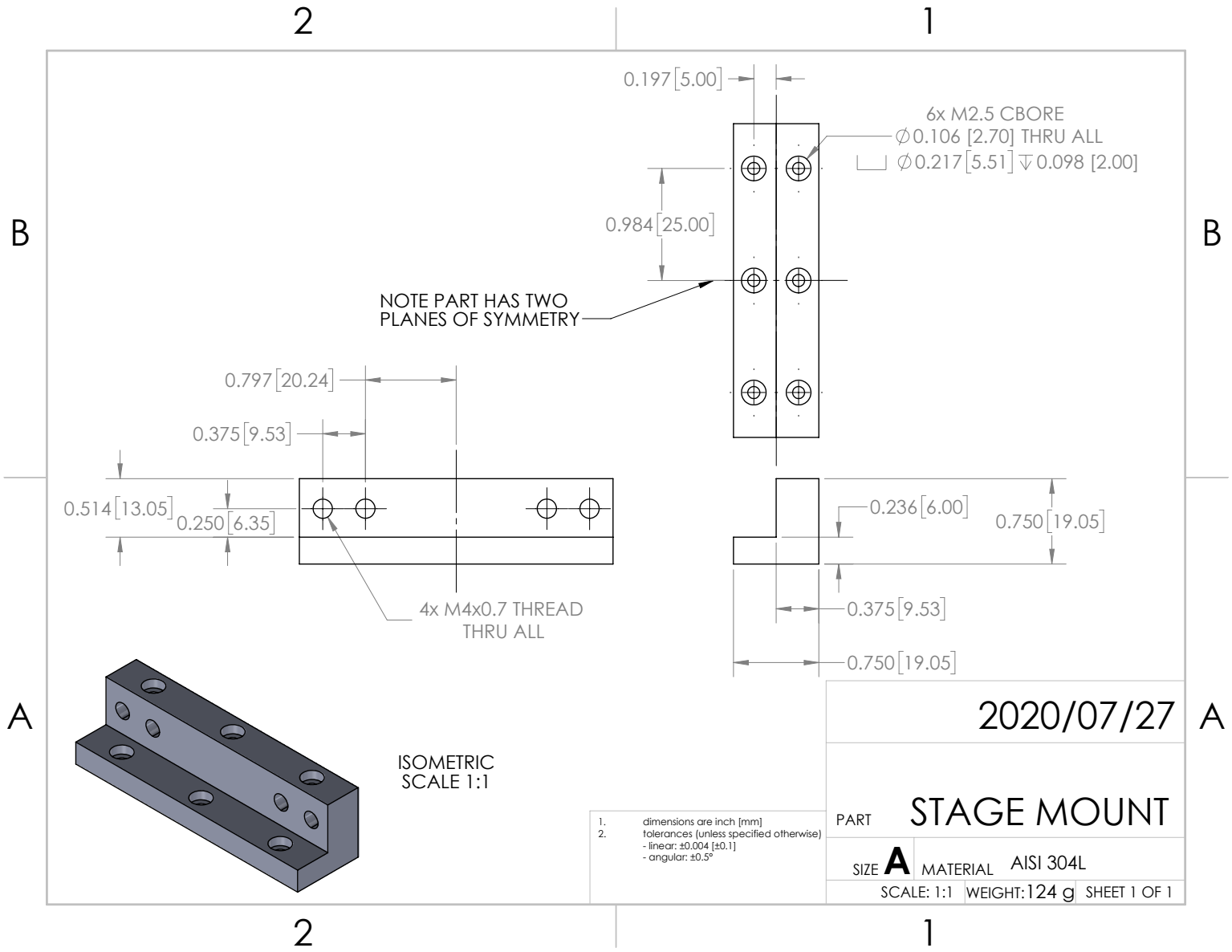

Figure B.15. Mounting fixture for bolting the upper glue fixture to the piezoactuator.

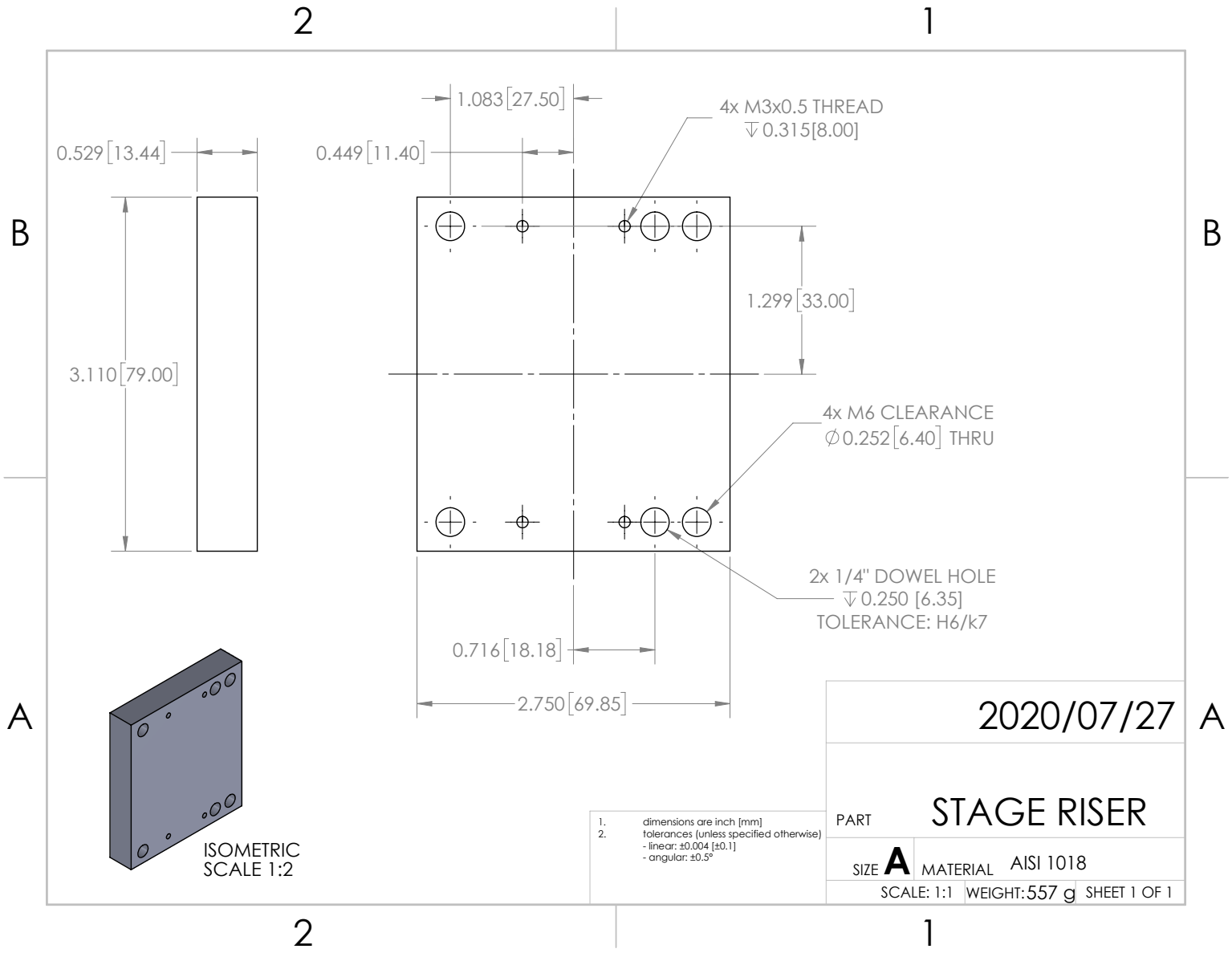

Figure B.16. Mounting plate for fixing the piezo-actuator to the tester frame.

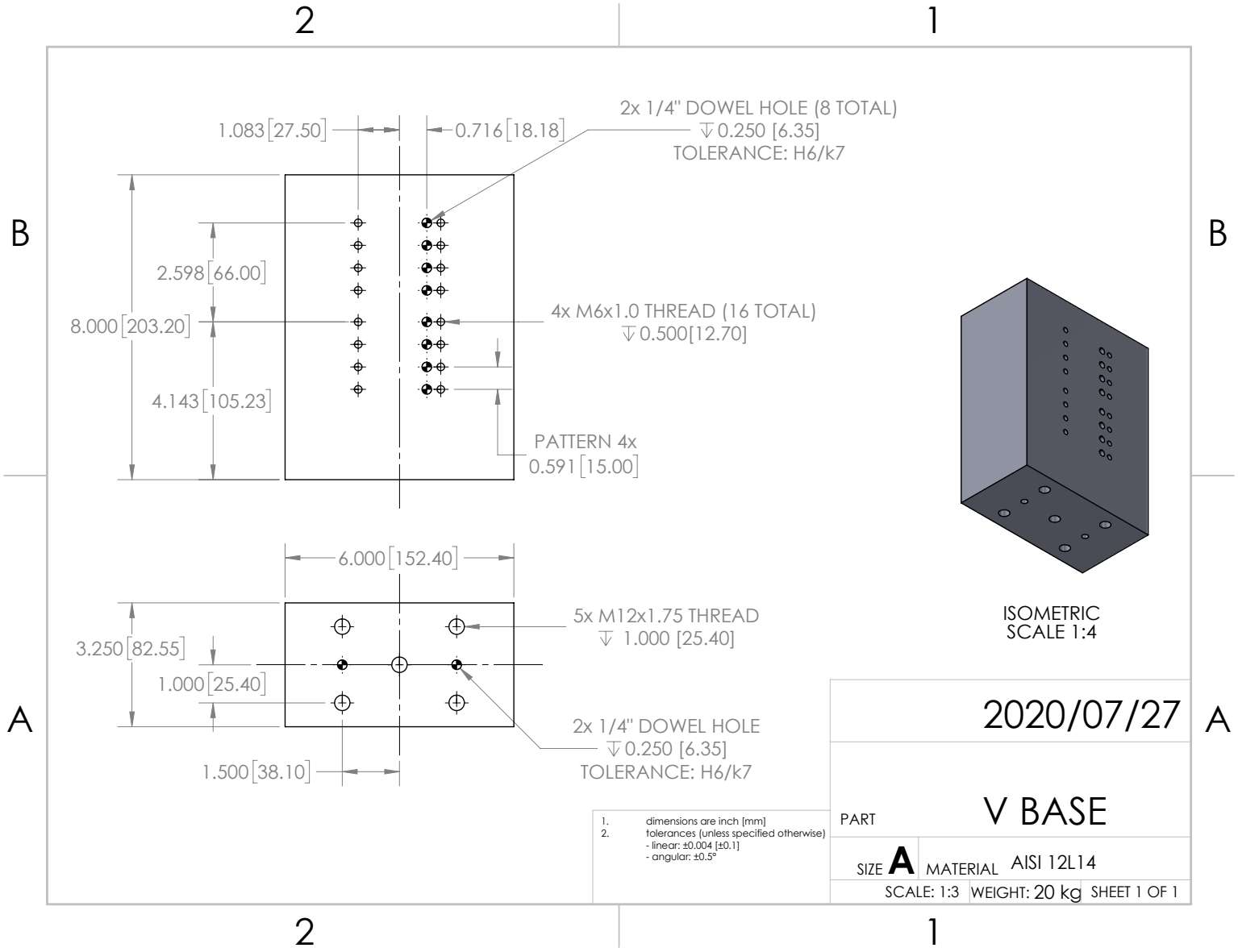

Figure B.17. One of two components that form the base of the tester.